International Journal of Pharmaceutics 515 (2016) 132–164

Contents lists available at ScienceDirect

International Journal of Pharmaceutics

journal homepage: www.elsevier.com/locate/ijpharm

Review

Nanomedicines for advanced cancer treatments: Transitioning towards responsive systems

Merel van Elk[a,b,c], Bruce P. Murphy[b,d,e], Tatiane Eufrásio-da-Silva[a,b,c], Daniel P. O'Reilly[a,b,c], Tina Vermonden[f], Wim E. Hennink[f], Garry P. Duffy[a,b,c], Eduardo Ruiz-Hernández[a,b,c,g,*]

[a] Tissue Engineering Research Group, Dept. of Anatomy, Royal College of Surgeons in Ireland (RCSI), Dublin 2, Ireland
[b] Trinity Centre for Bioengineering, Trinity College Dublin (TCD), Dublin 2, Ireland
[c] Advanced Materials Bio-engineering Research (AMBER) centre, RCSI, Dublin 2, Ireland
[d] Department of Mechanical and Manufacturing Engineering, School of Engineering, TCD, Dublin 2, Ireland
[e] AMBER centre, TCD, Dublin 2, Ireland
[f] Department of Pharmaceutics, Utrecht University, 3584 CG, Utrecht, The Netherlands
[g] School of Pharmacy, RCSI, Dublin 2, Ireland

ARTICLE INFO

Article history:
Received 5 August 2016
Received in revised form 4 October 2016
Accepted 5 October 2016
Available online 7 October 2016

Keywords:
Drug delivery
Cancer
Nanomedicine
Stimuli-responsive
Image guided therapies

ABSTRACT

The development of nanomedicines for the treatment of cancer focuses on the local targeted delivery of chemotherapeutic drugs to enhance drug efficacy and reduce adverse effects. The nanomedicines which are currently approved for clinical use are mainly successful in terms of improved bioavailability and tolerability but do not necessarily increase drug performance. Therefore, there is a need for improved drug carrier systems which are able to deliver high doses of anti-cancer drugs to the tumor. Stimuli responsive carriers are promising candidates since drug release can be triggered locally in the tumor via internal (i.e. pH, redox potential, metabolite or enzyme concentration) or external (i.e. heat, ultrasound, light, magnetic field) stimuli. This review summarizes the recent progress in the transition towards stimuli responsive nanomedicines (i.e. liposomes, polymeric micelles, nanogels and mesoporous silica nanoparticles) and other therapy modalities that are currently developed in the fight against cancer like the application of ultrasound, tumor normalization and phototherapy. Furthermore, the potential role of image guided drug delivery in the development of new nanomedicines and its clinical application is discussed.

Contents

* Corresponding author at: Tissue Engineering Research Group, Dept. of Anatomy, Royal College of Surgeons in Ireland (RCSI), Dublin 2, Ireland.
E-mail address: eduardorhernandez@rcsi.ie (E. Ruiz-Hernández).

http://dx.doi.org/10.1016/j.ijpharm.2016.10.013
0378-5173/

1. Introduction

The development of new medicinal compounds to face current healthcare challenges, especially in oncology, is commonly hindered by their poor solubility in water and non-specific cytotoxicity resulting in adverse side effects (Crawford et al., 2004; Gale, 1985; Gharib and Burnett, 2002; Bhattacharyya et al., 2015). Chemotherapeutics impair cell mitosis and thereby target fast dividing cells like cancer cells (Hanahan and Weinberg, 2000). A high dose of these drugs needs to be administered to achieve therapeutic levels, leading to various adverse effects because also other fast dividing, healthy cells are affected. Examples of adverse effects of chemotherapeutic drugs are neuropathy, nausea, general discomfort, myelosuppression (suppression of the bone marrow's production of blood cells and platelets), alopecia (hair loss), nephrotoxicity and cardiotoxicity (Crawford et al., 2004; Gale, 1985; Gharib and Burnett, 2002). Importantly, these adverse events often limit the dose and duration of the administered drugs. Another major problem is that cancer cells can become resistant towards chemotherapeutic drugs (Baguley, 2010; Szakács et al., 2006). Formulating cytostatic drugs in liposomal carriers or polymeric micelles, as well as in other nanoparticulate drug delivery systems, has demonstrated successful results in terms of therapeutic efficacy and tolerability, giving rise to several commercial products (Wicki et al., 2015a; Pérez-Herrero and Fernández-Medarde, 2015).

In general, drug delivery systems modify the pharmacokinetics of the loaded drug enabling a more favorable distribution (Nunez-Lozano et al., 2015). Given that drug carriers have sizes in the submicrometer range and they are surface modified by hydrophilic polymers, such as polyethylene glycol (PEG), they can avoid renal clearance and rapid uptake by cells of the reticuloendothelial system (RES) (Davis et al., 2008), therefore maximizing blood circulation time. Consequently, passive accumulation mechanisms can lead to high drug concentration in certain tissues. An example of this effect, attributed to certain tumor regions, (Kobayashi et al., 2014) inflammation (Yuan et al., 2012) and sites of bacterial infection (Maeda, 2013), is the enhanced permeation and retention (EPR) (Maeda and Matsumura, 1989a; Maeda et al., 1992; Matsumura and Maeda, 1986a; Seymour, 1992), by which different intravenously injected drug carriers can extravasate and later accumulate in the tissue, which is characterized by a leaky vasculature and poor lymphatic drainage (Maeda et al., 2000a; Maeda and Matsumura, 1989b; Matsumura and Maeda, 1986b). As a result, drug delivery systems enhance the therapeutic potential of the drug while reducing systemic side effects.

Despite the fact that PEGylated drug nanocarriers have a higher probability of ending up in tumors due to their extended time in the systemic circulation, there are a number of eventualities that may reduce the chances for an enhanced drug efficacy. For instance, in the case of polymeric micelles, instability might cause disassembly and thus hinder passive accumulation by the EPR effect (Chen et al., 2008; Savic et al., 2006). In fact, drug delivery to the tumor is rarely reported to be higher than 10% of the injected dose (Park, 2010; Bae and Park, 2011a; Ferris et al., 2016).

The conjugation of targeting moieties to the surface of drug nanocarriers has been suggested as a means to improve disposition in tumor and therapeutic efficacy. The overexpression of some receptors on the outer membrane of tumor cells facilitates recognition of drug delivery systems functionalized with biomolecules such as folic acid (FA), Arg-Gly-Asp (RGD) peptide or some other specific peptides or antibodies (Ruoslahti et al., 2010; Sudimack and Lee, 2000). This strategy has been broadly validated in *in vitro* experiments, and has also shown a significantly higher uptake of drug delivery systems in cancer cells within tumors *in vivo* (Kirpotin et al., 2006). However, active drug targeting generally speaking does not improve overall tumor accumulation of systemically administered nanomedicines *in vivo* (Kunjachan et al., 2014a), and with the exception of antibody-drug conjugates no drug delivery system employing this approach has yet been approved for clinical use (van der Meel et al., 2013). Further, it has been reported that nanoparticles or macromolecules with sizes of a few tens of nanometers could circulate in blood for long periods (half-life up to several hours), but they hardly penetrate into the tumor interstitium due to a high cell density and interstitial fluid pressure (Popovic et al., 2016; Dreher et al., 2006). For this reason, active targeting might not lead to improvements in the outcome over passively targeted nanomedicines. Active targeting however is often required for therapeutics, such as nucleic acid based drugs, which have their action intracellularly and as such do not spontaneously pass cellular membranes. The targeting ligand facilitates internalization of the drug-loaded nanoparticles leading to intracellular action of the drug after being released from its carrier system. It is worth mentioning that some stimuli-sensitive nanosystems have been designed to enhance tumor penetration after micelle disruption (Callahan et al., 2012) or cleavage of amide bonds (Li et al., 2016a) at the low pH characteristic of tumor sites.

Another challenge in local drug delivery is associated with the fact that the retention of the drug within the carrier should be strong enough to avoid premature leakage, but on the other hand the drug should be released from the carrier once the nanomedicine has reached its target site. Even in those cases in which a drug-loaded nanocarrier is able to reach the tumor region, an insufficient release of the cargo may hinder therapeutic efficacy (O'brien et al., 2004; Lammers et al., 2012). Overall, given the various constraints affecting drug accumulation in tumors, it is not surprising that most currently approved drugs do not substantially increase clinical performance after formulating them in nanocarriers (Venditto and Szoka, 2016).

The ability to trigger drug release on demand might therefore offer a renovated hope on the use of nanocarriers. A promising alternative to achieve site- and time-controlled release of therapeutics resides in the development of stimuli-responsive drug delivery systems. Ideally, such systems would entrap the drug in such a way that no premature release occurs at undesirable places in the body. Subsequently, drug release would be triggered

upon stimulation by external means (heat, ultrasound, light, magnetic field, *etc.*) or physiological cues (pH, redox potential, metabolite or enzyme concentration, *etc.*) at the site of action. ThermoDox®, a heat-activated liposomal formulation of an approved and frequently used drug for the treatment of a wide range of cancers, doxorubicin (DOX), exemplifies this concept (May and Li, 2013; Needham et al., 2013). The release of DOX from this formulation occurs upon heating to temperatures above the transition temperature of the used phospholipids (*ca.* 41 °C), at which the permeability of the liposome membrane is enhanced and the drug is released from the aqueous core into the outer medium. ThermoDox® together with radiofrequency ablation recently completed a phase III clinical trial in hepatocellular carcinoma patients (Needham, 2013).

Several types of stimuli-responsive materials have been proposed in the literature. In the field of polymeric drug delivery systems, sensitive hydrogels have been widely investigated to provide a triggered release of therapeutic agents. The mechanism of action of these systems is based on abrupt changes in volume in response to temperature, pH, electric field or protein concentration (Yang et al., 2015a; Griset et al., 2009; Shirakura et al., 2014). Inorganic nanocarriers have also been developed for this purpose, providing a stable structure to host the drug and the necessary anchoring groups to which a variety of responsive building blocks can be coupled (Vallet-Regi et al., 2011). Among the most intensively reported, silica-based materials, in particular mesoporous silica nanocarriers, have been chemically modified and combined with different inorganic nanoparticles (such as quantum dots and magnetic nuclei) or macromolecules to allow the construction of stimuli-responsive systems. (Li et al., 2014a; Han et al., 2015; Díez et al., 2014; Knezevic et al., 2013; Martin-Saavedra et al., 2010; Vallet-Regi and Ruiz-Hernandez, 2011)

In this article, we summarize recent developments on nanocarriers for anti-cancer drug delivery, with a particular focus on stimuli-responsive systems. Different material configurations have been attempted to enable these carriers to release the loaded drugs due to internal cues intracellularly or in the tumor microenvironment as well as external application of physical stimuli. We will discuss the use of biomaterials as carriers for drugs, the different options for triggered release and the interactions of these drug delivery systems with the biological milieu.

2. Liposomes

Nanosized drug delivery systems like liposomes have been developed for the encapsulation of chemotherapeutic drugs to improve their therapeutic efficacy and to reduce adverse events. Liposomes are unilamellar or multilamellar vesicles, which were first described in the 1960s by Bangham (Fig. 1A) (Bangham et al., 1965; Bangham and Horne, 1964). Liposomes consist mainly of phospholipids, which spontaneously form a lipid bilayer surrounding an aqueous core when dispersed in water via non covalent interactions. Hydrophilic drugs can be encapsulated in the aqueous core of the liposomes while hydrophobic drugs can be solubilized in the lipid bilayer.

Liposomes of the first generation are rapidly cleared from the systemic circulation by macrophages of the RES (Beaumier and Hwang, 1983; Gregoriadis and Ryman, 1972); approximately 50–80% of the liposomes were removed from the circulation within 15–30 min after administration. The circulation half-life of liposomes was significantly improved by coupling PEG on their surface. The reason for this improved half-life is that PEG is a hydrophilic polymer, which forms a steric barrier around the liposomes reducing protein adsorption on their surface and subsequent recognition by cells of the RES (Lasic et al., 1991; Allen et al., 1991; Gabizon et al., 1994; Torchilin et al., 1994). This improved circulation time allowed liposome accumulation in tumors via the EPR effect (Lammers et al., 2012; Maeda, 2010; Bae and Park, 2011b). So far, the discovery and development of liposomes have resulted in the approval of several liposomal formulations for the treatment of cancer (Doxil®/Caelyx®, Myocet®, DaunoXome® and Marqibo®, Table 1) (Wicki et al., 2015a; Allen and Cullis, 2013; Barenholz, 2012).

The efficacy of these liposomal formulations depends on their passive accumulation in tumors via the EPR effect. However, the actual accumulation of liposomes in tumors is less than 10% of the administered dose and the majority of the liposomes is still taken up by macrophages present in liver and spleen (Harrington et al., 2001). Moreover, the EPR effect is very heterogeneous and varies between tumor types, from patient to patient and even varies within the tumor (Lammers et al., 2012; Jain and Stylianopoulos, 2010). Furthermore, these liposomes are designed such that they exhibit a high stability in the blood circulation to prevent

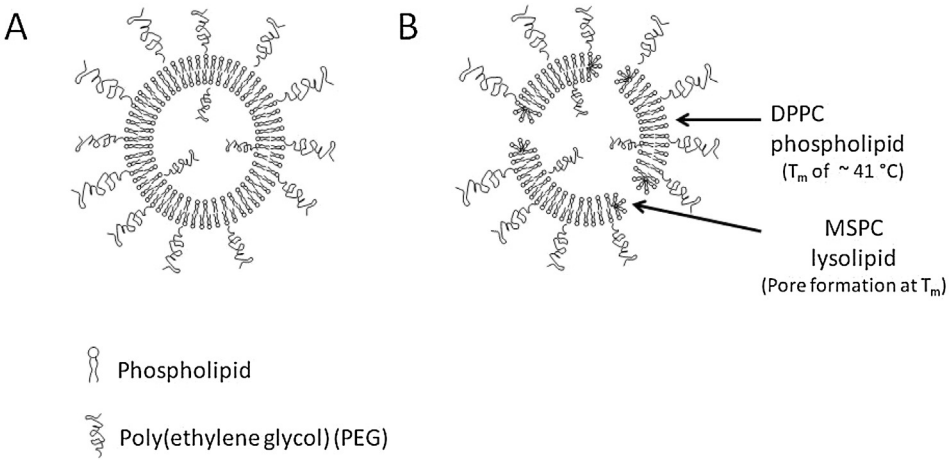

Fig. 1. Schematic representation of (A) a PEGylated liposome, and (B) a temperature sensitive liposome containing lysolipids. Lysolipids can form stable pores at the phase transition temperature of the liposome, inducing drug release.

Table 1
Overview of marketed liposomal formulations for cancer treatment (Wicki et al., 2015a; Allen and Cullis, 2013).

Product	Drug	Indication
Doxil®/Caelyx®	Doxorubicin	Kaposi's sarcoma Ovarian cancer Breast cancer Multiple myeloma
Myocet®	Doxorubicin	Breast cancer
DaunoXome®	Daunorubicin	Kaposi's sarcoma
Marqibo®	Vincristine	Acute lymphoblastic leukemia

premature release of the drug before arrival at the tumor site. Because of this high stability, the release of DOX from these liposomes is slow and uncontrolled resulting in a relatively low free drug concentration in the tumor and as a consequence, cytotoxic free drug concentrations are not always reached in the tumor (Bandak et al., 1999).

To increase the antitumor-activity of liposomal formulations, a higher concentration of free drug should be obtained in the tumor (Landon et al., 2011; Yarmolenko et al., 2010). Triggerable liposomal drug release systems have great opportunities to increase and control the drug concentration in the tumor. Several methods of triggered release have been described in literature (*e.g.* pH, light and ultrasound) (Leung and Romanowski, 2012; Ng et al., 2009; Obata et al., 2010) but so far heat has been the most intensively studied trigger for drug release (Fig. 2).

2.1. Responsive liposomes

Both internal and externally applied stimuli have been proposed to trigger the release from responsive liposomes. Among the former, the enhanced activity of reductases in cancers and inflammatory diseases (Ong et al., 2008), or changes in the intracellular pH (Mo et al., 2012) have been studied as triggers. On the other hand, gas-containing liposomes have been designed to respond to ultrasonic pulses (Huang, 2008), and the oxidation of lipid double bonds by singlet oxygen has been described as a mechanism to induce light-induced liposome permeabilization (Pashkovskaya et al., 2010). In the case of temperature triggered drug release, the goal is to achieve high drug concentrations in the tumor upon mild hyperthermia of the circulating liposomes. Therefore, the release from temperature sensitive liposomes should be ultrafast to facilitate a complete content release faster

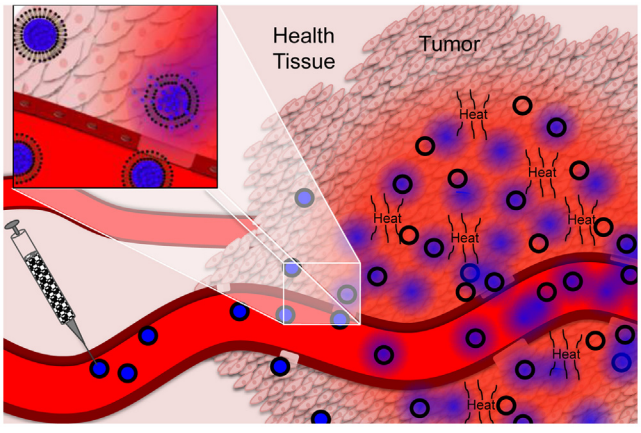

Fig. 2. Drug release from temperature sensitive liposomes in a tumor during mild hyperthermia. Liposomes pass through the preheated tumor vasculature after intravenous administration. Subsequently, the release from the liposomes present in the vasculature and the tumor tissue is triggered due to the mild hyperthermia treatment.

than the transit of the liposomes through the vasculature of the tumor. It has been reported that chemotherapeutic drugs and hyperthermia can act synergistically, leading to an enhanced cytotoxic effect of the drug (Landon et al., 2011; Hahn et al., 1975; Herman, 1983). The temperature threshold for mild hyperthermia lies around 43 °C because higher temperatures induce vascular occlusion and hemorrhage, resulting in a decreased blood flow, followed by a decreased drug delivery. Besides, a temperature in the whole tumor above 43 °C is difficult to achieve clinically (Landon et al., 2011; Hildebrandt et al., 2002; Thrall et al., 1992; Dewhirst and Sim, 1984). In this review, different temperature sensitive liposomes reported in literature are discussed (Table 2).

The first temperature sensitive liposomal formulation (traditional temperature sensitive liposomes or TTSL) was developed by Yatvin in 1979. These liposomes consisted of 1,2-dipalmitoyl-*sn*-*glycero*-3-phosphocholine (DPPC) and 1,2-distearoyl-*sn*-*glycero*-3-phosphocholine (DSPC) in a molar ratio of 3:1 and released neomycin (an antibiotic drug) at a temperature of 43–45 °C, which induced effective killing of E. Coli bacteria (Yatvin et al., 1978, 1981). The drug was released from these TSL at temperatures above the melting phase transition temperature (T_m) of the lipid bilayer. At the T_m, the lipids undergo a phase transition from a solid gel phase to a liquid crystalline phase. (Yatvin et al., 1978; Anyarambhatla and Needham, 1999) Upon heating, grain boundaries are formed between domains in the solid phase and domains in the liquid phase, leading to membrane permeability and subsequent drug release. The permeability of the lipid bilayer is highest at the T_m since solid and gel domains coexist at this temperature.

The first generation of TSL did not meet the optimal release requirements since the release rate was too slow and the temperature at which the release occurs is too high (43–45 °C) for clinical applications (Landon et al., 2011; Thrall et al., 1992; Dewhirst and Sim, 1984; Kong and Dewhirst, 1999). Low temperature sensitive liposomes (LTSL) were developed by Needham et al. to increase the release rate and simultaneously decrease the release temperature (Needham et al., 2000; Kong et al., 2000). DPPC was chosen as the main component of the LTSL since this phospholipid has a T_m of ~41 °C, which is ideal for the application of mild hyperthermia in the clinic. MSPC (1-stearoyl-2-hydroxy-*sn*-*glycero*-3-phosphocholine), a mono chain lysolipid that is able to form micelles, was added to the LTSL formulation to induce fast release of the content during mild hyperthermia (Fig. 3). At the phase transition temperature of the liposomes, the grain boundaries start to melt. As a result, the lipid mobility increases and the lysolipids accumulate in the grain boundaries causing the formation of pores which in turn induces fast release of the content (Fig. 1B). (Banno et al., 2010; Mills and Needham, 2005; Sandstrom et al., 2005; Winter et al., 2011; Ickenstein et al., 2003)

LTSL contain 1,2-distearoyl-*sn*-*glycero*-3-phosphoethanolamine-*N*-[amino(polyethylene glycol)-2000] (DSPE-PEG2000) not only to increase the half-life of the liposomes but it was also shown that DSPE-PEG2000 stabilizes the formed pores induced by the lysolipids (Needham et al., 2013). LTSL showed very rapid release kinetics of 80% the DOX loading in 20 s at 42 °C (Needham et al., 2000; Anyarambhatla and Needham, 1999). A complete tumor regression was obtained with LTSL in combination with mild hyperthermia (42 °C for 1 h) in a xenograft mouse model (Needham et al., 2000; Kong et al., 2000). As concluded by the authors, the reduction in tumor growth in mice treated with LTSL in combination with mild hyperthermia was more effective than the free drug, TTSL and non-temperature sensitive liposomes in combination with mild hyperthermia (Needham et al., 2000; Kong et al., 2000; Anyarambhatla and Needham, 1999; Needham and Dewhirst, 2001).

However, also shortcomings of LTSL have been reported. Approximately ~70% of the lysolipid desorbs from the LTSL within

Table 2
Overview of temperature sensitive liposomes under development for the treatment of cancer.

Liposome	Lipid composition	Drug encapsulated	T_m/LCST (°C)	Release	Animal model
TTSL (Yatvin et al., 1978)	DPPC:DPSC 3:1	Neomycin		44.5 °C (maximum release rate)	n.a.
LTSL (Needham et al., 2000; Kong et al., 2000)	DPPC:MSPC:DSPE-PEG 90:10:4	Doxorubicin	~41	>20% at 37 °C in 15 min 80% at 42 °C in 20 s	FaDu/mice
HaT (Tagami et al., 2011a, 2011c)	DPPC:Brij78 96:4	Doxorubicin	41	10–20% at 37 °C in 30 min >90% at 40–42 °C in 2.5 min	EMT-6/mice
$DPPG_2$ (Hossann et al., 2007; Limmer et al., 2014)	DPPC:DSPC:$DPPG_2$ 50:20:30	Doxorubicin	~42	11% at 37 °C in 3 h >95% at 42 °C in 2 min	BN175/rat gemcitabine
EOEOVE (Kono et al., 2011, 2010)	EPC:chol:poly(EOEOVE):PEG-PE 50:45:4:2	Doxorubicin	40.5	<10% at 37 °C in 30 min ~90% at 45 °C in 1 min	CT26/mice

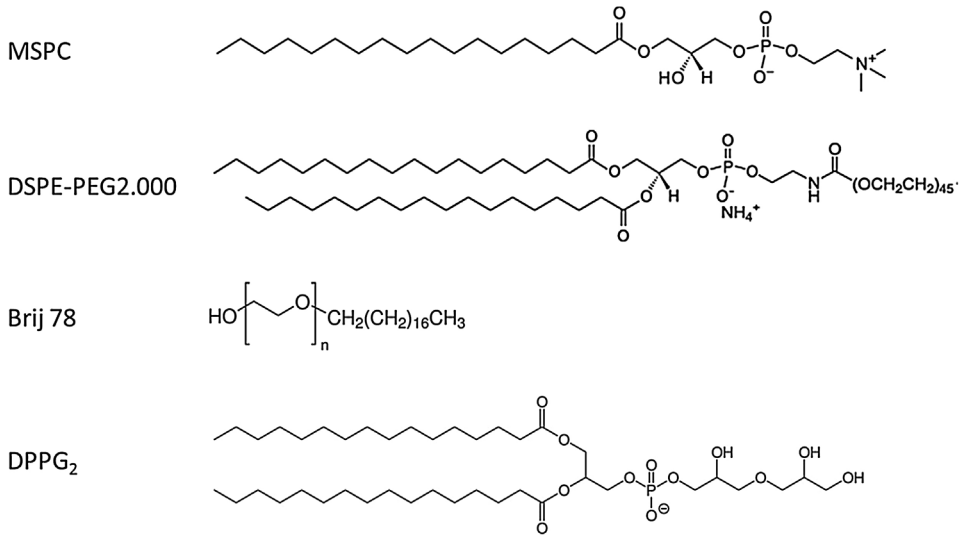

Fig. 3. Chemical structures of MSPC (1-stearoyl-2-hydroxy-*sn-glycero*-3-phosphocholine), DSPE-PEG2.000 (1,2-distearoyl-*sn-glycero*-3-phosphoethanolamine-*N*-[amino (polyethylene glycol)-2000]), Brij 78 and $DPPG_2$ (1,2-dipalmitoyl-*sn-glycero*-3-phosphoglyceroglycerol).

1 h after *in vivo* administration, which could hamper the maximal release *in vivo* from the LTSL (Banno et al., 2010; Sandstrom et al., 2005). Moreover, as demonstrated by de Smet et al., LTSL release more than 20% of DOX at 37 °C when incubated in serum rich medium for 15 mintues, which limits the amount of DOX delivered to the tumor tissue and induces exposure of healthy tissue to DOX (de Smet et al., 2010; Negussie et al., 2011).

Hyperthermia-activated cytotoxic liposomes (HaT, DPPC:Brij78 in a molar ratio of 96:4) were developed by Tagami et al. to simplify the LTSL formulation since Brij78 (Fig. 2) is a PEGylated single chain surfactant, which can replace MSPC (single chain lysolipid) and DSPE-PEG2000 of the LTSL formulation (Fig. 3) (Tagami et al., 2011a, 2011b). Quantitative DOX release was achieved from this HaT formulation within 3 min at 40–42 °C (Tagami et al., 2011b). The HaT formulation showed a faster DOX release rate at 40 and 41 °C compared to LTSL while the stability in serum at 37 °C and the circulation half-life (30 min) were similar for these two products (Tagami et al., 2011a, 2011c). The DOX delivery to a heated tumor (43 °C) was 1.4 fold increased when HaT was compared to LTSL, resulting in a significant enhanced tumor regression in Balb/c mice bearing EMT-6 tumors treated with the HaT formulation (Tagami et al., 2011a). Oxaliplatin (OXA) and gemcitabine (GEM) were passively loaded into HaT (HaT-OXA or HaT-GEM) and showed a temperature triggered release profile. Only 17% of the administered HaT-OXA remained in the circulation 1 h after injection and no increase in the amount of OXA released from HaT-OXA was observed in the heated tumor compared to free administered OXA. For the HaT-GEM, 82% of the administered dose remained in the blood circulation for 1 h and a 25 fold increase in drug deposition in the tumor was observed when HaT-GEM was delivered to a heated tumor compared to the free drug resulting in a complete tumor regression after a single dose of HaT-GEM. A significant shorter circulation time and antitumor efficacy were obtained by HaT-OXA in comparison with HaT-GEM. As suggested by the authors, OXA interacts with the phospholipids in the lipid bilayer, inducing a conformational change in the liposomal membrane, which results in an increased liver uptake and therefore an enhanced clearance from the blood circulation. Therefore, as concluded by May et al., less OXA is delivered to the tumor and no improvement in antitumor activity is observed (May et al., 2013).

The HaT formulation was further optimized by loading DOX with a Cu^{2+} gradient and post insertion of Brij78 (HaTII) in the phospholipid bilayer. The serum stability at 37 °C improved significantly whereas an enhanced drug release rate at 41–42 °C was observed. Compared to LTSL, the HaTII formulation showed a 2 times longer circulation time and a 2 fold increase in drug disposition in a heated EMT-6 tumor of a Balb/c mice resulting in an enhanced antitumor efficacy with complete growth inhibition (Tagami et al., 2012).

Thermosensitive liposomes composed of DPPC, DSPC and 1,2-dipalmitoyl-*sn-glycero*-3-phosphoglyceroglycerol ($DPPG_2$) have been developed to improve the liposomal stability in blood and to increase the circulation half-life. $DPPG_2$ is a synthetic phospholipid (Fig. 3) that is expected to prolong the circulation

time since this phospholipid has a hydrophilic glycerol chain, which extends from the liposomes and therefore likely forms a steric barrier around the liposomes, similar to PEG (Lindner et al., 2004). As shown by Lindner at al., since $DPPG_2$ is not able to form micelles at high concentrations, it can be incorporated into liposomes to a significantly higher extent (70%) than DSPE-PEG2000 (Lindner et al., 2004; Ashok et al., 2004). The half-life of $DPPG_2$-TSL was 9.6 h in hamsters and 5 h in rats (Lindner et al., 2004) compared to less than 1 h for LTSL in rats and mice (Tagami et al., 2011a; de Smet et al., 2011). DOX was quantitatively released within 2 min from $DPPG_2$-TSL at 42 °C and showed an improved stability in serum at 37 °C compared to LTSL with only 11% DOX release in 3 h at 37 °C (Hossann et al., 2007, 2012; Wang et al., 2008). The size of liposomes can influence the release kinetics since the membrane curvature increases for smaller liposomes, resulting in a looser packaging of the phospholipids, which increases the membrane permeability. The release kinetics of $DPPG_2$-TSL were less affected by the size of the liposomes compared to LTSL (Hossann et al., 2010). Hexadecylphosphocholine (HePC) was incorporated into $DPPG_2$-TSL since HePC is structurally related to MSPC (lysolipid in LTSL) and therefore its presence increased the release rate of $DPPG_2$-TSL to more than 80% release within 10 s at 43 °C in serum (Lindner et al., 2008).

A pharmacokinetic study in rats by Limmer et al. revealed that the half-life of GEM was extended from 4 min to 2.6 h by encapsulation of the drug into $DPPG_2$-TSL. The tumor growth of a BN175 tumor in the hind leg of a Brown Norway rat was significantly suppressed by $DPPG_2$-TSL in combination with mild hyperthermia compared to GEM in combination with mild hyperthermia or $DPPG_2$-TSL without mild hyperthermia (Limmer et al., 2014).

Another approach to prepare temperature sensitive liposomes concerns the modification of the liposomal surface with polymers displaying lower critical solution temperature (LCST) behavior. These polymers are water-soluble below its LCST, while above this temperature, hydrogen bonds between water molecules and amide bonds of the polymer become weaker resulting in less hydrated polymer chains. Consequently, the hydrophobic interactions between the isopropyl groups start to dominate and the polymer chains undergo a coil to globule transition, causing polymer precipitation. LCST polymers can be incorporated into liposomes by introducing a hydrophobic anchor in the polymer that solubilizes in the liposomal bilayer (Kono, 2001; van Elk et al., 2014).

Poly(*N*-isopropylacrylamide) (Poly(NIPAM)) is a temperature sensitive polymer with a LCST of 32 °C and NIPAM based polymers have often been used as carriers for drug delivery (Jalani et al., 2014; Peng et al., 2013; Saleem et al., 2013). NIPAM can be copolymerized with hydrophobic monomers which serve as an anchor for incorporation into liposomes. Kono et al. synthesized a copolymer of NIPAM and 1% octadecyl acrylate (ODA) via free radical polymerization (poly(NIPAM-co-ODA)). This copolymer had a LCST of 27 °C, which is slightly lower than the LCST of solely NIPAM due to the hydrophobic nature of the anchor unit. A temperature triggered release of calcein or carboxyfluorescein as fluorescence markers was observed when these polymers were coated onto DPPC or egg phosphocholine (EPC) liposomes even though their release was incomplete (<70% after 5 min at 40 °C) (Kono et al., 1994). In a study by Hayashi et al., an enhanced and complete calcein and DOX release was observed from 1,2-dioleoyl-*sn-glycero*-3-phosphoethanolamine (DOPE) liposomes coated with poly(NIPAM-co-ODA) (Hayashi et al., 1996; Kono et al., 1999a). DOPE itself does not self-assemble into liposomes but forms a nonbilayer structure (hexagonal H_{II}) (Allen et al., 1990; Ishida et al., 2001). However, liposomes containing DOPE can be prepared by stabilization with hydrated poly(NIPAM-co-ODA). Above the LCST, the polymer becomes dehydrated and loses its stabilizing properties and thereby induces drug release by liposome aggregation, fusion and membrane permeabilization (Hayashi et al., 1998).

The liposomes described above demonstrated that poly(NIPAM) is indeed able to trigger drug release from liposomes at elevated temperatures but these liposomes are clinically not suitable due to the low release temperature (under physiological temperature). Therefore, NIPAM was copolymerized with *N,N*-didodecylacrylamide (NDDAM, anchor) and various amounts of acrylamide (AAM) as hydrophilic monomer. The LCST of poly(NIPAM) increased from 28 to 46 °C when copolymerized with 10 −30% AAM. DOPE:EPC liposomes coated with poly(NIPAM-co-NDDAM-co-AAM) showed only a minimal content release below the LCST while an enhanced release was observed at temperatures above the polymer's LCST. Liposomes coated with a polymer having a higher AAM content and therefore a higher LCST, had a higher release temperature, demonstrating that by adjusting the LCST of the polymer the release could be tuned (Han et al., 2006; Hayashi et al., 1999).

In another study, the influence of the position of the lipid anchor on the release kinetics was investigated. Copolymers with lipid anchors randomly distributed over the polymer chains were prepared by free radical polymerization of NIPAM, acryloylpyrrolidine (APr) and *N,N*-didodecylacrylamide (NDDAM lipid anchor) (poly(NIPAM-co-APr-co-NDDAM)). Copolymers with a terminal anchor were obtained by free radical polymerization of NIPAM and APr and subsequent conjugation to *N,N*-didodecyl succinamic acid ($2C_{12}$) to obtain $2C_{12}$-poly(NIPAM-co-APr). Liposomes modified with a terminal anchor polymer ($2C_{12}$-poly(NIPAM-co-APr)) released its content more rapidly upon a small temperature change compared to liposomes coated with copolymers having random anchor units (poly(NIPAM-co-APr-co-NDDAM)). The polymer mobility might be more restricted when the lipid anchors are randomly distributed over the polymer chains compared to polymers with a terminal anchor. Therefore, terminal anchor polymers dehydrate faster, inducing a more rapid content release (Kono et al., 1999b).

Free radical polymerization is a method which has limited control over the average molecular weight and also results in polymers with a relatively high polydispersity. Therefore, Ta et al. synthesized a poly(NIPAM-co-propylacrylic acid) by reversible addition-fragmentation chain transfer (RAFT), obtaining polymers with a M_n of 30 kDa, a LCST of 42 °C (at pH 6.5) and a PDI of only 1.2. Liposomes modified with this polymer released DOX quantitatively within 5 min at 42 °C with a low release at 37 °C (<10% after 1 h incubation). The release at 42 °C was faster from poly(NIPAM-co-propylacrylic acid) coated liposomes compared to TTSL (Ta et al., 2010).

Besides RAFT, living cationic polymerization also provides a high level of control over the molecular weight and yields polymers with a low polydispersity. Using this method, block-copolymers of (2-ethoxy)ethoxyethyl vinyl ether (EOEOVE, temperature sensitive component) and octadecyl vinyl ether (ODVE, hydrophobic anchor) were synthesized with various molecular weights. Polymers with a higher molecular weight showed an enhanced release at a narrow temperature range near the LCST than polymers with a lower molecular weight (Kono et al., 2005). Presumably, polymers with a longer chain length form larger dehydrated blocks above the LCST, inducing a stronger interaction with the membrane and therefore induce an enhanced release. Poly(EOEOVE-b-ODVE) with a LCST of 40.5 °C released 90% of the loaded DOX at 45 °C within 1 min, but was however also rather unstable at 37 °C (30% release in 30 min). The stability at 37 °C was improved by PEGylation (< 10% DOX release in 30 min) while enhancing the release rate above the LCST even further. According to the authors, the partly dehydrated poly(EOEOVE-b-ODVE) might

interact with PEG on the surface of the liposomes, weakening the interaction between EOEOVE and the liposomes. Furthermore, PEGylation of the poly(EOEOVE-b-ODVE) modified liposomes increased the circulation time in mice while reducing the uptake by macrophages of the liver. The tumor growth was strongly suppressed after injection of these DOX loaded liposomes in combination with hyperthermia treatment while the tumor suppressive effect was less pronounced when only liposomes were administered without hyperthermia treatment (Kono et al., 2010). The accumulation of these liposomes in the tumor was monitored by coating of gadolinium chelates were coated to the PEGylated liposomes (Kono et al., 2011). Furthermore, as shown by Katagiri et al., Fe_3O_4 nanoparticles could be incorporated into the lipid bilayer of poly(EOEOVE-b-ODVE) modified liposomes via hydrophobic interactions. An alternating magnetic field (AMF) was used to heat the Fe_3O_4 nanoparticles and induce the release of a fluorescent marker (Katagiri et al., 2011).

Fatty acid conjugated elastin like polypeptides (ELP) display LCST behavior and can be coated onto DOX loaded liposomes (ELP-liposomes). Park et al. showed that ELP-liposomes release > 95% of the content in 10 s at 42 °C while less than 20% was released within 30 min at 37 °C in serum. ELP-liposomes had a plasma half-life of 2 h compared to a half-life of 0.9 h for LTSL. A significant delay in tumor growth was achieved by ELP-liposomes in combination with high intensity focused ultrasound (HIFU) compared to LTSL after one intravenous injection (Park et al., 2013). A 7 fold increase in cellular uptake of $\alpha_v\beta_3$ overexpressing cells was observed when ELP-liposomes were coupled to a cRGD binding moiety, which resulted in a 5 times higher tumor accumulation compared to ELP-liposomes in mice. This implies that tumors can be targeted through the interaction between cRGD grafted onto liposomes and $\alpha_v\beta_3$ integrin receptors on tumor-associated endothelial cells or tumors (Kim et al., 2014a).

3. Polymeric nanocarriers

3.1. Polymeric micelles

Amphiphilic block copolymers with *e.g.* an A-B or A-B-A architecture spontaneously form micelles with size ranging from 5 to 100 nm when these polymers are dispersed in an aqueous medium. The outer shell is formed by the hydrophilic block of the polymer while the inner core is formed by the hydrophobic part of the block copolymer. The inner core can be used to solubilize hydrophobic drugs (Kowalczuk et al., 2014) and because of this and their small size, polymeric micelles are very attractive drug delivery systems (Gong et al., 2012; Kataoka et al., 2012; Ruiz-Hernandez et al., 2014). It should be mentioned that equilibrium exists between the formed micelles and the soluble unimers. However an important advantage for the design of drug nanocarriers is that the polymer concentration at which polymeric micelles are formed (referred to as the critical micelle concentration or CMC) is quite low compared to the CMC of micelles formed with low molecular weight surfactants (Kataoka et al., 2012; Deng et al., 2012). Therefore, polymeric micelles are stable at relatively low polymer concentrations and are less susceptible to dilution compared to surfactant micelles. After intravenous injection, the stability of polymeric micelles can also be affected by interaction with various blood proteins which can lead to the dissociation or aggregation of the micelles and unwanted premature release of the cargo. However, the stability of polymeric micelles can be improved by cross-linking their inner core as shown by *e.g.* Rijcken et al. (2007) although this might not always lead to an enhanced circulation time of the encapsulated drug (Talelli et al., 2015).

Hydrophobic drugs can be solubilized in the hydrophobic core of micelles via physical interactions which may increase the solubility of common anti-cancer drugs like DOX, docetaxel and paclitaxel (PTX). Nevertheless, the physical loading of these drugs into micelles does not necessarily lead to improved circulation kinetics of the drug. In particular cases, it has been demonstrated that the pharmacokinetics of PTX loaded in micelles had comparable pharmacokinetics as the free drug (Shi et al., 2013). As a solution to this limitation, the circulation time of the loaded drug can be improved by chemically conjugating the drug to the polymer that forms the micelle (Talelli et al., 2010a; Crielaard et al., 2012; Wu et al., 2012). Although this chemical modification can adversely alter the pharmacological activity of the drug, micelles incorporating acetal-linked PTX prodrug have been reported in which the drug activity can be retained (Zhong et al., 2016; Gu et al., 2013). Another possibility, as suggested by Shi et al., consists of loading drugs via Π-Π stacking in which the aromatic groups of the drug interact with aromatic groups in the polymer chain. This strategy has shown to improve the pharmacokinetics of PTX and subsequently increase drug accumulation in the tumor, leading to complete tumor regression in xenograft models (Shi et al., 2015). Specific targeting moieties can be conjugated to the hydrophilic shell of the micelle to make them specific for the target cell, therefore enabling a selective delivery of the encapsulated drug. In a recent example illustrating this concept, Kutty et at. conjugated cetuximab and a ligand to target epithelial growth factor receptors (EGFR) to vitamin E D-α-tocopheryl polyethylene glycol succinate micelles for the treatment of triple negative breast cancer in mice. The targeted micelles accumulated in the tumor 2 h after administration and were retained in the tumor for at least 24 h. In contrast, non-targeted micelles were evenly distributed throughout the body. As a result, targeted micelles showed a 2 fold higher accumulation in the tumor compared to non-targeted micelles and delivered docetaxel more efficiently to the tumor resulting in a 2 fold smaller tumor volume after 15 days (Kutty et al., 2015).

An important challenge in the targeted delivery of micelles is intracellular autophagy in which the micelles are taken up by the cells and transported to the lysosomes for degradation. Zhang et al. showed that PEG-b-poly(D,L-lactide-co-glycolide) (PEG-b-PLGA) micelles internalized by MCF-7 breast cancer cells were subsequently translocated into lysosomes. By co-treatment with chloroquine, a known inhibitor for autophagy, the authors reported a 12-fold lower IC_{50} of docetaxel-loaded PEG-b-PLGA micelles. As a result, the combination of drug-loaded micelles and chloroquine significantly inhibited the tumor growth in a xenograft SCID mouse model (Zhang et al., 2014).

Several clinical trials have been conducted involving micelles loaded with chemotherapeutic drugs such as cisplatin (Plummer et al., 2011), PTX (Kato et al., 2012; Lee et al., 2013) and DOX (Matsumura et al., 2004; Cabral and Kataoka, 2014) (Table 3). Currently, Genexol-PM is the only micellar formulation approved for the treatment of cancer. These micelles are composed of a PEG-b-poly(D,L-lactic acid) diblock copolymer and are loaded with PTX. Phase I clinical trials with Genexol-PM have shown a maximum tolerated dose of 390 mg/m^2 which is higher than the usual dose range of PTX as its Taxol formulation (135–200 mg/m^2) (Kim et al., 2004). In subsequent trials, it was shown that patients suffering from breast cancer had a high response rate of 58.5% to Genexol-PM (Lee et al., 2008a).

Similarly to new liposome formulations, the development of stimuli-responsive micelles seems an attractive strategy to improve drug delivery to the tumor site therefore enhancing therapeutic efficacy (Oerlemans et al., 2010). Physiological (*i.e.* acidic pH, reducing environment) as well as external (*i.e.* increased

Table 3
Polymeric micelles under clinical investigation (Gong et al., 2012; Cabral and Kataoka, 2014; Wang et al., 2012; Kresge et al., 1992).

Formulation	Drug	Polymer	Indication	Status	Company
NC-6300	Epirubicin	PEG-b-poly(aspartate)	Various solid tumors	Phase I	Nanocarrier, Co.
NK911	Doxorubicin	PEG-b-poly(α,β-aspartic acid)	Various solid tumors	Phase II	Nippon Kayaku, Co
NK105	Paclitaxel	PEG-b-poly(α,β-aspartic acid)	Gastric cancer/Breast cancer	Phase III	Nippon Kayaku, Co.
NC-4016	Oxaliplatin	PEG-b-poly(L-glutamic acid)	Various solid tumors	Phase I	Nanocarrier, Co.
NK012	SN-38	PEG-b-poly(L-glutamic acid)	Triple negative breast cancer	Phase II	Nippon Kayaku, Co.
NC-6004	Cisplatin	PEG-b-poly(L-glutamic acid)	Pancreatic cancer	Phase III	Nanocarrier, Co.
BIND-014	Docetaxel	PEG-b-PLGA	Various cancers	Phase II	BIND Bioscience
SP1049C	Doxorubicin	Pluronic L61 and Pluronic F127	Various cancers	Phase II	Supratek Pharma Inc.
Genexol-PM	Paclitaxel	mPEG-b-PDLLA	Various cancers	Phase IV	Samyang Corporation

temperature, radiation) stimulants have been suggested for triggered release of micelles at the target site (Fig. 4).

3.2. Temperature responsive micelles

Temperature sensitive polymers display LCST behavior. Temperature has been exploited as an external trigger for the assembly of micelles (Rijcken et al., 2007; Zhang et al., 2005), the triggered release of the micellar content (Deng et al., 2015; Liu and Tong, 2005) and to increase the cellular uptake of micelles (Akimoto et al., 2009, 2010).

PolyNIPAM has been intensively investigated for the formation of self-assembling micelles. For instance, when NIPAM is polymerized with a hydrophilic block like PEG to form NIPAM-b-PEG, micelles can be formed by simply heating the polymer solution above the CP (Topp et al., 1997). Below the CP, the NIPAM block is hydrophilic making the polymer water soluble while this block becomes hydrophobic above the CP resulting in the formation of micelles. NIPAM-b-PEG has been synthesized via atom transfer radical polymerization (ATRP), generating polymers with a narrow molecular weight distribution. As reported by Zhang et al., the temperature at which NIPAM-b-PEG micelles with low and narrowly distributed molecular weight of PNIPAM block (PEG_{110}-b-$PNIPAM_{44}$) are formed increases from 33.7 to 38.4 °C when the copolymer concentration decreases from 2 to 0.2 mg/mL. Unlike PEG-b-PNIPAM or PEG-g-PNIPAM, the diameter of PEG_{110}-b-$PNIPAM_{44}$ micelles also increases with decreasing polymer concentrations. The authors hypothesize that this behavior can be due to the relatively slow micellization of PEG_{110}-b-$PNIPAM_{44}$ (Zhang et al., 2005). As stated above, the stability of self-assembling micelles can be improved by cross-linking of the core to prevent demicellization upon dilution or during incubation at temperatures below the CP of the polymer. As demonstrated by Zeng et al., the size of core cross-linked pNIPAM-b-p(ethylene oxide) micelles remains stable up to 2 weeks at low concentrations while no micelles were detected after 2 weeks during incubation with the reducing agent β-mercaptoethanol which degraded the cross-links (Zeng and Pitt, 2005).

A disadvantage of NIPAM based micelles is that they are not biodegradable. Therefore biodegradable core cross-linked PEG-b-poly(*N*-(2-hydroxypropyl) methacrylamide-lactate) (PEG-b-p(HPMAm-Lac_n)) micelles have been investigated. Micelles were formed by heating the copolymer aqueous solution above the CP followed by photo cross-linking of the micelle core. In these micelles, the lactate chains can be hydrolyzed at physiological conditions resulting in an increase of the CP that leads to the disintegration of the micelles. Rijcken et al. showed that these core cross-linked micelles present a significantly improved circulation kinetics compared to non-crosslinked micelles, with 58% of the injected dose present in the circulation after 4 h compared to only 6% of non-crosslinked micelles. This resulted in a 6 times higher tumor accumulation of the core cross-linked micelles compared to non-crosslinked micelles (Rijcken et al., 2007). Despite the longer circulation times, the authors found that the loaded drug (PTX) was rapidly removed from the circulation probably due to an insufficient retention inside the micelles (Rijcken, 2007). In order to solve this issue, Talelli et al. covalently linked the drug (DOX) to the micelle core via a pH sensitive hydrazone linker. It was shown that DOX was quantitatively released at pH 5 at 37 °C within 24 h while only 5% was released at pH 7.4. As a consequence, these micelles showed a substantial antitumor effect in a mouse model (B16F10 melanoma carcinoma) compared to free DOX (Talelli et al., 2010b). Another advantage of these micelles is that targeting ligands can be coupled to the terminal ends of the PEG chains. The coupling of an anti-EGFR nanobody to the micelles demonstrated an improvement in the cell association to EGFR expressing cancer cells (A431) (Talelli et al., 2011), and led to an improved *in vivo* therapeutic efficacy (Talelli et al., 2013).

In contrast to NIPAM-b-PEG micelles, when the temperature sensitive block is coupled to a hydrophobic block instead, the polymers assemble into micelles below the CP while the content of the micelles can be released at temperatures above the CP. Following this approach, Liu et al. reported the formation of temperature responsive micelles with poly(NIPAM-co-*N*,*N*-dimethylacrylamide)-b-poly(D,L-lactide-co-glycolide) (P(NIPAAm-co-DMAAm)-b-poly(PLGA)) copolymers (Liu and Tong, 2005). NIPAM was copolymerized with the hydrophilic monomer DMAAm to tailor the CP to 39 °C. Micelles prepared with this copolymer were loaded with DOX and had an average size around 100 nm. The authors also demonstrated that copolymers synthesized with larger PLGA blocks resulted in a decrease of the CMC and a higher drug loading, presumably due to the enhanced interaction between the PLGA block and DOX. In the release studies with these micelle formulations, an initial burst release was observed during incubation at 37 °C in PBS followed by a period without DOX release. At temperatures below the CP, the micelles present a stable core-shell structure in which DOX diffusion is hindered. The initial burst release was ascribed to the presence of DOX on the micellar surface or due to DOX located between the surface and the core. After exposing the micelles to a temperature above their CP (39.5 °C), more than 80% DOX was released within 8 h. As explained by Liu et al., the collapse of the outer shell might induce the deformation of the core-shell structure thus exposing the encapsulated DOX and triggering drug release (Liu and Tong, 2005).

The incorporation of magnetic nanoparticles into thermoresponsive polymeric micelles opens up the possibility to trigger the release by the application of an AMF (Kakwere et al., 2015; Wang et al., 2014; Sirivisoot and Harrison, 2015; Gobbo et al., 2015). Deng et al. recently developed magnetothermally responsive drug loaded micelles composed of the biodegradable star-block copolymer poly(ε-caprolactone)-block-poly(2-(2-methoxyethoxy)ethyl methacrylate-co-oligo(ethylene glycol)methacrylate) (PCL-b-P(MEO_2MA-co-OEGMA)). DOX as well as manganese and zinc doped ferrite magnetic nanoparticles (MZF, 8 nm) were encapsulated into these micelles (DOX-MZF-micelles, Fig. 5A). MZF

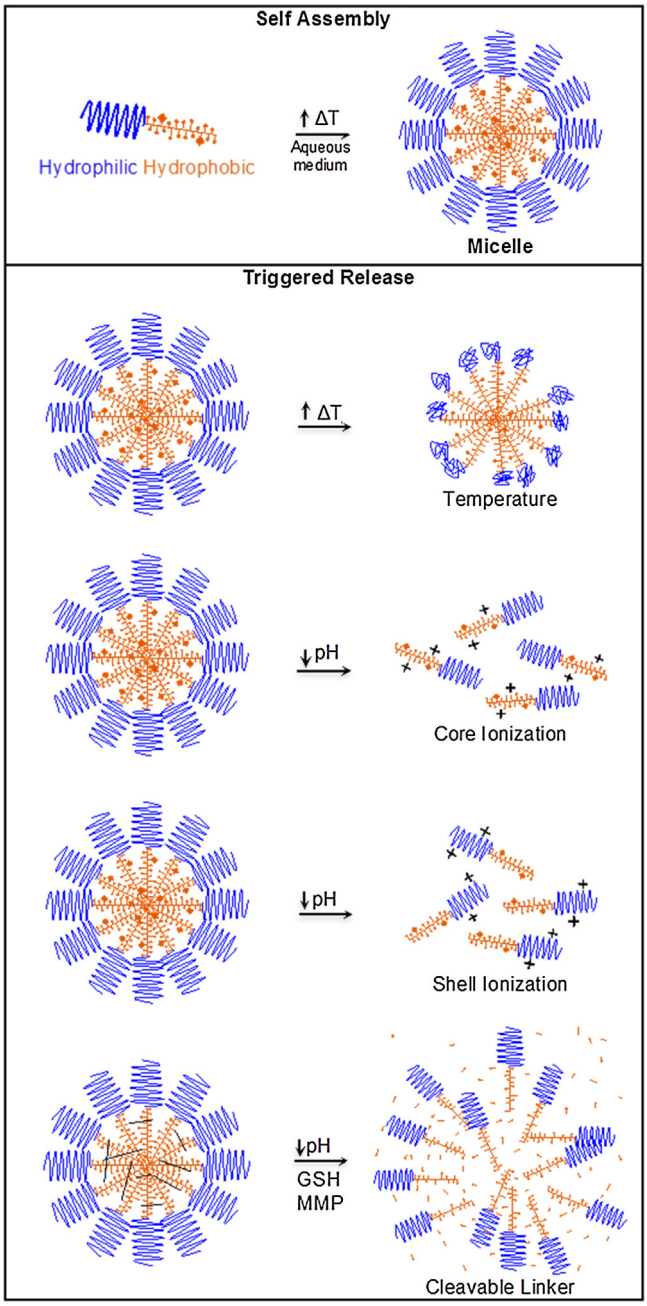

Fig. 4. Different categories of stimuli-responsive micelles. Micelles can be formed by self-assembly of temperature sensitive polymers dissolved in aqueous solution upon increasing the temperature. Triggered release of micelles can be induced by stimuli like temperature, pH and levels of gluthation (GSH) or matrix metalloproteinase (MMP).

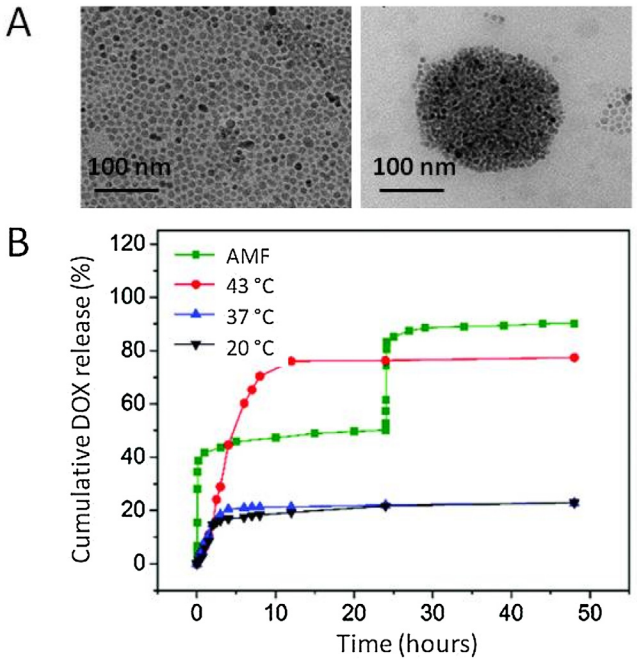

Fig. 5. (a) TEM image of MZF nanoparticles (left) and DOX-MF-micelles (right). (b) *In vitro* DOX release from DOX-MZF-micelles incubated at 20 °C, 37 °C, 43 °C or after AMF exposure (5 min per 24 h) (Deng et al., 2015). Adapted with permission of the Royal Society of Chemistry.

can be used as contrast agents in magnetic resonance imaging, and because they have a high specific absorption rate (SAR, which is the power a magnetic material dissipates upon exposure to AMF) too, self-heating is generated after exposure to AMF. The CP of PCL-b-P(MEO_2MA-co-OEGMA) was tuned to 43 °C by optimizing the ratio between MEO_2MA and OEGMA. At 37 °C the hydrophilic shell stabilized the micelle and only 20% of the DOX was released within 48 h (Fig. 5B). Importantly a higher release rate was observed when the micelles were heated above the CP, where the deformation of the micelles led to a release of 70% within 10 h. Remarkably, a quick exposure of 5 min to AMF produced a release of 35% of the DOX, after which the release rate declined. When AMF was applied for another 5 min 24 h later the release increased to 80%. As the authors conclude, AMF increases the temperature rapidly and efficiently, leading to a faster phase transition and a more pronounced DOX release. Consequently, the IC_{50} of DOX-MZF-micelles was 16 times lower after exposure to AMF (5 min per 24 h) compared to incubation at 37 °C, and 5 times lower compared to exposure to 43 °C (5 min per 24 h) (Deng et al., 2015).

Micelles composed of block-copolymers with a hydrophobic block and a temperature sensitive block are not only used to induce a temperature triggered release but can also present an improved cellular uptake. In the work by Akimoto et al., fluorescently labeled p(NIPAM-*co*-DMAAm)-b-poly(D,L-lactide) (p(NIPAM-co-DMAAm)-b-p(PLA)) micelles with a CP of 39 °C and a diameter of approximately 20 nm at 37 °C were prepared. Interestingly, the conformational change from hydrophilic to hydrophobic that occurs when these micelles passed their CP, promoted the interaction between the hydrophobic chains resulting in aggregation of the micelles. As a result, the size of the micelles increased to 600 nm when incubated above the CP. In the same manner, the hydrophobic interaction between micelles and cells increased leading to a 16-fold greater uptake when the micelles were incubated at 42 °C for 6 h as compared to 37 °C (Akimoto et al., 2009). As shown by the authors, p(NIPAM-co-DMAAm)-b-p(PLA) micelles localized in the Golgi apparatus and the endoplasmic reticulum after incubation with cells above the CP, suggesting the possibility of caveolae-mediated endocytosis (Akimoto et al., 2010).

3.3. pH sensitive micelles

pH sensitive micelles have a great potential in drug delivery due to the different pH values that exist in parts of the body (Felber et al., 2012). The pH of blood and most tissues is 7.4 while the pH in tumors can be between 5.7 and 7.1 due to an increased glycolysis which stimulates the production of lactic acid (Ojugo et al., 1999; Stubbs et al., 2000; Tannock and Rotin, 1989). An acidic pH (5–6) is also found in endosomes and lysosomes inside cells (Lafourcade

et al., 2008; Mindell, 2012). An example of a polymer that is frequently used in the development of pH sensitive micelles is poly (L-histidine) (Lee et al., 2003, 2005). The imidazole group of histidine (pKa of approximately 6) is protonated at acidic pH giving the polymer a positive charge. Zhang et al. reported the preparation of PEG-b-poly(L-histidine)-poly(lactic-co-glycolic acid) micelles with a size of 125 nm at pH 7.4. When incubated at pH 6, the size of the micelles increased till almost 500 nm due to the swelling and collapse of the micelle structure after protonation of the histidine units. Therefore less than 20% of the encapsulated andrographolide was released at pH 7.4 after 72 h while 70% was released at pH 5 during the same period (Zhang et al., 2015a).

Several micelles composed of ionizable pH sensitive polymers have also been developed to overcome multidrug resistance of cancer cells, which often hampers the success of chemotherapy. The quick efflux of DOX from cancer cells by overactivation of ATP binding transporters such as P-glycoprotein (P-gp) illustrates this critical issue (Gottesman et al., 2002). Suppression of ATP production by mitochondria can inhibit the drug efflux via P-gp. With this aim and since vitamin E derivates are known to suppress ATP production in mitochondria, micelles have been prepared from PEG-b-poly(2-(diisopropylamino)ethyl methacrylate) (PEG-b-PDPA) and a vitamin E derivate (D-α-tocopheryl polyethylene glycol 1000 succinate, TPGS). Spherical micelles were observed by Yu et al. at neutral pH while dissociation of the micelles took place at pH 6 due to the protonation of the PDPA block. In drug release assays, it was observed that 70% of the loaded DOX was released at lysosomal pH (5.5) within 8 h, which was 2 fold higher than the release at pH 7.4. In a control experiment, a 2 fold higher DOX concentration was observed in MCF-7 breast cancer cells after incubation of free DOX compared to PDPA/TPGS or PDPA. On the contrary, PDPA/TPGS showed a 4 fold higher DOX concentration in DOX-resistant MCF/ADR cells overexpressing P-gp compared to free DOX. When MCF/ADR cells were treated with PDPA, the IC_{50} of DOX showed a 5.3 fold decrease as compared to free DOX, which could be due to an increased uptake of DOX by PDPA micelles. In the case of PDPA/TPGS, the IC_{50} of DOX experienced a 23 fold decrease as compared to free DOX, which suggests that TPGS inhibits the drug efflux by P-gp. In a subsequent *in vivo* assay in a nude mouse model bearing an orthotopic MCF-7/ADR tumor, PDPA/TPGS showed the slowest tumor growth at an equivalent DOX dose (Yu et al., 2015).

In another study on the use of pH sensitive release, Xu et al. developed pH sensitive micelles consisting of P(PEGMA-b-(DEMA-co-APMA)) encapsulating MitoTPP (cationic porphyrin for mitochondrial targeting (Xu et al., 2015)) for the application of photodynamic therapy (PDT). The hydrophobic block of the polymer contains adenine, which was cross-linked with a uracil containing cross-linker under neutral pH through adenine/uracil nucleobase pairing (Fan et al., 2012). The micelles swelled in a medium of acidic pH due to the protonation of the tertiary amines and the disruption of the adenine/uracil nucleobase pairs. In these conditions, the micelles released 60% of the encapsulated MitoTPP within 30 h at pH 5.2 while only 7% was released at pH 7.4 during the same incubation time due to the charge repulsion between the positively charged MitoTPP and the positively charged polymer. Additionally, FA was conjugated to the micelles to trigger folate receptor mediated endocytosis, and these FA-decorated micelles showed a 2 times higher cell uptake compared to non-targeted formulation. Following the release of MitoTPP under acidic conditions and its accumulation in the mitochondria, singlet oxygen was generated under light irradiation inducing mitochondrial damage and subsequent cell apoptosis (Xu et al., 2014).

pH sensitive blocks are not only used as the core forming block of micelles but can also be used for the formation of the shell. Gao et al. showed this concept with poly(2-ethyl-2-oxazoline)-poly(D,L-lactide) (PEOz-PLA) micelles that were conjugated with cyclicRGDyk to facilitate integrin mediated endocytosis since this targeting ligand can bind to integrin $\alpha_v\beta_3$ expressing cells (Gao et al., 2015). A burst release of the loaded drug (PTX) was observed at pH 7.4 after which the remaining loaded drug was released in 1 day. In contrast, at pH 5 approximately 90% of the encapsulated PTX was released after 8 h. The authors suggest that the pH sensitive behavior might be due to the protonation of the PEOz block (pKa near neutral pH)(Wang and Hsiue, 2003) in an acidic environment resulting in electrostatic repulsion between the polymer chains that might induce loosening of the micellar structure. By using *in vivo* real time near-infrared (NIR) fluorescent imaging, a higher tumor accumulation of the cyclicRGDyk was observed as compared to non-targeted micelles, resulting in a higher antitumor efficacy. Furthermore, both cyclicRGDyk conjugated micelles and non-targeted micelles had better antitumor efficacy than Taxol®.

Polymeric micelles with pH cleavable chemical bonds are also used for triggered drug release. Acid labile bonds can be cleaved in a mild acidic environment while they remain stable at a pH of 7.4. Acetals (Yang et al., 2015b), hydrazones (Krüger et al., 2014) and benzoic imines (Gao et al., 2011) are examples of acid labile linkers used for pH-triggered drug delivery. Liu et al. synthesized PEG-b-poly(2,4,6-trimethoxybenzylidene-1,1,1-tris(hydroxymethyl) ethane methacrylate) polymers in which hydrolysable acetal groups were incorporated. DOX could be efficiently loaded in the formed micelles via hydrophobic and Π-Π interactions with the polymer chain. The hydrolysis of the acetal linker is pH dependent and therefore the micelles were stable at physiological conditions while a fast hydrolysis of the linker ocurred at pH 5, resulting in a 2 fold increase in DOX release. Moreover, cRGDfK was conjugated to the micelles (cRGD-PETM) to induce cellular uptake by ligand/receptor mediated endocytosis. cRGD-PETM micelles showed indeed an increased accumulation and retention of DOX in tumor tissues and presented a significantly better therapeutic effect compared to non-targeted micelles (Lin et al., 2015).

3.4. Redox sensitive micelles

Glutathion (GSH) is a reducing agent which is present in high concentrations (1–10 mM) in the cytosol and subcellular compartments. On the contrary, the concentration of GSH in body fluids like plasma and in extracellular matrices is much lower (2–20 μM) since it is readily oxidized to glutathione disulfide when GSH acts as a cofactor for antioxidant enzymes or by interaction with free radicals (Deshmukh et al., 2009). Further, the GSH concentration in the cytosol of cancer cells is more than a 4 fold higher compared to healthy cells due to genetic alteration in cancer cells (Kuppusamy et al., 2002; Wu et al., 2004). The difference in GSH concentration intracellular and extracellular can be used as a trigger to induce content release from a variety of drug delivery systems (Meng et al., 2009; Bruelisauer et al., 2014; Yang et al., 2016; Zou et al., 2016a, 2016b; Zhong et al., 2015).

Li et al. conjugated hyaluronic acid (HA) to deoxycholic acid via a cystamine reducible linker to form HA-SS-DOCA micelles that were loaded with PTX. Only 14% of the PTX was released from HA-SS-DOCA within 24 h in the presence of 10 μM GSH (concentration in plasma) while 55% was released within 4 h in the presence of 20 mM GSH (concentration in tumor cells), due to the destabilization of the hydrophobic core by the reducing agent GSH (Li et al., 2012). A significant increase in cellular uptake of HA-SS-DOCA was observed in CD44 (hyaluronic binding receptor) overexpressing MDA-MB-231 (human breast cancer) cells compared to micelles without HA, showing the specific binding and internalization via CD44 receptor mediated endocytosis. Furthermore, PTX-HA-SS-DOCA showed a significantly better delay in tumor growth with a 2

fold smaller tumor volume at day 20 compared to mice that received an equal dose of PTX as the non-sensitive PTX-HA-DOCA micelles and the Taxol® formulation (Lee et al., 2015).

Targeted redox sensitive micelles are not only developed for the treatment of breast cancer but also for several other cancer types. Guo et al. developed redox responsive micelles based on PEG-pLys-pPhe and conjugated with dehydroascorbic acid which recognizes GLUT-1 (glucose transporter overexpressed on hepatocarcinoma cells). An increased cellular uptake of DOX was observed by targeting the redox sensitive micelles, resulting in an enhanced tumor efficacy toward hepatocellular carcinoma tumors (Guo et al., 2015).

Besides GSH also high levels of reactive oxygen species (ROS) are present in tumor cells due to oncogene stimulation, malfunction of mitochondria and chronic inflammation in tumor tissue. The concentration of ROS is approximately 100 μM in tumor cells which is about 100 times higher than in normal cells (Pelicano et al., 2004). In an attempt to combine both stimuli, dual redox responsive micelles with a ROS sensitive diethyl sulfate (Des) component and a GSH sensitive disulfide containing cystamine (Cys) component (mPEG-bP(Des-Cys)) were designed for the targeted delivery of camptothecin (CPT) (Fig. 6A). After endocytosis by cancer cells, the high ROS levels will induce oxidation of the Des and subsequent swelling of the micelles while the increased level of GSH would cleave the cystamine leading to micelle dissociation, resulting in release of the content (Fig. 6B). CPT-loaded micelles were administered in HCT116 tumor bearing mouse and accumulated in the tumor and liver after 24 h. These micelles showed a significantly better antitumor effect compared to free administered CPT; the tumor volume increased 4.5 fold after administration of free CPT after 27 days while only an increase in tumor volume of 3.4% was observed for the CPT loaded micelles (Fig. 6C) (Chiang et al., 2015).

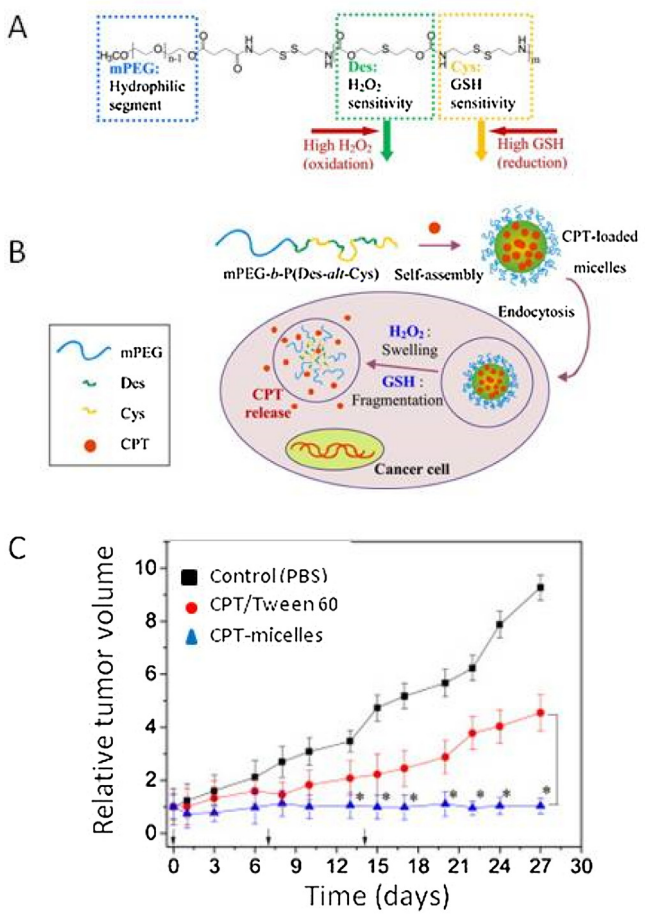

Fig. 6. (A) Chemical structure of mPEG-b-P(Des-Cys). (B) Dual redox-responsive micelles and CPT release triggered by ROS and GSH. As the dual redox-responsive micelles enter into cancer cells, which exhibit high levels of ROS and GSH, the structures of micelles are deformed, according to ROS-caused swollen effect and GSH-caused copolymer fragmentation. The encapsulated CPT could be released from micelles, leading to selectively location-controlled drug release and high tumor cytotoxicity. (C) *In vivo* tumor growth of HCT116 tumor-bearing mice after administration of PBS, free CPT + Tween 60 (to solubilize CPT) and CPT-micelles (Chiang et al., 2015). Reprinted with permission from Elsevier.

Combinational chemotherapy shows great promise for the treatment of cancer since with this approach several hallmarks of cancer can be targeted simultaneously. Co-delivery of drugs can result in an additive or even synergistic effect leading to a significant improvement in tumor regression, especially since the treatment with a single drug is often ineffective and can lead to drug resistance. To overcome these challenges, Gaspar et al. developed redox sensitive micelles composed of PEOz as the hydrophilic shield and PLA as the hydrophobic core, which was loaded with DOX. The polymer was grafted with redox sensitive PEI-SS (PPP-SS micelles) which condensates with super coiled mcDNA. DOX was released from these micelles in a sustained manner since it was incorporated in the PLA core while mcDNA showed a triggered release in disulfide reducing conditions with a 7.2 fold higher release within 4 h compared to non bioreducible micelles. PPP-SS-mcDNA was found in lysosomes of HeLa (cervix cancer) cells after 6 h incubation while the micelles were observed in the cytoplasm after 24 h, indicating efficient lysosomal escape which is of great importance for the delivery of mcDNA since entrapment in the lysosomes could lead to premature degradation (Yuan et al., 2015; Mintzer and Simanek, 2008). A 3D multicellular tumor spheroid model (MCTS) of HeLa and B16F10 melanoma cells showed successful GFP transgene expression mediated by PPP-SS-mcDNA with a significant portion of the cells transfected. This GFP expression was higher in comparison to formulations of mcDNA with non bioreducible micelles and Lipofectamine 2000. Intramural injection of PPP-SS-mcDNA led to a substantial expression of luciferase after 48 h and the luminescence signal was still observed after 8 days. Mice bearing subcutaneous B16F10 tumors were injected intratumoral with PPP-SS-mcDNA-DOX which resulted in a tumor volume reduction compared to administration of free DOX (Gaspar et al., 2015).

Redox sensitive micelles have also been used for the delivery of different classes of anticancer drugs like histone deacetylase (HDAC) inhibitors. Thailandespin (TDP-A) is a class I HDAC inhibitor with antiproliferative properties and is developed for the treatment of breast cancer. It has been shown that TDP-A inhibits cell proliferation, induces cell apoptosis, promotes the production of ROS and induces cell arrest in the G2/M phase (Wang et al., 2011). The hydrophobic TDP-A was encapsulated into disulfide cross-linked micelles composed of PEG-poly(lysine-cysteine)-cholic acid (PEG-Cys-L-CA). These micelles were completely disrupted within 30 min when incubated with 10 mM GSH inducing the release of TDP-A. Furthermore, a gradual accumulation of the micelles was observed in the tumor of a breast cancer xenograft mouse model and showed a significantly better tumor growth inhibition in this model compared to the FDA approved HDAC inhibitor FK228 (Xiao et al., 2015). However, no comparison with the intravenous administration of free TDP-A was shown in this study.

Wu et al. developed reduction and pH dual sensitive micelles based on lipoic acid and *cis*-1,2-cyclohexanedicarboxylic acid. These core cross-linked micelles showed excellent colloidal stability after extensive dilution and in the presence of high salt concentration, and released only 20% of the encapsulated drug (DOX) within 24 h at pH 7.4. On the contrary, these micelles fully

dissociated within 8.5 h in the presence of 10 mM DTT and also released DOX nearly quantitatively in the presence of 10 mM GSH at pH 5 within 24 h. Confocal microscopy studies revealed that these micelles delivered DOX efficiently within 12 h into the nuclei of HeLa cells (Wu et al., 2013).

3.5. MMP responsive micelles

Matrix metalloproteinase 2 (MMP-2) is excessively expressed in cancer cells (Nakopoulou et al., 2003) and can therefore be used as a trigger for drug release from micelles in tumors. The advantage of a release triggered by enzymes is the selectivity for the substrate. As a representative example, Chen et al. developed multifunctional micelles composed of PEG-b-poly(L-lysine) as the polymer backbone to which DOX was conjugated by means of an MMP-2 sensitive peptide linker. In addition, biotin was attached as targeting ligand to enhance uptake by cancer cells via ligand/receptor mediated endocytosis and intracellular release. A triggered DOX release occurred when the micelles were incubated in the presence of MMP-2 proteases due to the cleavage of the peptide linkage. Biotin-PEG-b-PLL-peptide-DOX micelles released 46% DOX within 6 h in the presence of MMP-2 while a negligible release was observed in buffer or when both MMP-2 and a MMP inhibitor were present in the incubation medium, demonstrating the selectivity of the peptide linker for cleavage by MMP-2. The cellular uptake of the micelles took place within 3 h when incubated with SCG-7 (squamous cell carcinoma) cells which have a high MMP expression while DOX entered the nuclei of the cells after 6 h incubation inducing cell apoptosis, again indicating that the peptide linker was cleaved by MMP-2 (Chen et al., 2015a).

3.6. Light responsive micelles

Light can be used as a safe and useful energy source for responsive drug delivery (Palumbo, 2007; Agostinis et al., 2011). Nomoto et al. developed three layer micelles (TPM), (poly-lysine)-dendrimeric photosensitizer-PEG, for light induced gene delivery (DPc-TPM, Fig. 7A). A dendrimeric photosensitizer (DPc, Fig. 7B) was incorporated into the intermediate layer of the micelle via carboxyl groups to induce a photochemical disruption of the endosomal/lysosomal membrane to facilitate cytoplasmic delivery of pDNA, which was condensed in the PLys core of the micelle (Fig. 7C). DPc and pDNA were incorporated into different layers of the micelle to prevent inactivation of the pDNA by DPs induced production of ROS after irradiation. The DPc became hydrophobic in the acidic environment of the endosome/lysosome due to protonation of the carboxylic groups, leading to translocation of the DPc to the endosomal/lysosomal membrane. Subsequently, photoirradiation induced disruption of the endosomal/lysosomal membrane and facilitated the translocation of pDNA to the cytoplasm. A 4.4 fold higher reporter gene transfer was observed in an *in vivo* subcutaneous HeLa tumor model after photo-irradiation compared to a non-irradiated tumor following systemic administration (Nomoto et al., 2014). Reprinted with permission from Macmillan Publishers Ltd.

3.7. Nanogels

Hydrogels are soft materials consisting of hydrophilic three-dimensional polymer networks that have a high water content (Vermonden et al., 2012). Nanogels are nanosized hydrogels (typically < 200 nm) that recently gained interest in the field of drug delivery including as delivery vehicles of tumor therapeutics. Both for hydrogels and nanogels, different methods to obtain 3D cross-linked polymer networks are available. A variety of different crosslinking chemistries have been employed and some of them fulfill the requirements for biomedical applications, including degradable crosslinks and triggered drug release (Zhang et al., 2015b; Jiang et al., 2014).

Attractive features of nanogels for drug delivery include their high loading capacity, good stability, possibilities to functionalize their surface with bioactive moieties, and depending on the used polymers pH and/or temperature responsiveness can be introduced easily to facilitate triggered release (Chacko et al., 2012; Raemdonck et al., 2009a). The properties of hydrogels and nanogels including swelling behavior, network structure, permeability for entrapped molecules and mechanical strength can change in response to a variety of stimuli. Besides for drug delivery, nanogels also find applications in imaging, diagnostics and biosensing (Oishi and Nagasaki, 2010; Le Goff et al., 2015; Nagahama et al., 2015).

Different anticancer drugs have been loaded into nanogels. The most frequently used drug in nanogel formulation is DOX, which can be explained by its relatively hydrophilic character enabling easy formulation in water-rich carriers combined with its effectiveness as anticancer agent for multiple types of tumors. But also other conventional anticancer drugs have been formulated in nanogels and a rather complete overview of the different drugs used has been published recently by Mishra et al. (Wani et al., 2014) Therefore, this section on nanogels is not aimed to give a comprehensive overview, but mostly to illustrate some promising strategies.

An elegant example of smart nanogels for DOX delivery was recently reported by Yang et al. (Yang et al., 2015a) They developed systems with both pH sensitive and redox sensitive properties. These nanogels are hydrophilic in the bloodstream at pH 7.4, but a decrease in the ionization degree of carboxyl groups at slightly lower pH values in tumor tissues leads to a reduced swelling of the gels enabling good cellular uptake. Due to the relatively high GSH concentrations intracellularly, the redox properties of the system resulted in disintegration of the nanogels and consequently rapid drug release was obtained within the target cells (Fig. 8).

Also the hydrophobic drug PTX has been loaded in pH sensitive nanoparticles that were prepared via a miniemulsion polymerization technique combining high-energy emulsification and free radical polymerization of an acrylate monomer, 5-methyl-2-(2,4,6-trimethoxyphenyl)-[1,3]-5-dioxanylmethyl methacrylate. Upon reaching tumor tissues, the acid-labile protecting group 2,4,6-trimethoxybenzaldehyde was cleaved thus exposing the hydroxyl groups of the nanoparticles, which transformed from hydrophobic to swollen hydrophilic gel particles (Griset et al., 2009). When exposed to mildly acidic pH, these particles swelled up to 350 times their original volume and consequently release their cargo. *In vivo* studies showed a reduced tumor growth in mice treated with these expansile particles compared to a treatment with free PTX at the same dose. In a follow-up study, these particles were coated with a lipid monolayer facilitating the possibility to attach a targeting ligand such as FA to enhance the potency of the formulation (Stolzoff et al., 2015).

As discussed above, nanogels can be used as delivery vehicles for classical low molecular weight chemotherapeutic drugs, but because of their hydrophilic nature, they are also very suitable to deliver proteins or protein fragments that can be used for *e.g.* tumor vaccination (Kageyama et al., 2008; Ferreira et al., 2013; Li et al., 2015). The group of Akiyoshi is a pioneer in this field with the development of cholesteryl pullulan (CHP) nanogels comprising a truncated HER2 protein as vaccine eliciting an immune response to HER2 expressing tumors (Kageyama et al., 2008). Moreover, also nucleic acids can be easily loaded based on electrostatic interactions between negatively charged nucleic acids and positively charged polymers (Raemdonck et al., 2009b; De Backer et al., 2015; Tamura et al., 2009; Luten et al., 2008). Raemdonck

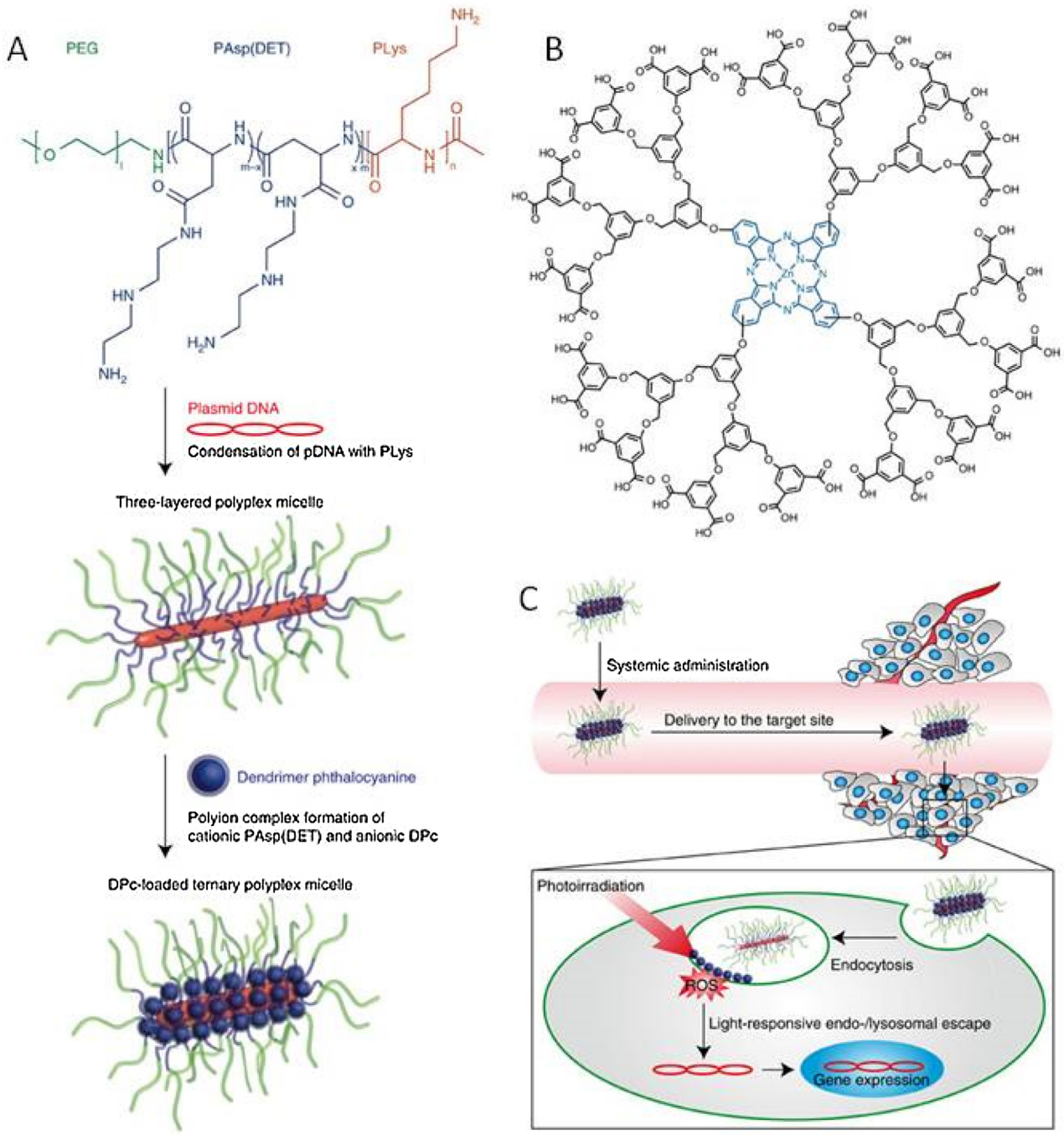

Fig. 7. (A) The three-layered polyplex micelle (DPc-TPM) composed of a pLys core condensed with plasmid DNA, a dendrimeric photosensitizer (DPc) at the intermediate layer and a PEG shell. (B) Chemical structure of DPc. (C) DPc-TPM circulates in the bloodstream and accumulates in the tumor via endocytosis. DPc is released from the DPc-TPM in the endosomes/lysosomes via protonation of the carboxylic group and subsequently interacts with the membrane of the endosomes/lysosomes through hydrophobic interactions. DPc generates ROS after photoirradiation, inducing destabilization of the membrane, facilitating endosomal escape for the pDNA (Nomoto et al., 2014). Reprinted with permission from Macmillan Publishers Ltd.

et al. developed nanogels based on cationic crosslinked dextran able to complex siRNA and showed that by coating these nanogels with a shell of pulmonary surfactants combined with a targeting ligand (Fig. 9), efficient gene silencing could be obtained in lung cancer cells (De Backer et al., 2015).

4. Mesoporous silica nanoparticles

Silica-based materials have been proposed for a variety of biomedical applications (Vallet-Regi and Ruiz-Hernandez, 2011; Alcaide et al., 2012; Kinnari et al., 2009; Serrano et al., 2008). Mesoporous silica can be synthesized as ordered pore arrays with hexagonal or cubic symmetries. SBA15- or MCM41-type structures were discovered in the early nineties of last century following a template-assisted process with the use of surfactants as structure-directing agents (Kresge et al., 1992; Lopez-Noriega et al., 2009; Ruiz-Hernández et al., 2010). The silica precursors undergo hydrolysis, condensation and self-assembly with ionic (*eg.* cetyl trimethylammonium bromide, CTAB) or non-ionic (*eg.* the Pluronic family) surfactants to create two- or three-dimensional networks

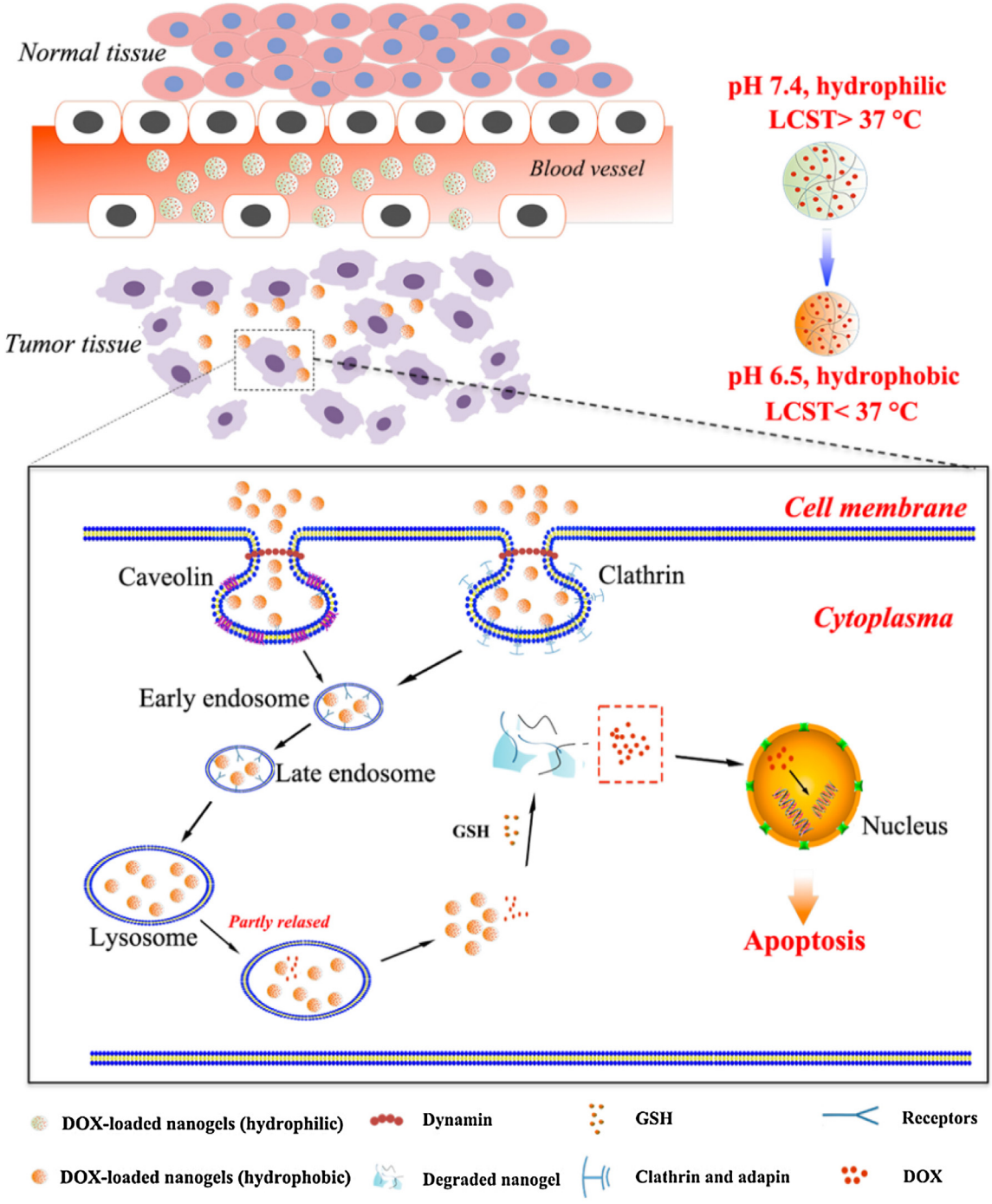

Fig. 8. Schematic illustration of the hydrophlicity/hydrophobicity reversible and redox-sensitive P(OEGMAs-ss-AA) nanogels for drug delivery in cancer (Yang et al., 2015a). Reprinted with permission from American Chemical Society.

in which a long-range ordered porosity is generated after surfactant removal (Arcos et al., 2008). The resulting materials are characterized by outstanding textural properties such as large surface areas (~1000 $m^2 \cdot g^{-1}$) and pore volumes (~1 $cm^3 \cdot g^{-1}$), and a tunable pore size in the mesoscale (2–50 nm). As a result, a relatively high loading of both hydrophilic and hydrophobic drugs can be achieved in this silica network.

Grün et al. suggested the synthesis and characterization of ordered mesoporous silica in the form of microspheres (Grun et al., 1997). By introducing surfactants in the sol-gel synthesis of monodisperse silica particles, it is possible to obtain size-controlled mesoporous spheres, which are suitable for application in high-resolution chromatographic separations. Furthermore, with modifications in the hydrolysis rate of the silica precursors, due to either tetraalkoxysilanes or alcohol co-solvents with different length of the alkyl chains, the size of mesoporous silica spheres can also be controlled in the submicrometric scale (*ca.* 20–700 nm). When larger amounts of alcohol with longer alkyl chains are employed in the synthesis, mesoporous particle growth is preferred to nucleation, thus producing larger silica spheres (Yamada et al., 2016). Even though a broad range of submicrometric particles may be safe for biomedical uses, the selection of the optimal size for each application will improve the pharmacokinetics, biodistribution and delivery of drugs at the target site.

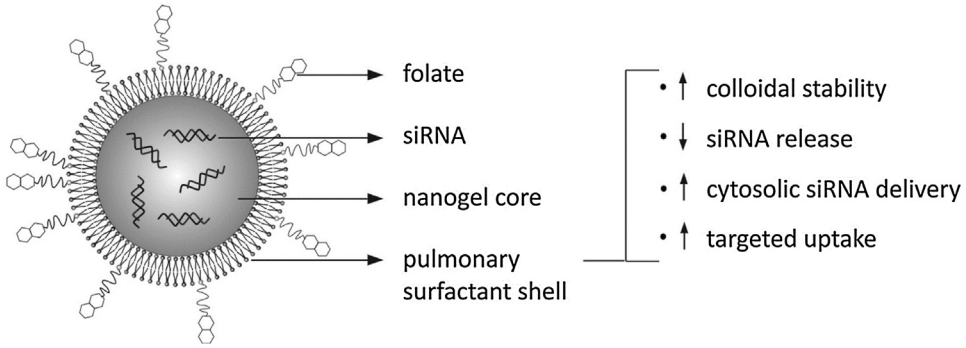

Fig. 9. Nanogel design for siRNA delivery to lung cancer cells (De Backer et al., 2015). Reprinted with permission from Elsevier.

Meng et al. suggested the integration of two synthetic strategies to obtain mesoporous silica nanoparticles (MSN) with 50–100 nm which are resistant to aggregation in protein-containing media with high ionic strength. Firstly, they combined two structure-directing agents, CTAB and Pluronic F127, to form the micellar template. By adding Pluronic F127, they not only affected the micelle packing behavior of CTAB resulting in smaller nanoparticles, but also improved the dispersion of MSN. Secondly, the adsorption of a polyethyleneimine (PEI)-PEG copolymer on the surface of the particles helped stabilizing the dispersion due to steric hindrance and electrostatic repulsion, and therefore reducing the hydrodynamic size of the formed nanospheres. This system showed a significantly higher EPR accumulation in a human squamous carcinoma in mice after intravenous administration when compared to both bigger particles (100–130 nm) and PEGylated MSN of the same size (Meng et al., 2016). In those cases where an efficient renal clearance is desired ("target or get out" strategy) (Benezra et al., 2016; Choi et al., 2007; Ashley et al., 2016), a fast hydrolysis and slow condensation rates can be applied together with a PEG-silane capping agent to stop particle growth. Ma et al. recently optimized the synthesis conditions to achieve a precise size control of MSN in the 6–15 nm range (Ashley et al., 2016). It should be highlighted that, in the context of drug delivery applications, the optimal size selection for MSN should not only take into account the threshold for an efficient internalization in cells (30–60 nm) (Jiang et al., 2008), but also the cargo capacity, which has been calculated to be proportional to the cube of the particle radius. (Ashley et al., 2016)

Since the first report a small molecule, ibuprofen, was loaded and released from MCM41-type silica two decades ago (Vallet-Regi et al., 2001), reports on drug delivery systems based on mesoporous silica have grown exponentially. Several different therapeutics including antibiotics, anti-inflammatories, proteins and genes have been controllably released from various silica matrices. One of the main advantages of mesoporous silica for its use as drug delivery agent is the enormous versatility for chemical modification. Silica-based carriers have been surface-functionalized with multiple organic groups in order to tune the retention of the loaded drug. By tailoring, for instance, the hydrophobicity of the surface, the release of a hydrophobic model drug such as ipriflavone can be adjusted to different time scales (Lopez-Noriega et al., 2016). Besides, and similarly to polymeric drug carriers, the degradation rate of MSN can be designed and tailored to provide the desired release kinetics. As reported by Ashley et al., the degree at which the silica core is condensed can be precisely controlled by amine-containing silanes. The addition of diverse amounts of the functionalizing group into the sol leads to a range of dissolution rates, from hours to weeks, that can be adapted for applications requiring burst or sustained release profiles (Ashley et al., 2016). Furthermore, the intrinsic resistance of silica structures to harsh body environments ensures protection from premature release of the loaded cytotoxic drugs. This feature is of particular importance to cancer treatment, where chemotherapy is often characterized by severe side-effects that prevent dose escalation to the required level. Overall, MSN constitutes an adjustable platform able to satisfy the needs of the changing clinical settings.

Concerning the biological testing of MSN, numerous studies have shown relatively good *in vitro* and *in vivo* biocompatibility. In order to assess the safety of intravenous administration, the interaction of MSN with mammalian red blood cells was compared with cytotoxic amorphous silica. The hemolytic properties of MSN and amorphous silica were remarkably different in the concentration range 20–100 μg/mL, in which MSN did not display toxicity toward red blood cells (Slowing et al., 2009; Lin and Haynes, 2009).

In vivo biodistribution and excretion in small animals have been evaluated, and despite accumulation in liver and spleen, as well as minor uptake by lungs, kidneys and heart, no significant acute inflammation and tissue toxicity were found after 1 month with MSN and PEGylated MSN (Yarmolenko et al., 2010; Fu et al., 2016). In spite of these encouraging results, there are indications that the cytotoxicity of MSN is highly dependent on the administration route (Fu et al., 2016; Hudson et al., 2008), and more insights into the toxicological profile regarding long-term effects or reproductive risks are clearly needed. Before MSN can be safely translated into clinical applications, a few challenges remain including effective clearance and mainly biodegradation. Although the well-defined porosity of MSN and their large surface area enhance degradation in physiological media, the greater stability compared to other drug delivery systems poses a safety issue. As explained by Chen et al. (Chen et al., 2013), the long-term effects of non-degraded MSNs *in vivo* have not been thoroughly studied. In order to combine efforts by different groups exploring potential clinical applications, standardization of the models and techniques for the *in vivo* assessment of MSN would be desired. Nonetheless, the approval by FDA for the first-in-human trials of ultrasmall multimodal silica nanoparticles (known as C-dots)(Phillips et al., 2014) for imaging of advanced melanoma shows promise for further developments.

Regarding cellular uptake of MSN, it has been documented that submicrometric particles can be efficiently internalized by non-phagocytic cells via pinocytosis and mainly clathrin-mediated endocytosis. Although the receptors for MSN in cells have not yet been identified, Slowing et al. showed that non-functionalized negatively charged MSN were endocytosed via clathrin-coated vesicles, as the uptake was inhibited by sucrose, commonly used in cell trafficking assays. In the case of MSN that were functionalized with amine-containing groups, 3-aminopropyl and guanidinopropyl, with only slightly negative zeta potential (approximately −4 mV), the uptake was inhibited by genistein, which is indicative of caveolae-mediated endocytosis (Slowing et al., 2006). Moreover,

the cell studies carried out with MSN have shown that the uptake process depends on dose, time and cell type. Chung et al. demonstrated cell-dependent uptake of positively charged MSN with different degree of surface modification in human mesenchymal stem cells and 3T3-L1 mouse embryonic cell line with differentiation activity to adipocyte (Chung et al., 2007). Interestingly, this dependence has also been found in the excretion of MSN by different cell lines. Yanes et al. evaluated the exocytosis of 3-(trihydroxysilyl)propyl methylphosphonate-functionalized MSN in lung cancer A549, breast cancer MDA-MB231 and MCF-7, melanoma PANC-1, and human embryonic stem H9 cell lines after 24 h incubation. The exocytosis efficiency varied from 87% in A549 to 4% in H9, and correlated well with the release of a lysosomal enzyme, β-hexosaminidase, from the different cell lines into the culture (Yanes et al., 2016). This observation suggests that the phosphonate-functionalized MSN undergo lysosomal exocytosis after fusion of the lysosomal membrane with the plasma membrane. As a result of this mechanism, MSN can be expelled from the cells thus limiting the window period for drug delivery. In this scenario, stimuli-responsive MSN can provide spatiotemporal control of the release in order to maximize intracellular drug delivery.

4.1. Responsive MSN

Stimuli-responsive MSN that can be activated by different external physical stimuli have been developed (Zhao et al., 2010). As described recently by Liu et al., nanoparticles with a mesoporous silica shell and gold nanorods in the core can be used to combine photothermal therapy with the release of chemotherapeutics. By using 1-tetradecanol (TD, melting point of 39 °C) as gatekeeper at the surface of the mesopores, the authors observed a rapid increase of DOX release upon stimulation with NIR radiation due to the diffusion of DOX through the hydrophobic and melted TD domains (Liu et al., 2015). Using a similar concept, Baeza et al. describe a thermoresponsive hybrid system in which magnetic nanoparticles were encapsulated in polymer-coated MSN (Baeza et al., 2012). In this system, MSN were surface functionalized with a thermoresponsive block copolymer of polyethyleneimine-pNIPAM that undergoes a conformational change at temperatures above its LCST, allowing the release of the loaded drugs to the outer media. Two different cargos (fluorescein and soybean trypsin inhibitor protein) were released from these particles upon heating of the magnetic nanoparticles under the application of an AMF (24 $kA \cdot m^{-1}$ and 100 kHz) (Martin-Saavedra et al., 2010; Baeza et al., 2012; Ruiz-Hernandez et al., 2011, 2007, 2008; Arcos et al., 2012). Different thermosensitive coatings have been suggested for magnetic MSN with the same goal. Kim et al. used hydroxypropyl cellulose (HPC) anchored to the surface of MSN to prevent the release of GEM from AMF-responsive nanoparticles in which drug release is triggered upon heating to 45 °C. As a result of the combination of hyperthermia and GEM release, *in vitro* tests with pancreatic cancer cells showed a reduction of cell viability of up to 82% (Kim et al., 2014b).

In order to design a nanosystem that can be triggered by HIFU, Qian et al. synthesized hollow periodic mesoporous organosilicas (HPMOs) using 1,4-bis(triethoxysilyl)benzene as silica precursor and CTAB as structure directing agent. Bridged phenyl groups were uniformly distributed within the framework of HPMOs providing Π-Π stacking with the loaded drug, DOX. The sensitivity of this interaction to ultrasound enables a HIFU-triggered release of DOX. In addition, the unique hollow structure of HPMOs modified the acoustic environment thus improving the efficiency of HIFU-mediated ablation therapy (Qian et al., 2014).

Despite the suitability to remotely activate drug release by an external trigger such as AMF or HIFU, (Chen et al., 2015b) an autonomous drug delivery system that is able to respond to the environmental cues characteristic of specific tissues is considered of great value. The selectivity of this kind of systems would depend on the stimulus that is chosen as a trigger of drug release.

The carrier system reported by Lai et al. in 2003 was the first device to achieve a stimuli-responsive release of a drug from MSN (Lai et al., 2003). In their work, MCM41-type MSN was surface-modified with 2-(propyldisulfanyl) ethylamine groups, which subsequently reacted with mercaptoacetic acid-functionalized cadmium sulfide (CdS) nanocrystals via an amidation reaction. As a result, CdS nanocrystals were chemically immobilized at the pore outlets of the particles. These engineered MSN loaded with vancomycin or ATP exhibited less than 1% release of these molecules over a period of 12 h. Upon contact with reducing molecules, such as dithiothreitol and mercaptoethanol, the CdS nanoparticles were removed from the surface of MSN thus triggering drug release. The ATP-loaded MSN demonstrated stimuli-responsive release in astrocyte cells after addition of mercaptoethanol, in which the released ATP induces an ATP-receptor mediated increase in intracellular calcium concentration. Similar approaches relying on cell-produced reducing agents such as cysteine and GSH have been reported. Kim et al., after demonstrating that cyclodextrins were able to act as gatekeepers to control the release from the pores of MSN (Park et al., 2009a, 2009b), developed a GSH-responsive MSN in which cyclodextrins were covalently attached to the surface of the silica by disulfide bonds. This system was able to retain DOX in the extracellular environment but released the drug inside GSH-rich A549 cancer cells (Kim et al., 2016).

In the case of pH-sensitive MSN, the aim is to target more acidic tissues like those in tumor and inflammatory regions, as well as the acidified pH inside the endosome after cellular uptake of the nanoparticles. The functionalization of mesoporous silica with pH-responsive chemical linkers has been used to provide a linkage with additional nanoparticles acting as gatekeepers of the drug release (Chen et al., 2014a). In a different approach, Diez et al. developed a pH responsive nanodevice comprising of a Janus type particle (Jiang et al., 2010) with a gold face and a MSN face (Diez et al., 2014). Glucose oxidase and esterase, as model molecules immobilized on the gold part, reduced the pH locally after catalyzing the conversion of glucose and ethyl butyrate into gluconic acid and butyric acid, respectively (Aznar et al., 2013). The MSN surface was functionalized with pH sensitive β-cyclodextrin based supramolecular nanovalves which capped the MSN pores at physiological conditions while opening the pores in an acidic environment (Fig. 10A). The MSN were tightly capped in the absence of the enzymes' substrate and hardly released DOX in 6 h. Addition of D-glucose, ethyl butyrate or a mixture of both agents reduced the pH in the medium and induced a triggered release of DOX (Fig. 10B) (Diez et al., 2014).

In order to combine two stimuli and thereby improve the delivery of a chemotherapeutic drug (DOX) and siRNA (silencing the expression of VEGF), Han et al. developed electrostatically self-assembled multilayered nanocomplexes (MLNs) (Fig. 11A) (Han et al., 2015). The core of MLNs consisted of a cationic TAT peptide modified mesoporous silica nanoparticle (TAT-MSN) which was used for DOX loading and TAT mediated DOX targeting to the nucleus (Smith et al., 2010) after dissociation of the MLNs. The anionic inner layer, composed of poly(allylamine hydrochloride)-citraconic anhydride (PAH—Cit), becomes positively charged after hydrolysis of the side chains in the acidic environment (Liu et al., 2008) of the endosome/lysosome facilitating MLNs dissociation and endosomal/lysosomal escape. The cationic galactose (Gal)-modified trimethyl chitosan-cysteine conjugate (GTC) in the outer layer encapsulated siVEGF, which was released in the cytosol after lysosomal escape due to cleavage of the disulfide bonds. Gal

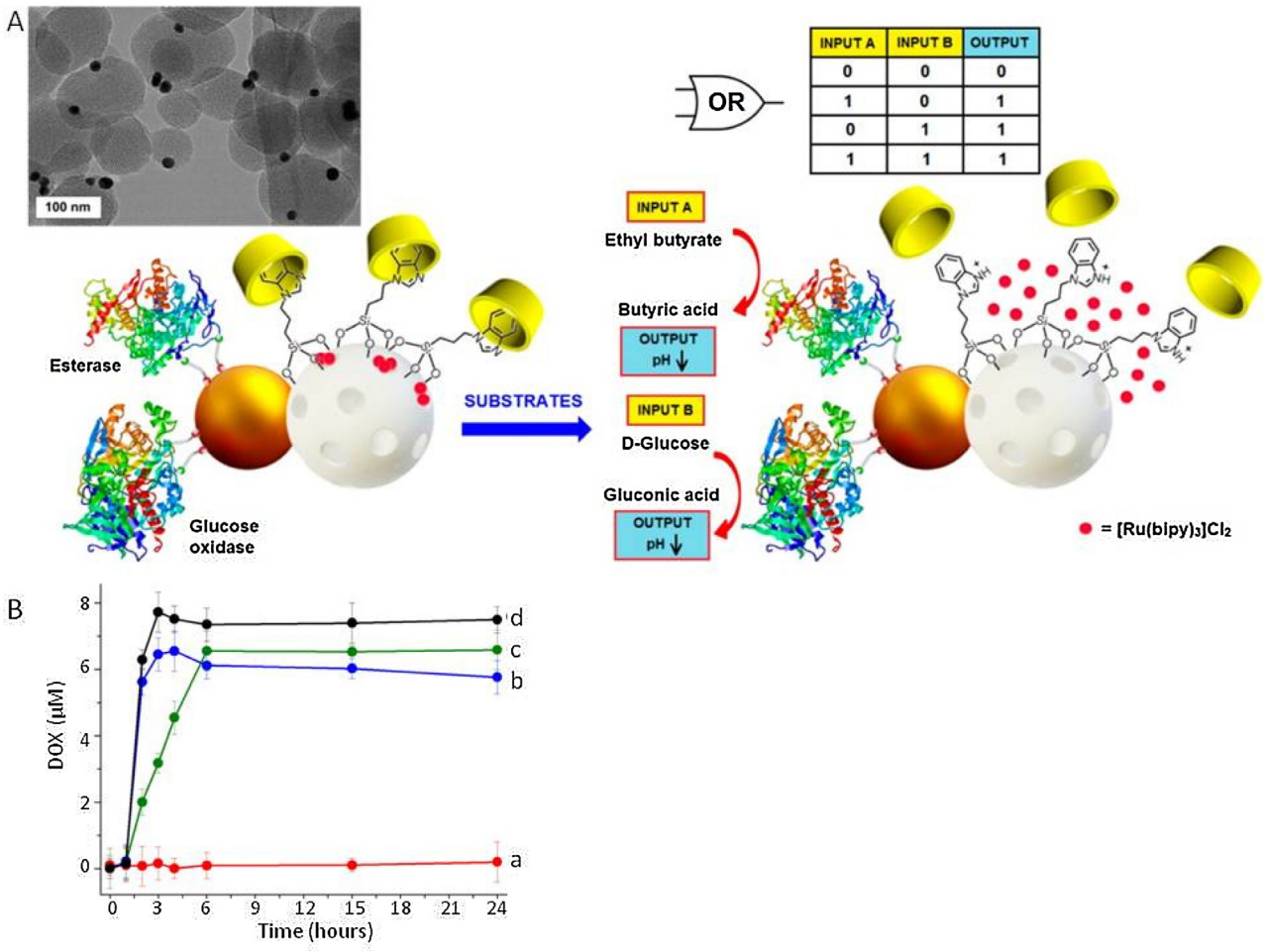

Fig. 10. (A) Schematic representation of Janus type particle in which the gold face is functionalized with enzymes to control the triggered drug release from MSN. TEM image (top) shows the presence of a gold face and a MSN face in the Janus-type nanoparticles. (B) DOX release of these particles in 20 mM Na_2SO_4, pH 7.5 (a) in the presence of ethyl butyrate (b), D-glucose (c) or a combination of both (d) (Diez et al., 2014). Adapted with permission from American Chemical Society.

induced active targeting to tumor cells via Gal receptor-mediated endocytosis (Han et al., 2013) (Fig. 11B). After the administration of MLNs to mice bearing a human hepato-carcinoma (QGY-7703) xenograft tumor, inhibition rates higher than 90% were found (Fig. 11C) (Han et al., 2015). Other stimuli-responsive MSN-based vectors have demonstrated a promising potential for gene-delivery (Weiss et al., 2016; Wu et al., 2016). Recently, Li et al. reported a dual intracellular responsive system by incorporating a short chain ammonium group with both a redox-sensitive disulfide bond and a pH-sensitive amide bond into MSN. This design demonstrated a high transfection efficiency of both plasmid DNA and siRNA in 293-T and HeLa cell lines (Li et al., 2016b).

5. Targeted therapies

5.1. Ultrasound

Ultrasound is an imaging modality which is cost effective, patient convenient and is used in the clinic for real time imaging. Furthermore, ultrasound can be used to purposefully destabilize drug delivery systems. Due to these advantageous properties and broad applicability it is possible to use ultrasound as a trigger for drug release and enhance its delivery to tumors.

Delivery of chemotherapeutic agents and therapeutic genes to the central nervous system through the blood brain barrier (BBB) remains a major challenge since uptake in the brain is essentially prevented by the tight junctions that are present between endothelial cells (Yao et al., 2015; Wu et al., 2015). Microbubbles (MBs) in combination with ultrasound exposure induce acoustic cavitation which leads to a temporal destruction of the tight junctions and an increase of the vascular permeability (Chai et al., 2014). Lin et al. developed liposomes with a high entrapment efficiency of plasmid DNA (73%, lpDNA containing luciferase reporter gene) for gene delivery to the brain using ultrasound mediated MBs to induce BBB's opening. A 5 fold increase in luciferase expression in the brain of mice was observed when lpDNA was administered in combination with MBs and focused ultrasound compared to lpDNA administration alone. The luciferase expression level was dose dependent and maximal 2 days post administration (Yang et al., 2015b). Presumably, exposure of the MBs to focused ultrasound induced bubble expansion and as a consequence stable cavitation inducing disruption of the liposomal bilayer and cell membranes, and thus enhancing the delivery of the reporter gene into the brain cells (Delalande et al., 2013).

Since MBs disrupt lipid cell membranes, they can also be used for intracellular dug delivery (Derieppe et al., 2015). However, some of the disadvantages of MBs are their relatively low stability and their micrometer size (Rapoport et al., 2011; Sheeran et al., 2015). Liquid perfluorocarbon (PFC) droplets are good alternatives for MBs since they undergo a phase transition upon ultrasound exposure and the resulting gas bubbles increase cellular drug uptake and can be used for vascular imaging (Rapoport, 2012). Lee

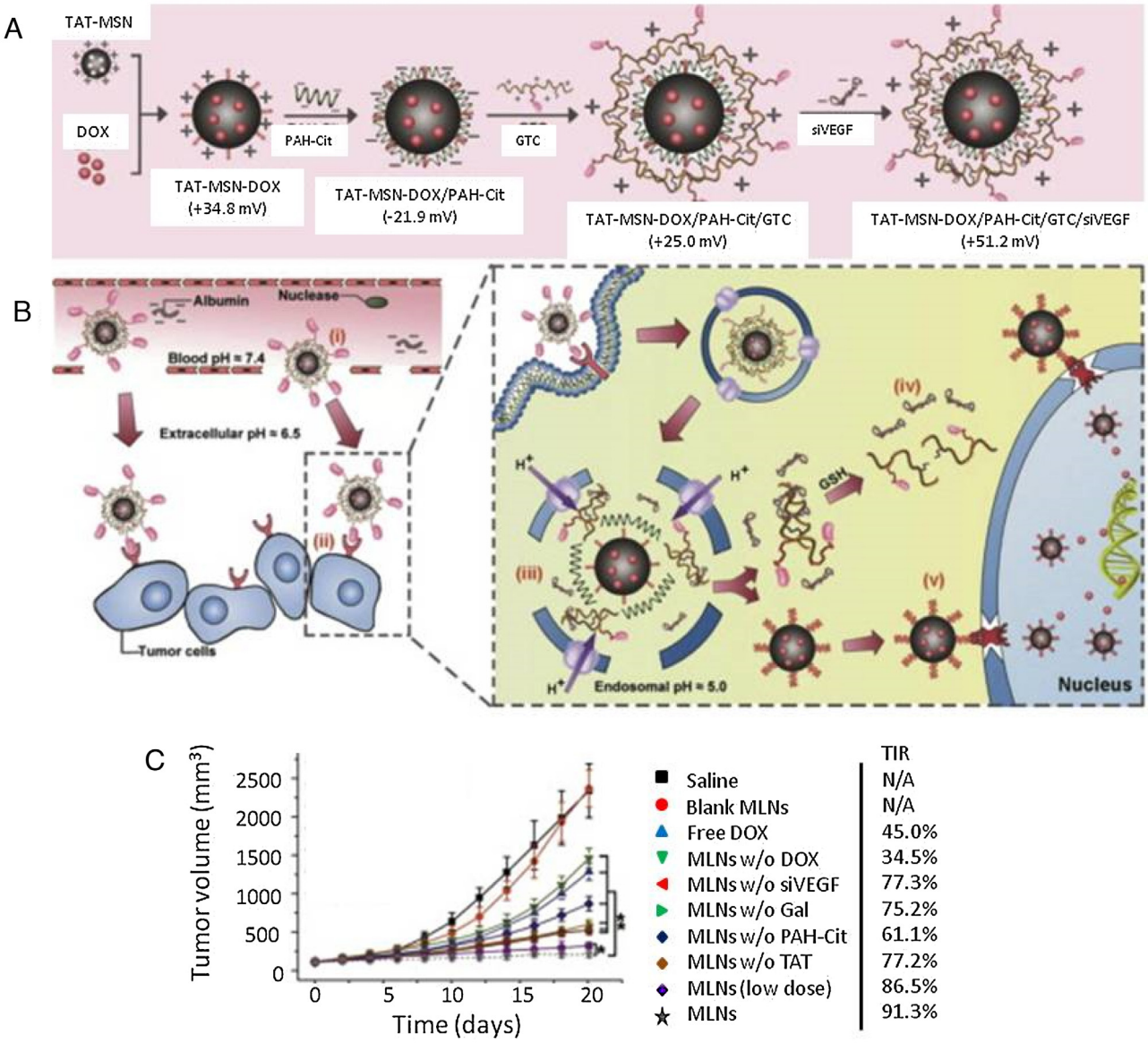

Fig. 11. (a) Schematic structure of MLNs which were constructed via layer-by-layer self-assembly driven by the electrostatic coverage of poly(allylamine hydrochloride)-citraconic anhydride (PAH-Cit) and galactose-modified trimethyl chitosan-cysteine conjugate (GTC) onto the TAT-MSN. (b) Schematic presentation of MLNs mediated delivery of DOX and siVEGF. MLNs maintained structural integrity in the blood and tumor environment, actively entered cancer cells via galactose receptor-mediated endocytosis and subsequently underwent structural disassembly and endosomal escape in response to intracellular acidity. siVEGF was released into the cytoplasm upon GSH-triggered disulfide cleavage and DOX was delivered into the nuclei via TAT-mediated targeting. (c) Tumor growth of mice bearing QYC-7703 xenograft tumors after treatment of MLNs or MLNs lacking one of the functionalities (Han et al., 2015). Reprinted with permission from Elsevier.

et al. prepared nanoparticles with a cross-linked human serum albumin (HSA)-PEG shell to generate a stable structure which encapsulated perfluoropentane nanodroplets (PFP), PTX and iron oxide nanoparticles (mpHSA-PFP). As PFP vaporized under ultrasound exposure, the nanodroplets were converted to MBs with a 56% decrease in nanodroplet population after a 15 s exposure. The iron oxide particles improved the conversion efficiency from droplets to MBs and made the mpHSA-PFP magnetically responsive. The vaporization from nanodroplets into MBs was monitored with passive acoustic mapping. Ninety percent of the loaded PTX was released after 3 min ultrasound exposure resulting in a 30% decrease in MCF-7 cells viability compared to a control formulation of mpHSA-PFP. This shows that an improved drug delivery can be achieved by using cavitation as a method of enhanced drug delivery (Lee et al., 2015). Ultrasound does not only improve drug delivery via an enhanced cellular delivery but it can also be used to mechanically trigger drug release (Lee et al., 2008b; Husseini et al., 2000). Recently Liang et al. developed ultrasound responsive diblock micelles composed of poly(propylene glycol) and PEG with mechano-labile (Cu(II))-terpyridine bonds between the blocks (PPG-Cu-PEG) (Liang et al., 2014). The Cu bonds were cleaved upon ultrasound exposure resulting in a decrease of the micelle size and release of the encapsulated pyrene (25% in 5 min, 75% in 30 min). Micelles with covalent crosslinks or strong metal-ligand bonds (Ru)(Meier et al., 2003) did not release their content, indicating that the release was induced by destroying the weak metal ligand bonds with Cu (Liang et al., 2014; Meier et al., 2003). Additionally, ultrasound can be used for non-invasive heating of tissue (via HIFU) as described before. Frequently, temperature triggered drug release is induced due to temperature sensitivity of the carrier system (Needham et al., 2000; Lindner et al., 2004; Liu and Tong, 2005). Chen et al. encapsulated ammonium bicarbonate

(ABC) into liposomes which simultaneously was used for active loading of DOX. At mild hyperthermia ABC decomposes leading to the formation of CO_2 bubbles (Chung et al., 2012; Lin et al., 2014) which induce defects in the lipid bilayer of the liposomes leading to drug release. ABC liposomes indeed released DOX rapidly at 42 °C and showed a longer circulation time in a mouse model compared to lysolipid containing liposomes. As a result, ABC liposomes had a higher antitumor efficacy compared to the lysolipid liposomes in combination with mild hyperthermia treatment (Chen et al., 2014c).

As shown by de Smet et al., temperature sensitive liposomes in combination with magnetic resonance (MR)-HIFU improved the drug distribution and liposome accumulation in rats (de Smet et al., 2013). It is of great importance that drug delivery and antitumor efficacy can also be monitored in larger animals since mild hyperthermia in humans should be applied in a region larger than 1 cm, which cannot be achieved in a small animal model (Staruch et al., 2015). Therefore, more recently, Staruch et al. evaluated the antitumor efficacy of TSL in combination with MR-HIFU in a Vx2 rabbit model. A more than 20 fold increase in DOX concentration was observed in a heated tumor compared to unheated ones (Staruch et al., 2012). Furthermore, the administration of TSL alone induced a relatively fast tumor progression and the maximum tumor diameter of 6 cm was reached within 24 days for all treated rabbits. Importantly, four out of 6 rabbits treated with MR-HIFU had a tumor diameter below 6 cm after 60 days (Staruch et al., 2015).

Often TSL are injected intravenously and accumulate not only in the tumor but also in healthy organs like liver and spleen. Furthermore, TSL can induce systemic side effects after intravenous administration due to leakiness in the bloodstream. With the aim to reduce off-target effects and optimize localized drug delivery in a multistep manner, Lopez-Noriega et al. encapsulated TSL in biodegradable and biocompatible chitosan/β-glycerophosphate hydrogels which gelate at body temperature (Ruel-Gariepy et al., 2000; Zhou et al., 2009). An initial burst release of DOX (10% of the loading) was observed from these hydrogels, which induced apoptosis in human A2780 ovarian carcinoma cells in culture. Subsequently, a second dose of DOX was released by triggering the TSL by mild hyperthermia. An enhanced cell death and decrease in dsDNA levels were observed two days after the mild hyperthermia pulse compared to non-pulsed hydrogels. These hydrogels show great promise in overcoming the pharmacokinetic restrictions associated with the intravenous administration of TSL and increasing the local control of drug delivery to the tumor (López-Noriega et al., 2014; Lopez-Noriega et al., 2014).

5.2. Tumor normalization

Tumor growth induces changes in the tissue microenvironment and large gaps between endothelial cells exist, inducing excessive leakiness in the tumor vasculature and allowing nanoparticle extravasation via the EPR effect (Maeda, 2010; Maeda et al., 2000b). Simultaneously, the tumor environment reduces the rate of nanoparticles delivered to cancer cells since the blood flow to the tumor is reduced (Jain, 1988) and a high interstitial fluid pressure (IFP) (Milosevic et al., 2004; Provenzano et al., 2012) exists due to the leaky vasculature (Egeblad et al., 2010). Furthermore, a dense ECM (Egeblad et al., 2010) is formed and tumor vessels collapse as a result of solid stress, hindering the penetration of nanoparticles deep within the tumor (Jain et al., 2014). The abnormal tumor microenvironment can therefore be used as a target to enhance drug delivery by vascular normalization.

Khawah et al. schematically suggest how vasculature normalization could enhance drug delivery to tumor tissue by restoring the vessel pores and the basement membrane (Fig. 12) (Khawar et al., 2015). A phase II clinical trial with cediranib (anti-angiogenic agent) revealed that patients with recurrent glioblastoma had a 6–9 month longer survival time likely because cediranib treatment increased blood perfusion compared to patients without increased blood perfusion (Jain, 2013; Batchelor et al., 2010). Despite these promising results, cediranib in combination with lomustine did not show a significant difference in progression free survival in patients with recurrent glioblastoma compared to lomustine treatment alone in a phase III clinical trial. This demonstrates the need for preselecting patients which are likely to respond to the treatment (Batchelor et al., 2013). Bevacizumab is a monoclonal

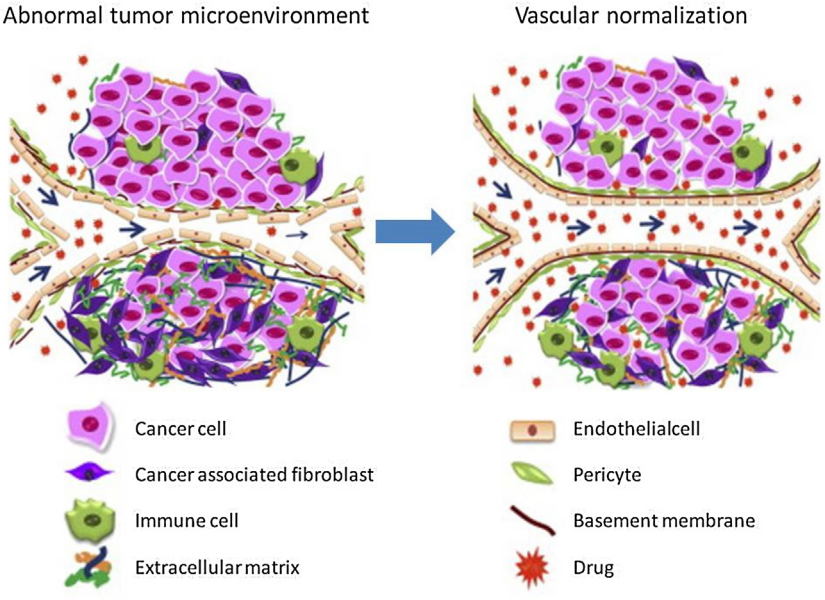

Fig. 12. The abnormal microenvironment in a tumor with *i.e.* leaky vasculature can be used as a target to enhance the drug delivery. After vascular normalization, the size of vessel pores and basement membrane is restored, which improves perfusion and may eventually improve drug penetration into tumor tissue (Khawar et al., 2015). Reprinted with permission from Elsevier.

antibody against vascular endothelial growth factor and is FDA approved as an anti-angiogenic drug. A significant decrease in vascular permeability of 30–70% was observed in tumor bearing rats 3 days after administration of bevacizumab. Concomitantly, the IFP in this model decreased with approximately 50% compared to the injection of saline. The delivery of melphalan (a chemotherapeutic agent) improved 2–6 fold after pre-treatment with bevacizumab compared to saline pre-treatment. Combination therapy of bevacizumab and melphalan increased the quadrupling time of the tumor volume with 37 to 113% depending on the tumor model (Turley et al., 2012).

Tailor et al. investigated whether not only small molecules but also larger drug carriers could benefit from tumor vascular normalization. Pazopanib, a small molecule inhibitor of VEGF decreased the mean vessel density and tumor IFP in a mouse model for non-small cell lung cancer. No difference in DOX concentration in the tumor was observed when Doxil was administered after pre-treatment with pazopanib and the control group. There was even a reduction in Doxil penetration in the tumor, presumably because the normalization of the vasculature decreased vessel permeability and causing that the liposomes were not able to accumulate in the tumor via the EPR effect (Tailor et al., 2010). To explore the size-dependent particle delivery after tumor vasculature normalization, Chauhan et al. evaluated the tumor accumulation of nanoparticles with varying sizes (12, 60 and 125 nm) after vasculature normalization by blocking the VEGF-receptor 2 with DC101 (anti-VEGF-receptor 2 antibody). A 3 fold enhancement in tumor deposition of 12 nm particles based on poly(imidazole)-coated quantum dots was observed compared to the control group while no enhancement was observed for the larger particles (60 and 125 nm). The delivery of these larger nanoparticles was even blocked in some of the tumors (Chauhan et al., 2012). In another study, Jiang et al. evaluated the tumor accumulation of particles based on quantum dots-PEG with 20 and 40 nm in a mouse model of breast cancer. Administration of DC101 for 3 days reduced the tumor vessel density at day 8 (Fig. 13A) and decreased vessel length and volume. An improved delivery and distribution of both the 20 and 40 nm particles was observed in the tumor, and the particles were detected further from the blood vessels compared to tumors with IgG treatment (control) instead of DC101 (Fig. 13B). Meanwhile, the larger particles had a higher diffusional hindrance and therefore the smaller particles were distributed more homogeneously throughout the tumor (Jiang et al., 2015).

PTX is a drug that is often encapsulated in drug delivery systems for the treatment of solid tumors (Singla et al., 2002), and inhibits angiogenesis by remodeling the vasculature (Myoung et al., 2001). In a recent work by Danhier et al., a more organized and less tortuous vasculature was observed 5 days after PTX-micelle (M-PTX), composed of a block of PEG and poly(trimethylene carbonate-co-ε-caprolactone) administration while the vasculature converted back to a less organized structure after 7 days (Fig. 14A). Administration of these micelles reduced the IFP 2 fold and increased the endothelial cell and pericyte population surrounding the blood vessels (Fig. 14B). M-PTX pretreatment improved the delivery of FITC-dextran (35 nm, 150 kDa) to the tumor and showed a 2 fold increase in tumor accumulation of albumin-evans blue (6 nm), [^{3}H]-M-PTX (24 nm) and iron oxides (30 nm) (Danhier et al., 2015).

5.3. Phototherapy

Phototherapy can be categorized in two subgroups namely photothermal therapy (PTT), in which an agent is used that efficiently absorbs NIR light thus generating heat and subsequently ablates the surrounding tumor, whereas photodynamic therapy (PDT) uses photosensitizers that transform oxygen to singlet

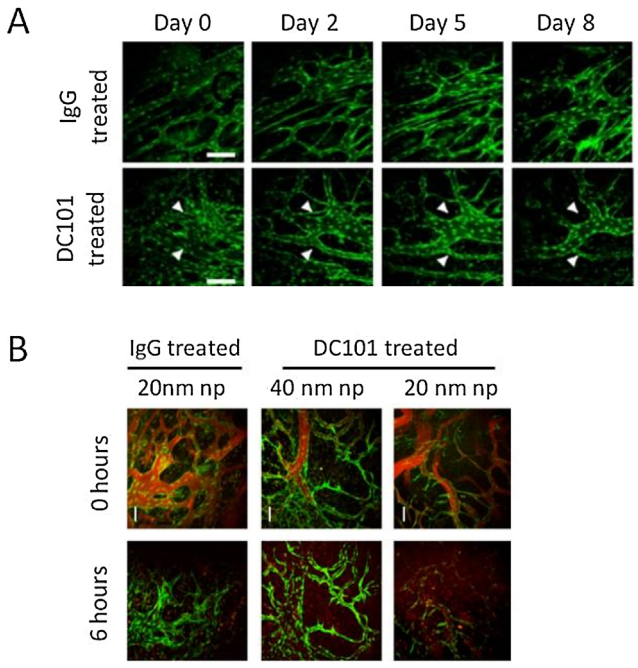

Fig. 13. (A) Vascular normalization of tumor xenograft model after treatment with DC101 or IgG as control. (B) Intratumoral delivery of 20 nm and 40 nm particles (red) after vascular normalization with DC101 or IgG (Jiang et al., 2015). Adapted with permission from American Chemical Society. (For interpretation of the references to colour in this figure legend, the reader is referred to the web version of this article.)

oxygen ($^1O_2$) which is a very reactive species that induces cell death because of its reaction with lipids, nucleic acids and other biomolecules present in cells.

Several nanoparticle formulations have been used for PTT (Liu et al., 2011; Wang et al., 2015; Zhou et al., 2015a). Although these nanoparticles showed enhanced antitumor activity, common disadvantages of these systems are that the particles are often non-biodegradable and are rapidly removed from the circulation due to capture by macrophages present in the liver and spleen (De Jong et al., 2008). Therefore, micelles composed of chitosan derivatives that contain self-doped polyaniline (PANI) were developed that form hydrogels (NMPA-CS) at pH 7 due to micelle aggregation resulting in the formation of a 3D-network (Hsiao et al., 2015). As demonstrated by Hsiao et al., the PANI in the hydrogel converted NIR light into heat and these hydrogels could be used for repeated thermo ablation since they are not washed out from the tumor. The photothermal effect was evaluated in Hep3 B human hepatocellular carcinoma cells and it was shown that cell death was dependent on the NIR exposure time, reaching cell death in the whole laser beam area after 5 min irradiation (Fig. 15A). Repeated PTT was achieved after administration of these hydrogels to mice bearing a Hep3 B tumor followed by exposure to a NIR laser. This could not be achieved with hollow gold nanospheres (HGNs) which probably leaked out rapidly from the tumor (Fig. 15B). A temperature above 50 °C was reached which induces protein denaturation and DNA damage (Roti Roti, 2008). Hep3 B tumors were irradiated every 4 days for a total of 4 treatments after administration of the hydrogels or HGNs. A decrease in tumor volume was observed for the hydrogel group during a period of 16 days whereas HGNs administration showed only a tumor regression in the first 4 days followed by regrowth of the tumor (Fig. 15C).

Chemotherapy and radiotherapy induce damage to the DNA but this can be repaired leading to regrowth of the tumor and multidrug resistance. On the contrary, PDT generates cytotoxic $^1O_2$

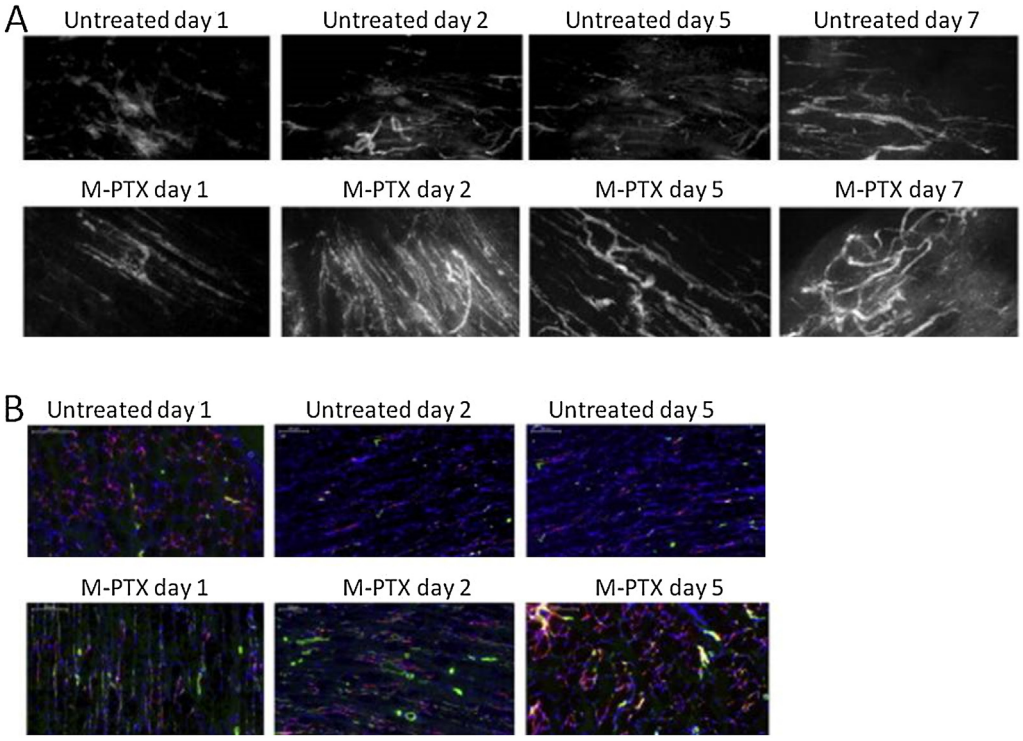

Fig. 14. (A) Vasculature normalization 1 to 7 days after administration of M-PTX (80 mg/kg) or without treatment. (B) Endothelial cells were stained with anti-CD31 (red) and pericyted with anti-α-SMA (green) after administration of M-PTX (80 mg/kg) or without treatment (Danhier et al., 2015). Reprinted with permission from Elsevier. (For interpretation of the references to colour in this figure legend, the reader is referred to the web version of this article.)

and it is expected that a combination of PDT, chemotherapy and radiotherapy can synergistically improve the therapeutic outcome. Fan et al. coated Gd-doped upconversing nanoparticles (Gd-UCNPs) with a mesoporous silica outer layer and encapsulated docetaxel (chemotherapeutic agent and radiosensitizer) in the cavity while hematoporphyrin (photo and radiosensitizer) was covalently grafted onto the outer silica layer (Fan et al., 2014). The Gd-UCNPs convert NIR light into UV light, which can activate photosensitizers (Park et al., 2012; Cui et al., 2012). Accumulation of these particles in the tumor was monitored via MR imaging (MRI) and upconversion luminescence. Upon NIR excitation and X-ray irradiation, a complete tumor regression was observed in a subcutaneous 4T1 tumor after *i.v.* administration of these particles, but the tumor regrew after 10 days. On the contrary, intratumoral injection of the particles did not result in a regrowth of the tumor indicating that the particles insufficiently accumulated in the tumor after *i.v.* injection (Fan et al., 2014).

Topete et al. combined PTT and PDT for better therapeutic efficiency. PLGA/chitosan nanoparticles were coated with branched gold nanoparticles for phototherapy. The nanoparticle shell was complexed with human serum albumin-indocyanine green (ICG, NIR fluorescent dye) for fluorescent imaging and PDT. The particles were loaded with DOX for combined chemotherapy, PTT, PDT and diagnostic imaging. Irradiation with a NIR laser enhanced the $^1O_2$ production and increased the temperature with 19 °C after 5 min irradiation, triggering the release of DOX since the reached temperature was higher than the T_g of PLGA. The viability of HeLa and MDA-MB-231 cells decreased to 20% after incubation with the nanoparticles and NIR light irradiation due to the combined chemotherapy (DOX), PTT (gold shell) and PDT (ICG) (Topete et al., 2014).

Chen et al. conjugated the photosensitizer Ce6, which could chelate Gd for MR imaging, with micelles based on poly(maleic anhydride-alt-1-octadecene)-PEG (Gong et al., 2014). Furthermore, the NIR dye IR825 was encapsulated in these micelles for fluorescent imaging and thermal ablation (Chai et al., 2014). After *i.v.* administration, the accumulation of the IR825/Ce6 micelles in the tumor was shown via triple model imaging using florescence imaging, MRI and photoacoustic imaging tomography (Fig. 16A). An increase in temperature in the tumor to 49 °C was achieved after 6 min laser irradiation (Fig. 16B). The growth of a 4T1 tumor was inhibited for the first 8 days following PTT treatment alone (808 nm for 6 min), after which a rapid regrowth was observed. PDT alone (660 nm for 1 h) inhibited tumor growth only partially while a combination of PTT and PDT significantly inhibited tumor growth compared to a single treatment regime (Fig. 16C) (Gong et al., 2014). In another study, IR825 absorbed to HSA (IR825-HSA) migrated rapidly to tumor associated sentinel lymph nodes (SLN), which often contain metastatic tumor cells, after intratumoral injection. The tumors were surgically removed and SLN were ablated by NIR exposure which improved the survival rate of Balb/c mice bearing a 4T1 tumor since ablation of SLN is expected to reduce metastasis (Fig. 16D) (Chen et al., 2014b).

It should be mentioned that the above described systems are rather complex and different components are needed for the different treatment modalities (*i.e.* PDT, PTT, chemotherapy and imaging). Therefore Li et al. developed a versatile multifunctional micellar system(Li et al., 2014b) able to encapsulate various chemotherapeutic drugs and metal ions for imaging (*e.g.* Gd for MRI (Sigward et al., 2015; Rigaux et al., 2014) and Cu for PET (Zhou et al., 2015b; Dale et al., 2015)). The micelles were composed of linear PEG-cysteine and dendritic oligomers of pyropheophorbide-a (Por, a porphyrin analogue) and cholic acid (CA). The micelles were cross-linked via disulfide bonds making them GSH as well as light sensitive. Cross-linking yielded stable particles in the circulation and showed good circulation kinetics, and therefore a higher tumor accumulation was observed compared to non-

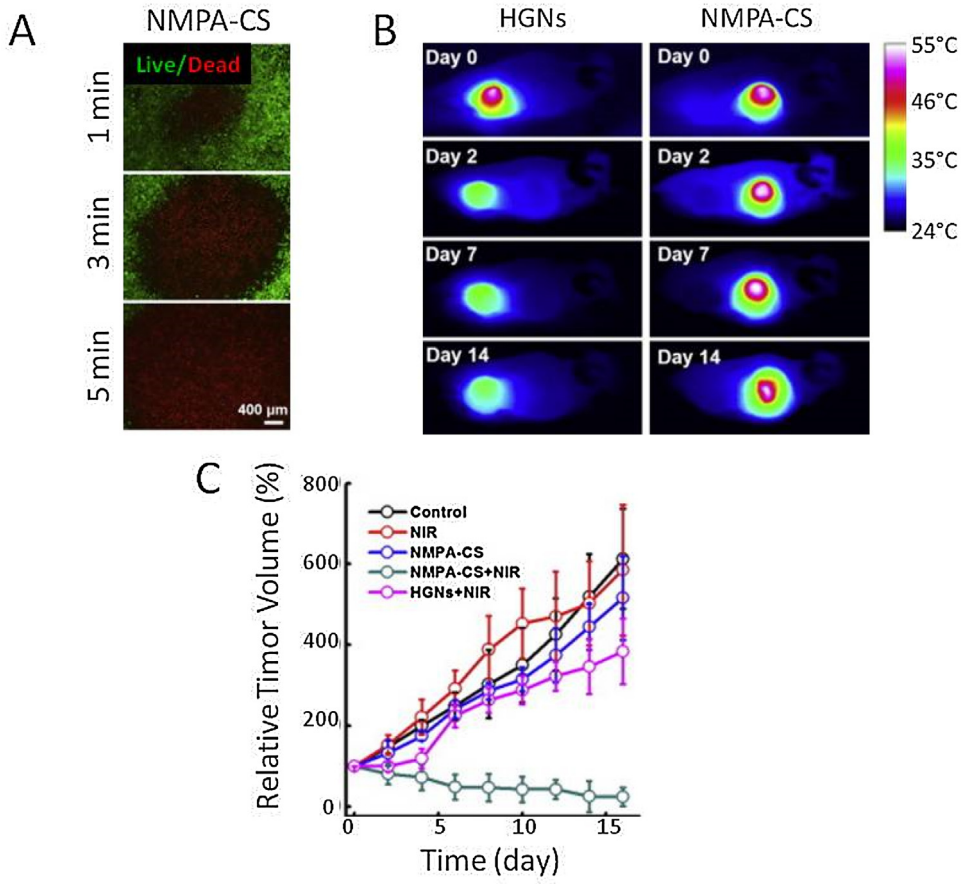

Fig. 15. (A) Photothermal killing of Hep3 B cells treated with NMPA-CS and exposed to a NIR laser (2 W/cm^2) for 1, 3 and 5 min. (B) Thermographic images of Hep3 B tumor-bearing mice that were intratumorally injected with a single dose of HGNs or NMPA-CS following exposure to a NIR laser (0.5 W/cm^2, 5 min) after 0, 2, 7 and 14 days. (C) Relative tumor volume of mice bearing Hep3 B tumors after treatment of HGNs and NMPA-CS in combination with or without exposure to a NIR laser (Hsiao et al., 2015). Reprinted with permission from Elsevier.

crosslinked micelles that dissociated in blood. The Por/CA core showed a high heat generation but low fluorescent signal due to quenching when the micelles were intact, but after dissociation the fluorescent signal increased and the heat generation was reduced. The micelles partly dissociated after cellular uptake likely due to the high intracellular concentration of GSH, allowing heating as well as fluorescence imaging. Furthermore, the Por/CA core can produce $^1O_2$ after dissociation and irradiation. As shown by Li et al., a complete tumor regression was observed in animals that received these micelles 12 days after irradiation and up to 32 days no tumor regrowth occurred. An important advantage of this system is that PDT and PTT are achieved using only one polymer and only 1 laser is needed for both therapies, while other systems need lasers with different wavelengths to combine both therapies (Gong et al., 2014).

6. Image guided chemotherapy

Image guided drug delivery has gained substantial interest in recent years and significant progress has been made in this field. Preclinical, image guided drug delivery is used to monitor the pharmacokinetics, distribution, target site accumulation and treatment efficacy of nanoparticles. Furthermore, imaging can be used to visualize and quantify drug release mainly for triggered nanosystems. In a clinical setting, imaging can be used for preselection of patients who will likely benefit from a treatment and could be used to predict the response and possible side effects (Ojha et al., 2015).

6.1. Tumor accumulation

A considerable number of nanosystems described in the literature are designed for passive accumulation in the tumor via the EPR effect (Kato et al., 2015; Chen et al., 2015d). Since the EPR effect is very heterogeneous and can vary even within a tumor (Bae and Park, 2011b), Theek et al. developed a method which predicts the extent of particle accumulation in the tumor. Contrast enhanced functional ultrasound (ceFU) imaging was used to assess the degree of tumor vascularization. Interestingly, a correlation was found between the number of particles that accumulated in the tumor and the extent of tumor vascularization (Theek et al., 2014). Since the EPR effect is very heterogeneous, not only passive targeting has received much attention for drug delivery, but also active targeting via coupling of targeting ligands to the surface of nanoparticles has been widely investigated (Cossu et al., 2015; Ahmed et al., 2013). To evaluate the effectiveness of active targeting over passive targeting, Kunjachan et al. functionalized RGD-conjugated polymeric nanoparticles (P-RGD, ~10 nm) and NGR-conjugated nanoparticles (P-NGR) with the NIR dye DY-676, while unmodified particles were functionalized with DY-750 (P-CON). Targeted nanoparticles and P-CON were co-injected intravenously into tumor bearing mice and particle accumulation

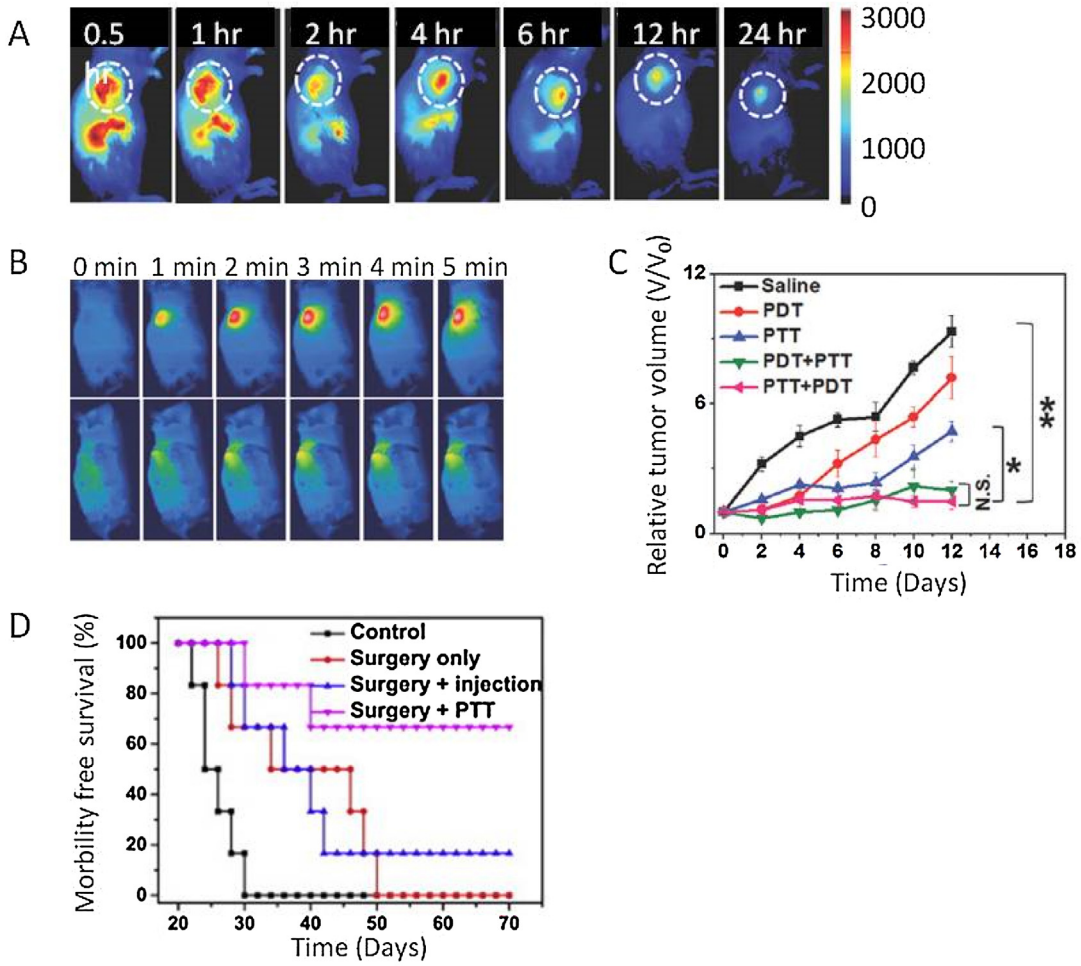

Fig. 16. (A) Fluorescent images of 4T1 tumor bearing mouse after i.v. administration of IR825/Ce6 micelles. (B) IR thermal images of 4T1 tumor-bearing mice under 808 nm laser irradiation (0.3 W/cm^2) after i.v. injection of IR825/Ce6 micelles (upper row) or saline (lower row). (C) Relative tumor volume of mice bearing 4T1 tumors after administration of IR825/Ce6 micelle after PTT treatment, PDT treatment or a combination of both (Gong et al., 2014). (d) Morbidity free survival of mice bearing 4T1 tumors after administration of IR825-HSA in combination with surgery and PTT (Chen et al., 2014b). Adapted with permission from Wiley online library (Gong et al., 2014). Reprinted with permission from Elsevier (Chen et al., 2014b).

was assessed for 72 h. Computed tomography-fluorescence molecular tomography (CT-FMT) imaging showed that P-RGD and P-NGR accumulated rapidly in the tumor (within 1 h) and bound to the endothelium, while after 48 h the particle concentration in the tumor decreased 50% (Fig. 17A and B). On the contrary, the formulation with no targeting ligands, P-CON, was hardly detected in the tumor after 1 h but accumulated more gradually, and after 48 h a prominent EPR mediated accumulation was observed. Thereby P-RGD and P-NGR showed a higher accumulation in healthy tissue compared to P-CON (Fig. 17C). This study shows that although particles can be directed to the tumor via active targeting in the first few hours after *i.v.* administration, passive targeting is more beneficial for long-circulating 10 nm particles (Kunjachan et al., 2014b). This phenomenon was also observed in other studies where modifying liposomes with HER2 (Kirpotin et al., 2006) and targeting nanoparticles with transferrin (Choi et al., 2010) did not improve tumor accumulation compared to untargeted systems. Meanwhile, these studies revealed that modifying the surface of these drug delivery systems with targeting ligands improves intracellular uptake of the particles. As a result, the delivery of for example siRNA can greatly benefit from active targeting since intracellular delivery is necessary to achieve a therapeutic effect (Bartlett et al., 2007).

One of the first clinical studies addressing the accumulation of liposomes in solid tumors revealed a low level of ^{111}In labeled PEGylated liposomes in a patient with breast cancer using gamma camera images (Harrington et al., 2001), which agrees with the fact that in clinical studies the response rate to free and encapsulated DOX was comparable (O'brien et al., 2004; Ranson et al., 1997). On the contrary, a high level of liposomal uptake was observed in several lesions in a patient with AIDS related Kaposi's carcinoma (Harrington et al., 2001), which correlates with another study that showed that liposomal DOX significantly improved the response rate from 25 to 46% compared to standard combination chemotherapy for the treatment of this malignancy (O'brien et al., 2004).

In addition to visualizing particle accumulation in a tumor, imaging can also be used to predict the therapeutic effect. To illustrate this concept, it was shown that the uptake of a radionuclide coupled to an antibody by neuroendocrine tumors was predictive for the overall survival of patients. Furthermore, a high uptake by the kidney was predictive for severe renal toxicity (Imhof et al., 2011). These studies showed the importance of imaging the accumulation of nanoparticles in a tumor. Patients with a high tumor accumulation after administration of nanoparticles are more likely to respond to drug-loaded nanoparticle

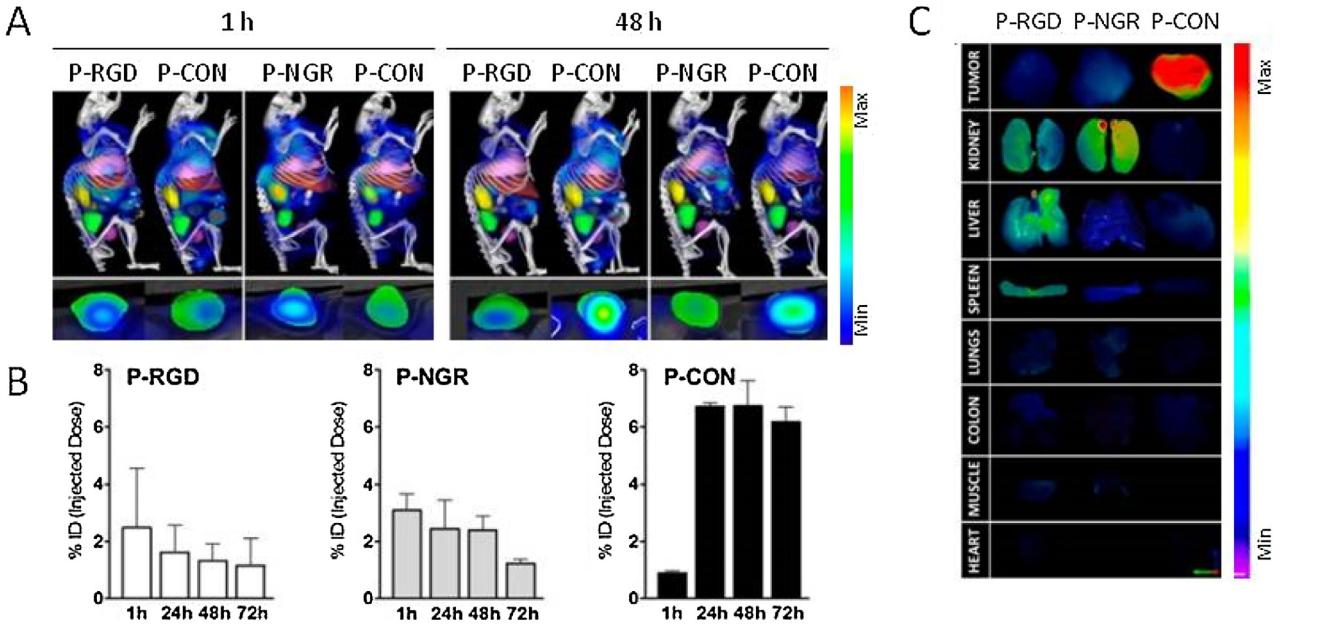

Fig. 17. (A) Hybrid computed tomography-fluorescence molecular tomography (CT-FMT) images of the biodistribution and tumor accumulation of P-RGD, P-NGR and P-CON at early (1 h) and late (48 h) time points post i.v. injection in highly leaky CT26 tumor-bearing mice. (B) Quantification of P-RGD, P-NGR and P-CON tumor accumulation 1 to 72 h post injection. (C) *Ex vivo* biodistribution of the above described nanoparticles in tumor and non-target organs (Theek et al., 2014). Adapted with permission from American Chemical Society.

treatment while patients who show hardly any accumulation in the tumor may probably benefit more from alternative treatments (Ojha et al., 2015).

6.2. Drug release

Drug delivery to the brain is challenging since the BBB prevents the passage of nanoparticles (Kievit and Zhang, 2011). Therefore, as stated above, MBs are used to enhance the permeability of the BBB by ultrasound exposure. To evaluate the enhanced permeability of the BBB after ultrasound exposure and subsequent drug delivery, Lammers et al. encapsulated ultrasmall superparamagnetic iron oxide (USPIO) nanoparticles in the shell of MBs based on poly(butyl cyanoacrylate). A significant increase in the R_2^* value was obtained in the brain of mice after administration of USPIO-MBs and subsequent ultrasound exposure (5 min), indicating an enhanced permeability of the BBB and the release of USPIO from MBs. Furthermore, injection of FITC-dextran prior to the administration of USPIO-MBs and ultrasound exposure resulted in an increased extravasation of the FITC-dextran (70 kDa, 3–5 nm) in the brain, showing that USPIO-MBs in combination with ultrasound exposure could mediate and monitor the enhanced BBB permeability and improved the delivery of macromolecules into the brain (Lammers et al., 2015).

Visualization of triggered drug release has been most intensively studied for temperature sensitive liposomes in combination with MR guided HIFU. Co-encapsulation of DOX and a Gd based contrast agent into LTSL resulted in a simultaneous and quantitative release at 42 °C indicating that the release of the contrast agent could be a good marker for *in vivo* release (Negussie et al., 2011; de Smet et al., 2011). Negussie et al. showed a signal increase on T_1 weighted images in a Vx2 rabbit tumor model after injection of LTSL co-encapsulating a contrast agent (ProHance® Gd-HP-DO3A) and DOX. A further increase in signal intensity of 9–22% was observed after four heating steps of 10 min indicating the release of the contrast agent (Fig. 18A) (Negussie et al., 2011). Comparable results were obtained in a rat study with subcutaneous 9L gliosarcoma tumors in the hind legs of the animals. Interestingly, some rats showed only a change in T_1 in the rim of the tumor 40 min after starting the first HIFU treatment, and only a small change in T_1 in the core was observed after 70 min (Fig. 18B). This relatively low change in T_1 correlated with a lower DOX concentration in the tumor compared to the rats which showed a more significant change in T_1. Likely, there was a difference in

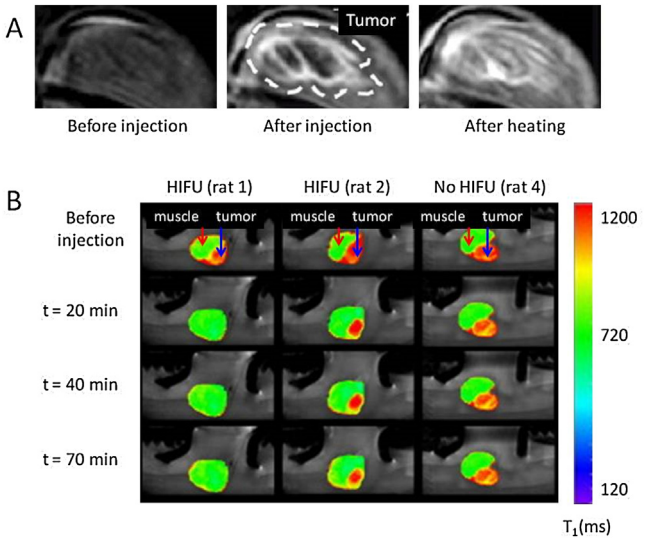

Fig. 18. (A) MR signal intensity before and after injection of TSL and after heating with MR-HIFU (four times for 10 min) (Negussie et al., 2011). (B) Anatomical MR images of tumor bearing rats and T_1 maps of the tumor and leg overlaid on the anatomical images at different time points: before the TSL injection, after the first hyperthermia period (t = 20 min), after the second hyperthermia period (t = 40 min) and 70 min after TSL injection. Left; HIFU treated tumor showing a large T_1 response (rat 1), middle; HIFU treated tumor showing a less sensitive response (rat 2) and right; untreated tumor (no HIFU, rat 4) (de Smet et al., 2011). Reprinted with permission from Taylor & Francis Ltd. (www.tandfonline.com). Adapted with permission from Elsevier (de Smet et al., 2011).

vascularization and permeability of the vessels from these rats (de Smet et al., 2011).

A slightly different approach was used by Kokuryo et al. to monitor the triggered release of DOX from liposomes. Polymer coated liposomes (EOEOVE, see Section on liposomes) loaded with DOX and a contrast agent (manganese-sulfate) were administered into mice bearing colon tumors 12 h prior to radiofrequency (RF) exposure (15 min, 42.5 °C) to ensure that the liposomes accumulated maximally in the tumor while liposomes were washed out from healthy tissue like liver and spleen thus limiting side effects. An increase in T_1 signal intensity was observed throughout the whole tumor after applying RF. As a result, the tumor size of mice treated with the liposomes in combination with RF was significantly smaller after 14 days compared to size of tumors in animals treated with the liposomes alone or RF exposure alone (Kokuryo et al., 2015). To enhance the delivery of drug to the tumor and visualize not only drug release but also particle distribution, van Elk et al. developed alginate microspheres for tumor embolization that encapsulated LTSL containing a contrast agent, Prohance® [Gd(HPDO3A)(H_2O)]. The microspheres could be visualized on a T_2^* weighted image since the microspheres were crosslinked with holmium ions while the temperature triggered release was observed in a T_1 weighted image (van Elk et al., 2015).

7. Perspectives

Cancer chemotherapy is currently limited by a high systemic toxicity that occurs as a result of high systemic dosing and the failure of non-targeted drugs to reach therapeutic doses at the target site either due to barriers around the tumor (aberrant vasculature), increased efflux of molecules from cancer cells (P-gp based efflux pumps) and the development of resistance to chemotherapeutic agents through co-activation of alternative signalling pathways (Lissa Nurrul Abdullah, 2013).

Nanoparticles currently on the market are capable of reducing systemic toxicity (Doxil, Depocyte) and passively targeting tumors (Wicki et al., 2015b). While this is an improvement over previous free drug regimens, it represents at best a non-specific method of depositing a chemotherapeutic drug depot into a tumor site with no regard for the future development of resistance or the type of tumor being targeted. Clinically, the recent emphasis is on the development of biologics and low molecular weight tyrosine kinase inhibitors which either synergise with classical chemotherapy (*e.g.* Tratuzumab and PTX) or can be used as monotherapy in certain malignancies to prevent further spread (*e.g.* Imatinib in Chronic Myelogenous Leukemia) (Al-Lazikani et al., 2012; Robert et al., 2006). As these cell signalling targets are limited, different methods of reducing systemic toxicity and therefore allowing higher therapeutic doses at the tumor site, and combining existing and newly developed therapies will be required (Bordon, 2015).

Having said that passive accumulation mechanisms of drug nanocarriers mainly rely on EPR, it should be remarked that this effect is dependent on tumor type and stage. Even though the EPR effect is common to almost all human solid tumors, with the exception of prostate and pancreatic cancer, large differences in accumulation can be found for the same carrier (Meng et al., 2016; Maeda, 2016). As stated above, size reduction of the carrier would lead to an enhanced EPR accumulation. Cabral et al. demonstrated that small micelles (30 nm) based on PEG-b-poly(glutamic acid) can penetrate a poorly permeable pancreatic tumor in mice, which was not achievable with larger sizes (50, 70 and 100 nm) (Cabral et al., 2016).

Another way to enhance nanocarrier accumulation in the tumor is by manipulating the local microenvironment. Angiotensin II-mediated blood pressure elevation and the infusion of nitric oxide donors, such as nitroglycerin, have both been successfully tested in human cancers. In a remarkable approach, Lo et al. reported on the application of local hyperthermia, mediated by NIR-activated gold nanorods, provoking a partial denaturation of tumor-associated collagen matrix. The resulting denatured fibrils could then be recognized by fibronectin fragment-functionalized nanoparticles leading to enhanced accumulation (Tailor et al., 2010).

In line with this two-particle strategy, the local tumor heating provided by gold nanorods resulted in additional signals that can be exploited for the same purpose. For instance, a stress-related protein, p32, is upregulated on the surface of tumor cells. By employing a specific peptide that binds to p32 receptors, peptide-targeted liposomes accumulated to a greater extent upon thermal treatment (Park et al., 2016; von Maltzahn et al., 2016). In another interesting strategy, magnetic accumulation of nanoparticles has been shown after the implantation of a magnetic micromesh in a human glioblastoma mouse model. By creating a magnetic gradient in the tumor tissue, the authors observed the retention of magnetic particles in the tumor neovasculature and surrounding tumor tissues (Fu et al., 2016). Given the low efficiency of EPR and specific ligand-mediated active targeting for drug carriers accumulation in tumors, more of these alternative strategies are expected for evaluation in animal models and clinical trials in the coming years.

A number of clinical trials currently in progress illustrate how novel nanomedicines can drive forward new biotechnological advances in the treatment of cancer (Table 4). A longstanding concept in oncology is the production of cancer vaccines, a form of immunotherapy which stimulates the patient's own immune system to target tumor cells (Bordon, 2015). However due to the complex mechanisms tumors use to avoid immune detection initially, and the fact that cancer cells are derived from self, such vaccines require a greater degree of complexity than their infectious disease counterparts. A number of vaccines are now in development which utilise the carrying capacity of liposomes to deliver complex immunogenic payloads thus creating and sustaining an immune response against neoplastic cells (Schwendener, 2014; Karkada et al., 2014). This offers a major advance on previous technologies based on simple antigen-adjuvant combinations and is a promising avenue for nanotechnology development.

Another example of cancer therapeutics is gene therapy. By suppressing oncogenes and promoting tumor suppressors, insertion of plasmids, microRNAs and oligonucleotides could fundamentally change the way we treat and manage malignant neoplasms (Esquela-Kerscher and Slack, 2006; Siddash et al., 2005). However, a number of barriers exist in the treatment of malignant neoplasms using these modalities including inadvertent insertion of gene products into normal tissue (possibly leading to tissue damage or the development of new malignancies) and the presence in plasma of multiple RNAases and DNAases preventing delivery of uncoated gene derived products. Nanoparticles can avoid both these processes acting as targeted vectors for the insertion of nucleotide based therapies into malignant cells (Chen et al., 2015c; Gonzalez et al., 2011). A number of therapies in clinical trials at present are utilising nanoparticles (Table 4) and will hopefully bring a new clinical dawn for the therapeutic usage of these modalities.

A number of substantial clinical problems currently exists which limit the efficacy of cancer chemotherapy and emerge from some basic principles of cancer biology. Tumors are often heterogeneous with multiple microenvironments due to the accumulation of different mutations in different cancer stem cells and the different Darwinian pressures each portion of the tumor is exposed to (Zellmer and Zhang, 2014). For instance cells in the periphery will typically have a readily available blood supply while those in the centre are more hypoxic. This selects for very different

Table 4
Current clinical trials involving nanomedicines.

Product (Company)	Novel Therapeutic Strategy	Platform	Drug	Indication	Status	Clinical Trial number
DPX-0907	Immunotherapy (cancer vaccine)	Liposome	HLA-A2 restricted cancer antigens	Breast cancer Ovarian cancer Prostate cancer	Phase I/ II	NCT01095848
Tecemotide	Immunotherapy (cancer vaccine)	Liposome	MUC1 antigen	Non small cell lung cancer	Phase III	NCT02049151
Lipovaxin- MM	Cancer vaccine	Liposome	Melanoma antigens	Malignant Melanoma	Phase I	NCT01052142
Chol FUS 1	Gene therapy vector	Liposome	FUS 1 gene	Non small cell lung cancer		NCT00059605
MRX-34	microRNA mimetic delivery	Liposome	MiR-34 mimetic	Primary liver Cancer Small cell lung carcinoma Lymphoma Melanoma ALL CLL Multiple myeloma MDS	Phase I	NCT01829971
BP1001	Delivery of antisense oligonucleotides	Liposome	L-GRB2 antisense oligonucleotide	CML AML ALL MDS	Phase I	NCT01159028
Dye labeled silica	Diagnostic	Silica nano particles	cRGDY-PEG-Cy5.5 dye	Melanoma of the head and neck Prostate cancer Cervical cancer Uterine cancer	Phase 0	NCT02106598
Rhenium nanoliposomes	Diagnostic/therapeutic	Liposome	Rhenium Radiotherapy	Glioblastoma Astrocytoma	Phase I/ II	NCT01906385

cells with possibly different susceptibilities in a small area. For example the hypoxic centre of a tumor is typically resistant to both radio and chemotherapy due to the lack of drugs reaching it and the low level of oxygen available for free radical production (Jensen, 2009). A device that delivers radiosensitisers and normalises the vasculature centrally while utilising classical chemotherapy to debulk peripheral cells would be enormously beneficial clinically. Recent publications have illustrated a prototypical small scale device which could possibly achieve this in heterogenous tumors such as glioblastoma multiforme (Oliver Jonas et al., 2015).

Additionally, previous research has shown that combinations of chemotherapeutic agents often synergise when they are dosed in a temporally independent fashion, forcing the cancer cell into dependence on a second pro-survival or anti-apoptopic pathway before a second agent is utilised for cytotoxicity (Lee et al., 2012). Advanced function nanoparticles offer the ability to combine drug regimens for synergistic killing and space the dosing of each component in time increasing their efficacy. As the nanoparticles would be delivered in a bolus, changes in the tumor microenvironment following the release of the first agent would not affect drug penetration and by utilising current technology drug release can be triggered externally (by using thermosensitive and photosensitive materials) or internally (by changes in pH or enzymes overexpressed by the tumor) (Wicki et al., 2015b; Junttila and de Sauvage, 2013; Van der Veldt et al., 2012).

After intensive research efforts dedicated over the years to the development of lipid-derived and polymeric nanoparticles for the controlled release of therapeutics, drug delivery system options based on MSN may represent a solid addition to the current arsenal of nanomedicines against cancer. Given the high chemical and thermal stability, and the flexibility to be modified with many different functional groups, mesoporous silica nanoparticles aimed for biomedical applications has attracted an enormous research effort in the last decade. From the most basic model of adsorbing a small molecule on the silica surface to the highly sophisticated systems incorporating nanovalves for multiple drug delivery, hundreds of different designs were proposed and the biomaterials community has developed the expertise to initiate the steps towards clinical translation.

Notably, multifunctional nanocarriers based on MSN can be designed to have theranostic potential. In addition to the ability to deliver drugs in a controlled manner, these particles can be easily doped with fluorescent dyes, quantum dots and MRI contrast agents to image the delivery site. Moreover, MSN have been proposed as a carrier of multicomponent cargo. The ability to combine the intracellular delivery of small drugs, siRNA and toxins at the same time and in a traceable manner represents a great promise for synergistic treatments to fight complex diseases (Ashley et al., 2016).

Ultimately the goal in nanoparticle development is a single nanocarrier capable of diagnosis (such as the particles described in NCT02106598, Table 4), therapeutic dosing and controlled triggered release (similar to clinically available Thermodox®). Nanoparticles will increase the therapeutic scope of both investigational and clinically approved chemotherapeutics by reducing the associated toxicities while integrating with other biotechnological advances to produce targeted, triggerable release platforms for greater debulking of tumor mass and reduction of metastatic tumor load. This will improve patient prognosis and reduce the lifelong after effects of chemotherapy including the risk of a new malignancies.

Acknowledgements

We thank the following for funding this work: RCSI Seed funding Scheme, EU FP7 AMCARE, H2020 FP7 DRIVE. This publication has emanated from research supported in part by a research grant from Science Foundation Ireland (SFI) under Grant Number SFI/12/RC/2278.

References

Agostinis, P., Berg, K., Cengel, K.A., Foster, T.H., Girotti, A.W., Gollnick, S.O., et al., 2011. Photodynamic therapy of cancer: an update. CA. Cancer J. Clin. 61, 250–281.
Ahmed, E., Morton, S.W., Hammond, P.T., Swager, T.M., 2013. Fluorescent multiblock π-conjugated polymer nanoparticles for in vivo tumor targeting. Adv. Mater. 25, 4504–4510.
Akimoto, J., Nakayama, M., Sakai, K., Okano, T., 2009. Temperature-induced intracellular uptake of thermoresponsive polymeric micelles. Biomacromolecules 10, 1331–1336.

Akimoto, J., Nakayama, M., Sakai, K., Okano, T., 2010. Thermally controlled intracellular uptake system of polymeric micelles possessing poly (N-isopropylacrylamide)-based outer coronas. Mol. Pharm. 7, 926–935.
Al-Lazikani, B., Banerji, U., Workman, P., 2012. Combinatorial drug therapy for cancer in the post-genomic era. Nat. Biotechnol. 30, 679–692.
Alcaide, M., Ramirez-Santillan, C., Feito, M.J., Matesanz, M.D., Ruiz-Hernandez, E., Arcos, D., et al., 2012. In vitro evaluation of glass–glass ceramic thermoseed-induced hyperthermia on human osteosarcoma cell line. J. Biomed. Mater. Res. A 100A, 64–71.
Allen, T.M., Cullis, P.R., 2013. Liposomal drug delivery systems: from concept to clinical applications. Adv. Drug Deliv. Rev. 65, 36–48.
Allen, T., Hong, K., Papahadjopoulos, D., 1990. Membrane contact, fusion and hexagonal (HII) transitions in phosphatidylethanolamine liposomes. Biochemistry 29, 2976–2985.
Allen, T., Hansen, C., Martin, F., Redemann, C., Yau-Young, A., 1991. Liposomes containing synthetic lipid derivatives of poly (ethylene glycol) show prolonged circulation half-lives in vivo. Biochim. Biophys. Acta (BBA)-Biomembr. 1066, 29–36.
Anyarambhatla, G.R., Needham, D., 1999. Enhancement of the phase transition permeability of DPPC liposomes by incorporation of MPPC: a new temperature-sensitive liposome for use with mild hyperthermia. J. Liposome Res. 9, 491–506.
Arcos, D., López-Noriega, A., Ruiz-Hernández, E., Ruiz, L., González-Calbet, J.M., Vallet-Regí, M., 2008. Syntesis of mesoporous microparticles for biomedical applications. Key Eng. Mater. Trans. Technol. Publ. 181–194.
Arcos, D., Fal-Miyar, V., Ruiz-Hernandez, E., Garcia-Hernandez, M., Luisa Ruiz-Gonzalez, M., Gonzalez-Calbet, J., et al., 2012. Supramolecular mechanisms in the synthesis of mesoporous magnetic nanospheres for hyperthermia. J. Mater. Chem. 22, 64–72.
Ashley, C.E., Carnes, E.C., Phillips, G.K., Padilla, D., Durfee, P.N., Brown, P.A., et al., 2016. The targeted delivery of multicomponent cargos to cancer cells by nanoporous particle-supported lipid bilayers. Nat. Mater. 10, 389–397.
Ashok, B., Arleth, L., Hjelm, R.P., Rubinstein, I., Önyüksel, H., 2004. In vitro characterization of PEGylated phospholipid micelles for improved drug solubilization: effects of PEG chain length and PC incorporation. J. Pharm. Sci. 93, 2476–2487.
Aznar, E., Villalonga, R., Gimenez, C., Sancenon, F., Marcos, M.D., Martinez-Manez, R., et al., 2013. Glucose-triggered release using enzyme-gated mesoporous silica nanoparticles. Chem. Commun. (Camb.) 49, 6391–6393.
Bae, Y.H., Park, K., 2011a. Targeted drug delivery to tumors: myths, reality and possibility. J. Controlled Release 153, 198–205.
Bae, Y.H., Park, K., 2011b. Targeted drug delivery to tumors: myths, reality and possibility. J. Controlled Release 153, 198.
Baeza, A., Guisasola, E., Ruiz-Hernandez, E., Vallet-Regi, M., 2012. Magnetically triggered multidrug release by hybrid mesoporous silica nanoparticles. Chem. Mater. 24, 517–524.
Baguley, B.C., 2010. Multiple drug resistance mechanisms in cancer. Mol. Biotechnol. 46, 308–316.
Bandak, S., Goren, D., Horowitz, A., Tzemach, D., Gabizon, A., 1999. Pharmacological studies of cisplatin encapsulated in long-circulating liposomes in mouse tumor models. Anticancer Drugs 10, 911–920.
Bangham, A.D., Horne, R., 1964. Negative staining of phospholipids and their structural modification by surface-active agents as observed in the electron microscope. J. Mol. Biol. 8 660–IN10.
Bangham, A., Standish, M.M., Watkins, J., 1965. Diffusion of univalent ions across the lamellae of swollen phospholipids. J. Mol. Biol. 13 238–IN27.
Banno, B., Ickenstein, L.M., Chiu, G.N.C., Bally, M.B., Thewalt, J., Brief, E., et al., 2010. The functional roles of poly (ethylene glycol)-lipid and lysolipid in the drug retention and release from lysolipid-containing thermosensitive liposomes in vitro and in vivo. J. Pharm. Sci. 99, 2295–2308.
Barenholz, Y., 2012. Doxil® – the first FDA-approved nano-drug: lessons learned. J. Controlled Release 160, 117–134.
Bartlett, D.W., Su, H., Hildebrandt, I.J., Weber, W.A., Davis, M.E., 2007. Impact of tumor-specific targeting on the biodistribution and efficacy of siRNA nanoparticles measured by multimodality in vivo imaging. Proc. Natl. Acad. Sci. 104, 15549–15554.
Batchelor, T.T., Duda, D.G., di Tomaso, E., Ancukiewicz, M., Plotkin, S.R., Gerstner, E., et al., 2010. Phase II study of cediranib, an oral pan-vascular endothelial growth factor receptor tyrosine kinase inhibitor, in patients with recurrent glioblastoma. J. Clin. Oncol. JCO 26, 3988 (2009).
Batchelor, T.T., Mulholland, P., Neyns, B., Nabors, L.B., Campone, M., Wick, A., et al., 2013. Phase III. randomized trial comparing the efficacy of cediranib as monotherapy, and in combination with lomustine, versus lomustine alone in patients with recurrent glioblastoma. J. Clin. Oncol. 31, 3212–3218.
Beaumier, P.L., Hwang, K.J., 1983. Effects of liposome size on the degradation of bovine brain sphingomyelin/cholesterol liposomes in the mouse liver. Biochim. Biophys. Acta (BBA)-Biomembr. 731, 23–30.
Benezra, M., Penate-Medina, O., Zanzonico, P.B., Schaer, D., Ow, H., Burns, A., et al., 2016. Multimodal silica nanoparticles are effective cancer-targeted probes in a model of human melanoma. J. Clin. Invest. 121, 2768–2780.
Bhattacharyya, J., Bellucci, J.J., Weitzhandler, I., McDaniel, J.R., Spasojevic, I., Li, X., et al., 2015. A paclitaxel-loaded recombinant polypeptide nanoparticle outperforms Abraxane in multiple murine cancer models. Nat. Commun. 6.
Bordon, Y., 2015. Immunotherapy: checkpoint parley. Nat. Rev. Cancer 15, 3.
Bruelisauer, L., Gauthier, M.A., Leroux, J.-C., 2014. Disulfide-containing parenteral delivery systems and their redox-biological fate. J. Controlled Release 195, 147–154.
Cabral, H., Kataoka, K., 2014. Progress of drug-loaded polymeric micelles into clinical studies. J. Controlled Release 190, 465–476.
Cabral, H., Matsumoto, Y., Mizuno, K., Chen, Q., Murakami, M., Kimura, M., et al., 2016. Accumulation of sub-100 nm polymeric micelles in poorly permeable tumours depends on size. Nat. Nanotechnol. 6, 815–823.
Callahan, D.J., Liu, W.E., Li, X.H., Dreher, M.R., Hassouneh, W., Kim, M., et al., 2012. Triple stimulus-responsive polypeptide nanoparticles that enhance intratumoral spatial distribution. Nano Lett. 12, 2165–2170.
Chacko, R.T., Ventura, J., Zhuang, J., Thayumanavan, S., 2012. Polymer nanogels: a versatile nanoscopic drug delivery platform. Adv. Drug Deliv. Rev. 64, 836–851.
Chai, W.-Y., Chu, P.-C., Tsai, M.-Y., Lin, Y.-C., Wang, J.-J., Wei, K.-C., et al., 2014. Magnetic-resonance imaging for kinetic analysis of permeability changes during focused ultrasound-induced blood–brain barrier opening and brain drug delivery. J. Controlled Release 192, 1–9.
Chauhan, V.P., Stylianopoulos, T., Martin, J.D., Popović, Z., Chen, O., Kamoun, W.S., et al., 2012. Normalization of tumour blood vessels improves the delivery of nanomedicines in a size-dependent manner. Nat. Nanotechnol. 7, 383–388.
Chen, H., Kim, S., Li, L., Wang, S., Park, K., Cheng, J.-X., 2008. Release of hydrophobic molecules from polymer micelles into cell membranes revealed by Forster resonance energy transfer imaging. Proc. Natl. Acad. Sci. U. S. A. 105, 6596–6601.
Chen, Y., Chen, H., Shi, J., 2013. In vivo bio-safety evaluations and diagnostic/therapeutic applications of chemically designed mesoporous silica nanoparticles. Adv. Mater. 25, 3144–3176.
Chen, M., He, X., Wang, K., He, D., Yang, S., Qiu, P., et al., 2014a. A pH-responsive polymer/mesoporous silica nano-container linked through an acid cleavable linker for intracellular controlled release and tumor therapy in vivo. J. Mater. Chem. B 2, 428–436.
Chen, Q., Liang, C., Wang, X., He, J., Li, Y., Liu, Z., 2014b. An albumin-based theranostic nano-agent for dual-modal imaging guided photothermal therapy to inhibit lymphatic metastasis of cancer post surgery. Biomaterials 35, 9355–9362.
Chen, K.-J., Chaung, E.-Y., Wey, S.-P., Lin, K.-J., Cheng, F., Lin, C.-C., et al., 2014c. Hyperthermia-mediated local drug delivery by a bubble-generating liposomal system for tumor-specific chemotherapy. ACS Nano 8, 5105–5115.
Chen, W.-H., Luo, G.-F., Lei, Q., Jia, H.-Z., Hong, S., Wang, Q.-R., et al., 2015a. MMP-2 responsive polymeric micelles for cancer-targeted intracellular drug delivery. Chem. Commun. 51, 465–468.
Chen, Y., Chen, H., Shi, J., 2015b. Nanobiotechnology promotes noninvasive high-Intensity focused ultrasound cancer surgery. Adv. Healthcare Mater. 4.
Chen, Y., Gao, D.Y., Huang, L., 2015c. In vivo delivery of miRNAs for cancer therapy: challenges and strategies. Adv. Drug Deliv. Rev. 81, 128–141.
Chen, Y., Ai, K., Liu, J., Sun, G., Yin, Q., Lu, L., 2015d. Multifunctional envelope-type mesoporous silica nanoparticles for pH-responsive drug delivery and magnetic resonance imaging. Biomaterials 60, 111–120.
Chiang, Y.-T., Yen, Y.-W., Lo, C.-L., 2015. Reactive oxygen species and glutathione dual redox-responsive micelles for selective cytotoxicity of cancer. Biomaterials 61, 150–161.
Choi, H.S., Liu, W., Misra, P., Tanaka, E., Zimmer, J.P., Ipe, B.I., et al., 2007. Renal clearance of quantum dots. Nat. Biotechnol. 25, 1165–1170.
Choi, C.H.J., Alabi, C.A., Webster, P., Davis, M.E., 2010. Mechanism of active targeting in solid tumors with transferrin-containing gold nanoparticles. Proc. Natl. Acad. Sci. 107, 1235–1240.
Chung, T.-H., Wu, S.-H., Yao, M., Lu, C.-W., Lin, Y.-S., Hung, Y., et al., 2007. The effect of surface charge on the uptake and biological function of mesoporous silica nanoparticles 3T3-L1 cells and human mesenchymal stem cells. Biomaterials 28, 2959–2966.
Chung, M.F., Chen, K.J., Liang, H.F., Liao, Z.X., Chia, W.T., Xia, Y., et al., 2012. A liposomal system capable of generating CO2 bubbles to induce transient cavitation, lysosomal rupturing, and cell necrosis. Angew. Chem. 124, 10236–10240.
Cossu, I., Bottoni, G., Loi, M., Emionite, L., Bartolini, A., Di Paolo, D., et al., 2015. Neuroblastoma-targeted nanocarriers improve drug delivery and penetration, delay tumor growth and abrogate metastatic diffusion. Biomaterials 68, 89–99.
Crawford, J., Dale, D.C., Lyman, G.H., 2004. Chemotherapy-induced neutropenia. Cancer 100, 228–237.
Crielaard, B.J., Rijcken, C.J.F., Quan, L., van der Wal, S., Altintas, I., van der Pot, M., et al., 2012. Glucocorticoid-loaded core-cross-linked polymeric micelles with tailorable release kinetics for targeted therapy of rheumatoid arthritis. Angew. Chem. Int. Ed. 51, 7254–7258.
Cui, S., Yin, D., Chen, Y., Di, Y., Chen, H., Ma, Y., et al., 2012. In vivo targeted deep-tissue photodynamic therapy based on near-infrared light triggered upconversion nanoconstruct. ACS Nano 7, 676–688.
Díez, P., Sánchez, A., Gamella, M., Martínez-Ruíz, P., Aznar, E., de la Torre, C., et al., 2014. Toward the design of smart delivery systems controlled by integrated enzyme-based biocomputing ensembles. J. Am. Chem. Soc. 136, 9116–9123.
Dale, A.V., An, G.I., Pandya, D.N., Ha, Y.S., Bhatt, N., Soni, N., et al., 2015. Synthesis and evaluation of new generation cross-bridged bifunctional chelator for Cu radiotracers. Inorg. Chem..
Danhier, F., Danhier, P., De Saedeleer, C.J., Fruytier, A.-C., Schleich, N., des Rieux, A., et al., 2015. Paclitaxel-loaded micelles enhance transvascular permeability and retention of nanomedicines in tumors. Int. J. Pharm. 479, 399–407.
Davis, M.E., Chen, Z., Shin, D.M., 2008. Nanoparticle therapeutics: an emerging treatment modality for cancer. Nat. Rev. Drug Discov. 7, 771–782.
De Backer, L., Braeckmans, K., Stuart, M.C.A., Demeester, J., De Smedt, S.C., Raemdonck, K., 2015. Bio-inspired pulmonary surfactant-modified nanogels: a promising siRNA delivery system. J. Controlled Release 206, 177–186.

De Jong, W.H., Hagens, W.I., Krystek, P., Burger, M.C., Sips, A.J., Geertsma, R.E., 2008. Particle size-dependent organ distribution of gold nanoparticles after intravenous administration. Biomaterials 29, 1912–1919.
Delalande, A., Kotopoulis, S., Postema, M., Midoux, P., Pichon, C., 2013. Sonoporation mechanistic insights and ongoing challenges for gene transfer. Gene 525, 191–199.
Deng, C., Jiang, Y., Cheng, R., Meng, F., Zhong, Z., 2012. Biodegradable polymeric micelles for targeted and controlled anticancer drug delivery: promises, progress and prospects. Nano Today 7, 467–480.
Deng, L., Ren, J., Li, J., Leng, J., Qu, Y., Lin, C., et al., 2015. Magnetothermally responsive star-block copolymeric micelles for controlled drug delivery and enhanced thermo-chemotherapy. Nanoscale 7, 9655–9663.
de Smet, M., Langereis, S., van den Bosch, S., Grull, H., 2010. Temperature-sensitive liposomes for doxorubicin delivery under MRI guidance. J. Controlled Release 143, 120–127.
de Smet, M., Heijman, E., Langereis, S., Hijnen, N.M., Grull, H., 2011. Magnetic resonance imaging of high intensity focused ultrasound mediated drug delivery from temperature-sensitive liposomes: an in vivo proof-of-concept study. J. Controlled Release 150, 102–110.
de Smet, M., Hijnen, N.M., Langereis, S., Elevelt, A., Heijman, E., Dubois, L., et al., 2013. Magnetic resonance guided high-intensity focused ultrasound mediated hyperthermia improves the intratumoral distribution of temperature-sensitive liposomal doxorubicin. Invest. Radiol. 48, 395–405.
Derieppe, M., Rojek, K., Escoffre, J.-M., de Senneville, B.D., Moonen, C., Bos, C., 2015. Recruitment of endocytosis in sonopermeabilization-mediated drug delivery: a real-time study. Phys. Biol. 12, 046010.
Deshmukh, M., Kutscher, H., Stein, S., Sinko, P., 2009. Nonenzymatic, self-elimination degradation mechanism of glutathione. Chem. Biodivers. 6, 527–539.
Dewhirst, M.W., Sim, D.A., 1984. The utility of thermal dose as a predictor of tumor and normal tissue responses to combined radiation and hyperthermia. Cancer Res. 44, 4772–4780.
Diez, P., Sanchez, A., Gamella, M., Martinez-Ruiz, P., Aznar, E., de la Torre, C., et al., 2014. Toward the design of smart delivery systems controlled by integrated enzyme-based biocomputing ensembles. J. Am. Chem. Soc. 136, 9116–9123.
Dreher, M.R., Liu, W.G., Michelich, C.R., Dewhirst, M.W., Yuan, F., Chilkoti, A., 2006. Tumor vascular permeability, accumulation, and penetration of macromolecular drug carriers. J. Natl. Cancer Inst. 98, 335–344.
Egeblad, M., Nakasone, E.S., Werb, Z., 2010. Tumors as organs: complex tissues that interface with the entire organism. Dev. Cell 18, 884–901.
Esquela-Kerscher, A., Slack, F.J., 2006. Oncomirs – microRNAs with a role in cancer. Nat. Rev. Cancer 6, 259–269.
Fan, J., Zeng, F., Wu, S., Wang, X., 2012. Polymer micelle with pH-triggered hydrophobic–hydrophilic transition and de-cross-linking process in the core and its application for targeted anticancer drug delivery. Biomacromolecules 13, 4126–4137.
Fan, W., Shen, B., Bu, W., Chen, F., He, Q., Zhao, K., et al., 2014. A smart upconversion-based mesoporous silica nanotheranostic system for synergetic chemo-/radio-/photodynamic therapy and simultaneous MR/UCL imaging. Biomaterials 35, 8992–9002.
Felber, A.E., Dufresne, M.-H., Leroux, J.-C., 2012. pH-sensitive vesicles, polymeric micelles, and nanospheres prepared with polycarboxylates. Adv. Drug Deliv. Rev. 64, 979–992.
Ferreira, S.A., Gama, F.M., Vilanova, M., 2013. Polymeric nanogels as vaccine delivery systems. Nanomed. Nanotechnol. Biol. Med. 9, 159–173.
Ferris, D.P., Lu, J., Gothard, C., Yanes, R., Thomas, C.R., Olsen, J.C., et al., 2016. Synthesis of biomolecule-Modified mesoporous silica nanoparticles for targeted hydrophobic drug delivery to cancer cells. Small 7, 1816–1826.
Fu, A., Wilson, R.J., Smith, B.R., Mullenix, J., Earhart, C., Akin, D., et al., 2016. Fluorescent magnetic nanoparticles for magnetically enhanced cancer imaging and targeting in living subjects. Acs Nano 6, 6862–6869.
Gabizon, A., Catane, R., Uziely, B., Kaufman, B., Safra, T., Cohen, R., et al., 1994. Prolonged circulation time and enhanced accumulation in malignant exudates of doxorubicin encapsulated in polyethylene-glycol coated liposomes. Cancer Res. 54, 987–992.
Gale, R.P., 1985. Antineoplastic chemotherapy myelosuppression: mechanisms and new approaches. Exp. Hematol. 13 (Suppl 16), 3–7.
Gao, Y., Ma, R., An, Y., Shi, L., 2011. Nanogated vessel based on polypseudorotaxane-capped mesoporous silica via a highly acid-labile benzoic-imine linker. J. Controlled Release 152, e81–e82.
Gao, Y., Zhou, Y., Zhao, L., Zhang, C., Li, Y., Li, J., et al., 2015. Enhanced antitumor efficacy by cyclic RGDyK-conjugated and paclitaxel-loaded pH-responsive polymeric micelles. Acta Biomater..
Gaspar, V.M., Baril, P., Costa, E.C., de Melo-Diogo, D., Foucher, F., Queiroz, J.A., et al., 2015. Bioreducible poly (2-ethyl-2-oxazoline)–PLA–PEI-SS triblock copolymer micelles for co-delivery of DNA minicircles and Doxorubicin. J. Controlled Release 213, 175–191.
Gharib, M.I., Burnett, A.K., 2002. Chemotherapy-induced cardiotoxicity: current practice and prospects of prophylaxis. Eur. J. Heart Fail. 4, 235–242.
Gobbo, O.L., Sjaastad, K., Radomski, M.W., Volkov, Y., Prina-Mello, A., 2015. Magnetic nanoparticles in cancer theranostics. Theranostics 5, 1249–1263.
Gong, J., Chen, M., Zheng, Y., Wang, S., Wang, Y., 2012. Polymeric micelles drug delivery system in oncology. J. Controlled Release 159, 312–323.
Gong, H., Dong, Z., Liu, Y., Yin, S., Cheng, L., Xi, W., et al., 2014. Engineering of multifunctional nano-micelles for combined photothermal and photodynamic therapy under the guidance of multimodal imaging. Adv. Funct. Mater. 24, 6492–6502.
Gonzalez, B., Ruiz-Hernandez, E., Feito, M.J., Lopez de Laorden, C., Arcos, D., Ramirez-Santillan, C., et al., 2011. Covalently bonded dendrimer-maghemite nanosystems: nonviral vectors for in vitro gene magnetofection. J. Mater. Chem. 21, 4598–4604.
Gottesman, M.M., Fojo, T., Bates, S.E., 2002. Multidrug resistance in cancer: role of ATP–dependent transporters. Nat. Rev. Cancer 2, 48–58.
Gregoriadis, G., Ryman, B.E., 1972. Fate of protein-containing liposomes injected into rats. Eur. J. Biochem. 24, 485–491.
Griset, A.P., Walpole, J., Liu, R., Gaffey, A., Colson, Y.L., Grinstaff, M.W., 2009. Expansile nanoparticles synthesis, characterization, and in vivo efficacy of an acid-responsive polymeric drug delivery system. J. Am. Chem. Soc. 131, 2469–2471.
Grun, M., Lauer, I., Unger, K.K., 1997. The synthesis of micrometer- and submicrometer-size spheres of ordered mesoporous oxide MCM-41. Adv. Mater. 9, 254.
Gu, Y.D., Zhong, Y.N., Meng, F.H., Cheng, R., Deng, C., Zhong, Z.Y., 2013. Acetal-linked paclitaxel prodrug micellar nanoparticles as a versatile and potent platform for cancer therapy. Biomacromolecules 14, 2772–2780.
Guo, Y., Zhang, Y., Li, J., Zhang, Y., Lu, Y., Jiang, X., et al., 2015. Cell microenvironment-controlled antitumor drug releasing-nanomicelles for GLUT1-targeting hepatocellular carcinoma therapy. ACS Appl. Mater. Interfaces 7, 5444–5453.
Hahn, G.M., Braun, J., Har-Kedar, I., 1975. Thermochemotherapy synergism between hyperthermia (42–43 degrees) and adriamycin (of bleomycin) in mammalian cell inactivation. Proc. Natl. Acad. Sci. U. S. A. 72, 937–940.
Han, H.D., Shin, B.C., Choi, H.S., 2006. Doxorubicin-encapsulated thermosensitive liposomes modified with poly (N-isopropylacrylamide-co-acrylamide): drug release behavior and stability in the presence of serum. Eur. J. Pharm. Biopharm. 62, 110–116.
Han, L., Tang, C., Yin, C., 2013. Effect of binding affinity for siRNA on the in vivo antitumor efficacy of polyplexes. Biomaterials 34, 5317–5327.
Han, L., Tang, C., Yin, C., 2015. Dual-targeting and pH/redox-responsive multi-layered nanocomplexes for smart co-delivery of doxorubicin and siRNA. Biomaterials 60, 42–52.
Hanahan, D., Weinberg, R.A., 2000. The hallmarks of cancer. Cell 100, 57–70.
Harrington, K.J., Mohammadtaghi, S., Uster, P.S., Glass, D., Peters, A.M., Vile, R.G., et al., 2001. Effective targeting of solid tumors in patients with locally advanced cancers by radiolabeled pegylated liposomes. Clin. Cancer Res. 7, 243–254.
Hayashi, H., Kono, K., Takagishi, T., 1996. Temperature-controlled release property of phospholipid vesicles bearing a thermo-sensitive polymer. Biochim. Biophys. Acta (BBA)-Biomembr. 1280, 127–134.
Hayashi, H., Kono, K., Takagishi, T., 1998. Temperature-dependent associating property of liposomes modified with a thermosensitive polymer. Bioconjugate Chem. 9, 382–389.
Hayashi, H., Kono, K., Takagishi, T., 1999. Temperature sensitization of liposomes using copolymers of N-isopropylacrylamide. Bioconjugate Chem. 10, 412–418.
Herman, T.S., 1983. Temperature dependence of adriamycin, cis-diamminedichloroplatinum, bleomycin, and 1,3-bis(2-chloroethyl)-1-nitrosourea cytotoxicity in vitro. Cancer Res. 43, 517–520.
Hildebrandt, B., Wust, P., Ahlers, O., Dieing, A., Sreenivasa, G., Kerner, T., et al., 2002. The cellular and molecular basis of hyperthermia. Crit. Rev. Oncol. Hematol. 43, 33–56.
Hossann, M., Wiggenhorn, M., Schwerdt, A., Wachholz, K., Teichert, N., Eibl, H., et al., 2007. In vitro stability and content release properties of phosphatidylglyceroglycerol containing thermosensitive liposomes. Biochim. Biophys. Acta 1768, 2491–2499.
Hossann, M., Wang, T., Wiggenhorn, M., Schmidt, R., Zengerle, A., Winter, G., et al., 2010. Size of thermosensitive liposomes influences content release. J. Controlled Release 147, 436–443.
Hossann, M., Syunyaeva, Z., Schmidt, R., Zengerle, A., Eibl, H., Issels, R.D., et al., 2012. Proteins and cholesterol lipid vesicles are mediators of drug release from thermosensitive liposomes. J. Controlled Release 162, 400–406.
Hsiao, C.W., Chen, H.L., Liao, Z.X., Sureshbabu, R., Hsiao, H.C., Lin, S.J., et al., 2015. Effective photothermal killing of pathogenic bacteria by using spatially tunable colloidal gels with nano-localized heating sources. Adv. Funct. Mater. 25, 721–728.
Huang, S.L., 2008. Liposomes in ultrasonic drug and gene delivery. Adv. Drug Deliv. Rev. 60, 1167–1176.
Hudson, S.P., Padera, R.F., Langer, R., Kohane, D.S., 2008. The biocompatibility of mesoporous silicates. Biomaterials 29, 4045–4055.
Husseini, G.A., Myrup, G.D., Pitt, W.G., Christensen, D.A., Rapoport, N.Y., 2000. Factors affecting acoustically triggered release of drugs from polymeric micelles. J. Controlled Release 69, 43–52.
Ickenstein, L.M., Arfvidsson, M.C., Needham, D., Mayer, L.D., Edwards, K., 2003. Disc formation in cholesterol-free liposomes during phase transition. Biochim. Biophys. Acta (BBA)-Biomembr. 1614, 135–138.
Imhof, A., Brunner, P., Marincek, N., Briel, M., Schindler, C., Rasch, H., et al., 2011. Response, survival, and long-term toxicity after therapy with the radiolabeled somatostatin analogue [90Y-DOTA]-TOC in metastasized neuroendocrine cancers. J. Clin. Oncol. 29, 2416–2423.
Ishida, T., Kirchmeier, M., Moase, E., Zalipsky, S., Allen, T., 2001. Targeted delivery and triggered release of liposomal doxorubicin enhances cytotoxicity against human B lymphoma cells. Biochim. Biophys. Acta (BBA)-Biomembr. 1515, 144–158.

Jain, R.K., Stylianopoulos, T., 2010. Delivering nanomedicine to solid tumors. Nat. Rev. Clin. Oncol. 7, 653–664.
Jain, R.K., Martin, J.D., Stylianopoulos, T., 2014. The role of mechanical forces in tumor growth and therapy. Annu. Rev. Biomed. Eng. 16, 321.
Jain, R.K., 1988. Determinants of tumor blood flow: a review. Cancer Res. 48, 2641–2658.
Jain, R.K., 2013. Normalizing tumor microenvironment to treat cancer: bench to bedside to biomarkers. J. Clin. Oncol. 31, 2205–2218.
Jalani, G., Jung, C.W., Lee, J.S., Lim, D.W., 2014. Fabrication and characterization of anisotropic nanofiber scaffolds for advanced drug delivery systems. Int. J. Nanomed. 9, 33.
Jensen, R.L., 2009. Brain tumor hypoxia: tumorigenesis, angiogenesis, imaging, pseudoprogression, and as a therapeutic target. J. Neurooncol. 92, 317–335.
Jiang, W., Kim, B.Y.S., Rutka, J.T., Chan, W.C.W., 2008. Nanoparticle-mediated cellular response is size-dependent. Nat. Nanotechnol. 3, 145–150.
Jiang, S., Chen, Q., Tripathy, M., Luijten, E., Schweizer, K.S., Granick, S., 2010. Janus particle synthesis and assembly. Adv. Mater. (Deerfield Beach, Fla) 22, 1060–1071.
Jiang, Y., Chen, J., Deng, C., Suuronen, E.J., Zhong, Z., 2014. Click hydrogels, microgels and nanogels: emerging platforms for drug delivery and tissue engineering. Biomaterials 35, 4969–4985.
Jiang, W., Huang, Y., An, Y., Kim, B.Y., 2015. Remodelling tumor vasculature to enhance delivery of intermediate-sized nanoparticles. ACS Nano 9, 8689–8696.
Junttila, M.R., de Sauvage, F.J., 2013. Influence of tumour micro-environment heterogeneity on therapeutic response. Nature 501, 346–354.
Kageyama, S., Kitano, S., Hirayama, M., Nagata, Y., Imai, H., Shiraishi, T., et al., 2008. Humoral immune responses in patients vaccinated with 1–146 HER2 protein complexed with cholesteryl pullulan nanogel. Cancer Sci. 99, 601–607.
Kakwere, H., Leal, M.P., Materia, M.E., Curcio, A., Guardia, P., Niculaes, D., et al., 2015. Functionalization of strongly interacting magnetic nanocubes with (thermo) responsive coating and their application in hyperthermia and heat-triggered drug delivery. ACS Appl. Mater. Interfaces 7, 10132–10145.
Karkada, M., Berinstein, N.L., Mansour, M., 2014. Therapeutic vaccines and cancer: focus on DPX-0907. Biologics 8, 27–38.
Katagiri, K., Imai, Y., Koumoto, K., Kaiden, T., Kono, K., Aoshima, S., 2011. Magnetoresponsive on-demand release of hybrid liposomes formed from Fe3O4 nanoparticles and thermosensitive block copolymers. Small 7, 1683–1689.
Kataoka, K., Harada, A., Nagasaki, Y., 2012. Block copolymer micelles for drug delivery: design, characterization and biological significance. Adv. Drug Deliv. Rev. 64, 37–48.
Kato, K., Chin, K., Yoshikawa, T., Yamaguchi, K., Tsuji, Y., Esaki, T., et al., 2012. Phase II. Study of NK105, a paclitaxel-incorporating micellar nanoparticle, for previously treated advanced or recurrent gastric cancer. Invest. New Drugs 30, 1621–1627.
Kato, Y., Zhu, W., Backer, M.V., Neoh, C.C., Hapuarachchige, S., Sarkar, S.K., et al., 2015. Noninvasive imaging of liposomal delivery of superparamagnetic iron oxide nanoparticles to orthotopic human breast tumor in mice. Pharm. Res. 1–10.
Khawar, I.A., Kim, J.H., Kuh, H.-J., 2015. Improving drug delivery to solid tumors: priming the tumor microenvironment. J. Controlled Release 201, 78–89.
Kievit, F.M., Zhang, M.Q., 2011. Cancer nanotheranostics: improving imaging and therapy by targeted delivery across biological barriers. Adv. Mater. 23, H217–H247.
Kim, T.-Y., Kim, D.-W., Chung, J.-Y., Shin, S.G., Kim, S.-C., Heo, D.S., et al., 2004. Phase I and pharmacokinetic study of Genexol-PM, a cremophor-free, polymeric micelle-formulated paclitaxel, in patients with advanced malignancies. Clin. Cancer Res. 10, 3708–3716.
Kim, M.S., Lee, D.-W., Park, K., Park, S.-J., Choi, E.-J., Park, E.S., et al., 2014a. Temperature-triggered tumor-specific delivery of anticancer agents by cRGD-conjugated thermosensitive liposomes. Colloids Surf. B: Biointerfaces 116, 17–25.
Kim, D.-H., Guo, Y., Zhang, Z., Procissi, D., Nicolai, J., Omary, R.A., et al., 2014b. Temperature-sensitive magnetic drug carriers for concurrent gemcitabine chemohyperthermia. Adv. Healthcare Mater. 3, 714–724.
Kim, H., Kim, S., Park, C., Lee, H., Park, H.J., Kim, C., 2016. Glutathione-induced intracellular release of guests from mesoporous silica nanocontainers with cyclodextrin gatekeepers. Adv. Mater. 22, 4280.
Kinnari, T.J., Esteban, J., Gomez-Barrena, E., Zamora, N., Fernandez-Roblas, R., Nieto, A., et al., 2009. Bacterial adherence to SiO(2)-based multifunctional bioceramics. J. Biomed. Mater. Res. A 89A, 215–223.
Kirpotin, D.B., Drummond, D.C., Shao, Y., Shalaby, M.R., Hong, K., Nielsen, U.B., et al., 2006. Antibody targeting of long-circulating lipidic nanoparticles does not increase tumor localization but does increase internalization in animal models. Cancer Res. 66, 6732–6740.
Knezevic, N.Z., Ruiz-Hernandez, E., Hennink, W.E., Vallet-Regi, M., 2013. Magnetic mesoporous silica-based core/shell nanoparticles for biomedical applications. RSC Adv. 3, 9584–9593.
Kobayashi, H., Watanabe, R., Choyke, P.L., 2014. Improving conventional enhanced permeability and retention (EPR) effects; what is the appropriate target? Theranostics 4, 81.
Kokuryo, D., Nakashima, S., Ozaki, F., Yuba, E., Chuang, K.-H., Aoshima, S., et al., 2015. Evaluation of thermo-triggered drug release in intramuscular-transplanted tumors using thermosensitive polymer-modified liposomes and MRI. Nanomed. Nanotechnol. Biol. Med. 11, 229–238.
Kong, G., Dewhirst, M.W., 1999. Hyperthermia and liposomes. Int. J. Hyperthermia 15, 345–370.
Kong, G., Anyarambhatla, G., Petros, W.P., Braun, R.D., Colvin, O.M., Needham, D., et al., 2000. Efficacy of liposomes and hyperthermia in a human tumor xenograft model: importance of triggered drug release. Cancer Res. 60, 6950–6957.
Kono, K., Hayashi, H., Takagishi, T., 1994. Temperature-sensitive liposomes: liposomes bearing poly (N-isopropylacrylamide). J. Controlled Release 30, 69–75.
Kono, K., Henmi, A., Yamashita, H., Hayashi, H., Takagishi, T., 1999a. Improvement of temperature-sensitivity of poly (N-isopropylacrylamide)-modified liposomes. J. Controlled Release 59, 63–75.
Kono, K., Nakai, R., Morimoto, K., Takagishi, T., 1999b. Thermosensitive polymer-modified liposomes that release contents around physiological temperature. Biochim. Biophys. Acta (BBA)-Biomembr. 1416, 239–250.
Kono, K., Murakami, T., Yoshida, T., Haba, Y., Kanaoka, S., Takagishi, T., et al., 2005. Temperature sensitization of liposomes by use of thermosensitive block copolymers synthesized by living cationic polymerization: effect of copolymer chain length. Bioconjugate Chem. 16, 1367–1374.
Kono, K., Ozawa, T., Yoshida, T., Ozaki, F., Ishizaka, Y., Maruyama, K., et al., 2010. Highly temperature-sensitive liposomes based on a thermosensitive block copolymer for tumor-specific chemotherapy. Biomaterials 31, 7096–7105.
Kono, K., Nakashima, S., Kokuryo, D., Aoki, I., Shimomoto, H., Aoshima, S., et al., 2011. Multi-functional liposomes having temperature-triggered release and magnetic resonance imaging for tumor-specific chemotherapy. Biomaterials 32, 1387–1395.
Kono, K., 2001. Thermosensitive polymer-modified liposomes. Adv. Drug Deliv. Rev. 53, 307–319.
Kowalczuk, A., Trzcinska, R., Trzebicka, B., Mueller, A.H.E., Dworak, A., Tsvetanov, C. B., 2014. Loading of polymer nanocarriers: factors, mechanisms and applications. Prog. Polym. Sci. 39, 43–86.
Krüger, H.R., Schütz, I., Justies, A., Licha, K., Welker, P., Haucke, V., et al., 2014. Imaging of doxorubicin release from theranostic macromolecular prodrugs via fluorescence resonance energy transfer. J. Controlled Release 194, 189–196.
Kresge, C.T., Leonowicz, M.E., Roth, W.J., Vartuli, J.C., Beck, J.S., 1992. Ordered mesoporous molecular-sieves synthesized by a liquid-crystal template mechanism. Nature 359, 710–712.
Kunjachan, S., Pola, R., Gremse, F., Theek, B., Ehling, J., Moeckel, D., et al., 2014a. Passive versus active tumor targeting using RGD- and NGR-Modified polymeric nanomedicines. Nano Lett. 14, 972–981.
Kunjachan, S., Pola, R., Gremse, F., Theek, B., Ehling, J., Moeckel, D., et al., 2014b. Passive versus active tumor targeting using RGD-and NGR-modified polymeric nanomedicines. Nano Lett. 14, 972–981.
Kuppusamy, P., Li, H., Ilangovan, G., Cardounel, A.J., Zweier, J.L., Yamada, K., et al., 2002. Noninvasive imaging of tumor redox status and its modification by tissue glutathione levels. Cancer Res. 62, 307–312.
Kutty, R.V., Chia, S.L., Setyawati, M.I., Muthu, M.S., Feng, S.-S., Leong, D.T., 2015. In vivo and ex vivo proofs of concept that cetuximab conjugated vitamin E TPGS micelles increases efficacy of delivered docetaxel against triple negative breast cancer. Biomaterials 63, 58–69.
López-Noriega, A., Hastings, C.L., Ozbakir, B., O'Donnell, K.E., O'Brien, F.J., Storm, G., et al., 2014. Hyperthermia-Induced drug delivery from thermosensitive liposomes encapsulated in an injectable hydrogel for local chemotherapy. Adv. Healthcare Mater. 3, 854–859.
Lafourcade, C., Sobo, K., Kieffer-Jaquinod, S., Garin, J., Van Der Goot, F.G., 2008. Regulation of the V-ATPase along the endocytic pathway occurs through reversible subunit association and membrane localization. PLoS One 3, e2758.
Lai, C.Y., Trewyn, B.G., Jeftinija, D.M., Jeftinija, K., Xu, S., Jeftinija, S., et al., 2003. A mesoporous silica nanosphere-based carrier system with chemically removable CdS nanoparticle caps for stimuli-responsive controlled release of neurotransmitters and drug molecules. J. Am. Chem. Soc. 125, 4451–4459.
Lammers, T., Kiessling, F., Hennink, W.E., Storm, G., 2012. Drug targeting to tumors: principles, pitfalls and (pre-) clinical progress. J. Controlled Release 161, 175–187.
Lammers, T., Koczera, P., Fokong, S., Gremse, F., Ehling, J., Vogt, M., et al., 2015. Theranostic USPIO-loaded microbubbles for mediating and monitoring blood-brain barrier permeation. Adv. Funct. Mater. 25, 36–43.
Landon, C.D., Park, J.Y., Needham, D., Dewhirst, M.W., 2011. Nanoscale drug delivery and hyperthermia: the materials design and preclinical and clinical testing of low temperature-sensitive liposomes used in combination with mild hyperthermia in the treatment of local cancer. Open Nanomed. J. 3, 38–64.
Lasic, D., Martin, F., Gabizon, A., Huang, S., Papahadjopoulos, D., 1991. Sterically stabilized liposomes: a hypothesis on the molecular origin of the extended circulation times. Biochim. Biophys. Acta (BBA)-Biomembr. 1070, 187–192.
Le Goff, G.C., Srinivas, R.L., Hill, W.A., Doyle, P.S., 2015. Hydrogel microparticles for biosensing. Eur. Polym. J. 386–412.
Lee, E.S., Shin, H.J., Na, K., Bae, Y.H., 2003. Poly(L-histidine)-PEG block copolymer micelles and pH-induced destabilization. J. Controlled Release 90, 363–374.
Lee, E.S., Na, K., Bae, Y.H., 2005. Doxorubicin loaded pH-sensitive polymeric micelles for reversal of resistant MCF-7 tumor. J. Controlled Release 103, 405–418.
Lee, K.S., Chung, H.C., Im, S.A., Park, Y.H., Kim, C.S., Kim, S.-B., et al., 2008a. Multicenter phase II trial of Genexol-PM, a cremophor-free, polymeric micelle formulation of paclitaxel, in patients with metastatic breast cancer. Breast Cancer Res. Treat. 108, 241–250.
Lee, M.-H., Lin, H.-Y., Chen, H.-C., Thomas, J.L., 2008b. Ultrasound mediates the release of curcumin from microemulsions. Langmuir 24, 1707–1713.
Lee, M.J., Ye, A.S., Gardino, A.K., Heijink, A.M., Sorger, P.K., MacBeath, G., et al., 2012. Sequential application of anticancer drugs enhances cell death by rewiring apoptotic signaling networks. Cell 149, 780–794.
Lee, S.Y., Park, H.S., Lee, K.Y., Kim, H.J., Jeon, Y.J., Jang, T.W., et al., 2013. Paclitaxel-loaded polymeric micelle (230 mg/m2) and cisplatin (60 mg/m2) vs. paclitaxel

(175 mg/m2) and cisplatin (60 mg/m2) in advanced non–small-cell lung cancer: a multicenter randomized Phase IIB trial. Clin. Lung Cancer 14, 275–282.
Lee, J.Y., Carugo, D., Crake, C., Owen, J., de Saint Victor, M., Seth, A., et al., 2015. Nanoparticle-loaded protein–polymer nanodroplets for improved stability and conversion efficiency in ultrasound imaging and drug delivery. Adv. Mater. 27, 5484–5492.
Leung, S.J., Romanowski, M., 2012. Light-activated content release from liposomes. Theranostics 2, 1020–1036.
Li, J., Huo, M., Wang, J., Zhou, J., Mohammad, J.M., Zhang, Y., et al., 2012. Redox-sensitive micelles self-assembled from amphiphilic hyaluronic acid-deoxycholic acid conjugates for targeted intracellular delivery of paclitaxel. Biomaterials 33, 2310–2320.
Li, J., Liu, F., Shao, Q., Min, Y., Costa, M., Yeow, E.K., et al., 2014a. Enzyme-responsive cell-penetrating peptide conjugated mesoporous silica quantum dot nanocarriers for controlled release of nucleus-targeted drug molecules and Real-Time intracellular fluorescence imaging of tumor cells. Adv. Healthcare Mater. 3, 1230–1239.
Li, Y., Lin T-y Luo, Y., Liu, Q., Xiao, W., Guo, W., et al., 2014b. A smart and versatile theranostic nanomedicine platform based on nanoporphyrin. Nat. Commun. 5.
Li, D., Kordalivand, N., Fransen, M.F., Ossendorp, F., Raemdonck, K., Vermonden, T., et al., 2015. Reduction-Sensitive dextran nanogels aimed for intracellular delivery of antigens. Adv. Funct. Mater. 25, 2993–3003.
Li, H.J., Du, J.Z., Du, X.J., Xu, C.F., Sun, C.Y., Wang, H.X., et al., 2016a. Stimuli-responsive clustered nanoparticles for improved tumor penetration and therapeutic efficacy. Proc. Natl. Acad. Sci. U. S. A. 113, 4164–4169.
Li, Y., Hei, M., Xu, Y., Qian, X., Zhu, W., 2016b. Ammonium salt modified mesoporous silica nanoparticles for dual intracellular-responsive gene delivery. Int. J. Pharm. 511, 689–702.
Liang, B., Tong, R., Wang, Z., Guo, S., Xia, H., 2014. High intensity focused ultrasound responsive metallo-supramolecular block copolymer micelles. Langmuir 30, 9524–9532.
Limmer, S., Hahn, J., Schmidt, R., Wachholz, K., Zengerle, A., Lechner, K., et al., 2014. Gemcitabine treatment of rat soft tissue sarcoma with phosphatidyldiglycerol-based thermosensitive liposomes. Pharm. Res. 31, 2276–2286.
Lin, Y.-S., Haynes, C.L., 2009. Synthesis and characterization of biocompatible and size-tunable multifunctional porous silica nanoparticles. Chem. Mater. 21, 3979–3986.
Lin, T., Zhang, Y., Wu, J., Zhao, X., Lian, H., Wang, W., et al., 2014. A floating hydrogel system capable of generating CO2 bubbles to diminish urinary obstruction after intravesical instillation. Pharm. Res. 31, 2655–2663.
Lin, C.-Y., Hsieh, H.-Y., Pitt, W.G., Huang, C.-Y., Tseng, I.-C., Yeh, C.-K., et al., 2015. Focused ultrasound-induced blood-brain barrier opening for non-viral, non-invasive, and targeted gene delivery. J. Controlled Release 212, 1–9.
Lindner, L.H., Eichhorn, M.E., Eibl, H., Teichert, N., Schmitt-Sody, M., Issels, R.D., et al., 2004. Novel temperature-sensitive liposomes with prolonged circulation time. Clin. Cancer Res. 10, 2168–2178.
Lindner, L.H., Hossann, M., Vogeser, M., Teichert, N., Wachholz, K., Eibl, H., et al., 2008. Dual role of hexadecylphosphocholine (miltefosine) in thermosensitive liposomes: active ingredient and mediator of drug release. J. Controlled Release 125, 112–120.
Lissa Nurrul Abdullah, E.K.H.C., 2013. Mechanisms of chemoresistance in cancer stem cells. Clin. Translat. Med. 2, 1–9.
Liu, S., Tong, Y., 2005. Yang Y-Y. Incorporation and in vitro release of doxorubicin in thermally sensitive micelles made from poly (N-isopropylacrylamide-co-N, N-dimethylacrylamide)-b-poly (D, L-lactide-co-glycolide) with varying compositions. Biomaterials 26, 5064–5074.
Liu, X., Zhang, J., Lynn, D.M., 2008. Polyelectrolyte multilayers fabricated from 'Charge-Shifting' anionic polymers: a new approach to controlled film disruption and the release of cationic agents from surfaces. Soft Matter 4, 1688–1695.
Liu, H., Chen, D., Li, L., Liu, T., Tan, L., Wu, X., et al., 2011. Multifunctional gold nanoshells on silica nanorattles: a platform for the combination of photothermal therapy and chemotherapy with low systemic toxicity. Angew. Chem. 123, 921–925.
Liu, J., Detrembleur, C., De Pauw-Gillet, M.-C., Mornet, S., Jerome, C., Duguet, E., 2015. Gold nanorods coated with mesoporous silica shell as drug delivery system for remote near infrared light-activated release and potential phototherapy. Small 11, 2323–2332.
Lopez-Noriega, A., Ruiz-Hernandez, E., Stevens, S.M., Arcos, D., Anderson, M.W., Terasaki, O., et al., 2009. Mesoporous microspheres with doubly ordered core-shell structure. Chem. Mater. 21, 18–20.
Lopez-Noriega, A., Ruiz-Hernandez, E., Quinlan, E., Storm, G., Hennink, W.E., O'Brien, F.J., 2014. Thermally triggered release of a pro-osteogenic peptide from a functionalized collagen-based scaffold using thermosensitive liposomes. J. Controlled Release 187, 158–166.
Lopez-Noriega, A., Arcos, D., Vallet-Regi, M., 2016. Functionalizing mesoporous bioglasses for long-Term anti-Osteoporotic drug delivery. Chem.– Eur. J. 16, 10879–10886.
Luten, J., van Nostrum, C.F., De Smedt, S.C., Hennink, W.E., 2008. Biodegradable polymers as non-viral carriers for plasmid DNA delivery. J. Controlled Release 126, 97–110.
Maeda, H., 2010. Tumor-selective delivery of macromolecular drugs via the EPR effect: background and future prospects. Bioconjugate Chem. 21, 797–802.
Maeda, H., 2013. The link between infection and cancer: tumor vasculature, free radicals, and drug delivery to tumors via the EPR effect. Cancer Sci. 104, 779–789.
Maeda, H., 2016. Tumor-Selective delivery of macromolecular drugs via the EPR effect: background and future prospects. Bioconjugate Chem. 21, 797–802.
Maeda, H., Matsumura, Y., 1989a. Tumoritropic and lymphotropic principles of macromolecular drugs. Crit. Rev. Ther. Drug Carrier Syst. 6, 193–210.
Maeda, H., Matsumura, Y., 1989b. Tumoritropic and lymphotropic principles of macromolecular drugs. Crit. Rev. Ther. Drug Carrier Syst. 6, 193–210.
Maeda, H., Seymour, L.W., Miyamoto, Y., 1992. Conjugates of anticancer agents and polymers – advantages of macromolecular therapeutics in vivo. Bioconjugate Chem. 3, 351–362.
Maeda, H., Wu, J., Sawa, T., Matsumura, Y., Hori, K., 2000a. Tumor vascular permeability and the EPR effect in macromolecular therapeutics: a review. J. Controlled Release 65, 271–284.
Maeda, H., Wu, J., Sawa, T., Matsumura, Y., Hori, K., 2000b. Tumor vascular permeability and the EPR effect in macromolecular therapeutics: a review. J. Controlled Release 65, 271–284.
Martin-Saavedra, F.M., Ruiz-Hernandez, E., Bore, A., Arcos, D., Vallet-Regi, M., Vilaboa, N., 2010. Magnetic mesoporous silica spheres for hyperthermia therapy. Acta Biomater. 6, 4522–4531.
Matsumura, Y., Maeda, H.A., 1986a. New concept for macromolecular therapeutics in cancer-chemotherapy – mechanism of tumoritropic accumulation of proteins and the antitumor agent smancs. Cancer Res. 46, 6387–6392.
Matsumura, Y., Maeda, H., 1986b. A new concept for macromolecular therapeutics in cancer chemotherapy: mechanism of tumoritropic accumulation of proteins and the antitumor agent smancs. Cancer Res. 46, 6387–6392.
Matsumura, Y., Hamaguchi, T., Ura, T., Muro, K., Yamada, Y., Shimada, Y., et al., 2004. Phase I. Clinical trial and pharmacokinetic evaluation of NK911, a micelle-encapsulated doxorubicin. Br. J. Cancer 91, 1775–1781.
May, J.P., Li, S.-D., 2013. Hyperthermia-induced drug targeting. Expert Opin. Drug Deliv. 10, 511–527.
May, J.P., Ernsting, M.J., Undzys, E., Li, S.-D., 2013. Thermosensitive liposomes for the delivery of gemcitabine and oxaliplatin to tumors. Mol. Pharm. 10, 4499–4508.
Meier, M.A., Lohmeijer, B.G., Schubert, U.S., 2003. Relative binding strength of terpyridine model complexes under matrix-assisted laser desorption/ionization mass spectrometry conditions. J. Mass Spectrom. 38, 510–516.
Meng, F., Hennink, W.E., Zhong, Z., 2009. Reduction-sensitive polymers and bioconjugates for biomedical applications. Biomaterials 30, 2180–2198.
Meng, H., Xue, M., Xia, T., Ji, Z., Tarn, D.Y., Zink, J.I., et al., 2016. Use of size and a copolymer design feature to improve the biodistribution and the enhanced permeability and retention effect of doxorubicin-loaded mesoporous silica nanoparticles in a murine xenograft tumor model. Acs Nano 5, 4131–4144.
Mills, J.K., Needham, D., 2005. Lysolipid incorporation in dipalmitoylphosphatidylcholine bilayer membranes enhances the ion permeability and drug release rates at the membrane phase transition. Biochim. Biophys. Acta 1716, 77–96.
Milosevic, M., Fyles, A., Hedley, D., Hill, R., 2004. The human tumor microenvironment: invasive (needle) measurement of oxygen and interstitial fluid pressure. Seminars in Radiation Oncology. Elsevier, pp. 249–258.
Mindell, J.A., 2012. Lysosomal acidification mechanisms. Annu. Rev. Physiol. 74, 69–86.
Mintzer, M.A., Simanek, E.E., 2008. Nonviral vectors for gene delivery. Chem. Rev. 109, 259–302.
Mo, R., Sun, Q., Xue, J.W., Li, N., Li, W.Y., Zhang, C., et al., 2012. Multistage pH-responsive liposomes for mitochondrial-targeted anticancer drug delivery. Adv. Mater. 24, 3659–3665.
Myoung, H., Hong, S.-D., Kim, Y.-Y., Hong, S.-P., Kim, M.-J., 2001. Evaluation of the anti-tumor and anti-angiogenic effect of paclitaxel and thalidomide on the xenotransplanted oral squamous cell carcinoma. Cancer Lett. 163, 191–200.
Nagahama, K., Sano, Y., Kumano, T., 2015. Anticancer drug-based multifunctional nanogels through self-assembly of dextran–curcumin conjugates toward cancer theranostics. Bioorg. Med. Chem. Lett. 25, 2519–2522.
Nakopoulou, L., Tsirmpa, I., Alexandrou, P., Louvrou, A., Ampela, C., Markaki, S., et al., 2003. MMP-2 protein in invasive breast cancer and the impact of MMP-2/TIMP-2 phenotype on overall survival. Breast Cancer Res. Treat. 77, 145–155.
Needham, D., Dewhirst, M.W., 2001. The development and testing of a new temperature-sensitive drug delivery system for the treatment of solid tumors. Adv. Drug Deliv. Rev. 53, 285–305.
Needham, D., Anyarambhatla, G., Kong, G., Dewhirst, M.W., 2000. A new temperature-sensitive liposome for use with mild hyperthermia: characterization and testing in a human tumor xenograft model. Cancer Res. 60, 1197–1201.
Needham, D., Park, J.-Y., Wright, A.M., Tong, J., 2013. Materials characterization of the low temperature sensitive liposome (LTSL): effects of the lipid composition (lysolipid and DSPE–PEG2000) on the thermal transition and release of doxorubicin. Faraday Discuss. 161, 515–534.
Needham, D., 2013. Reverse engineering of the low temperature-sensitive liposome (LTSL) for treating cancer. Park, K. (Ed.), Biomater. Cancer Ther. Diagn.Prevent. Ther. 270–348.
Negussie, A.H., Yarmolenko, P.S., Partanen, A., Ranjan, A., Jacobs, G., Woods, D., et al., 2011. Formulation and characterisation of magnetic resonance imageable thermally sensitive liposomes for use with magnetic resonance-guided high intensity focused ultrasound. Int. J. Hyperthermia 27, 140–155.
Ng, L.-T., Yuba, E., Kono, K., 2009. Modification of liposome surface with pH-responsive polyampholytes for the controlled-release of drugs. Res. Chem. Intermed. 35, 1015–1025.
Nomoto, T., Fukushima, S., Kumagai, M., Machitani, K., Matsumoto, Y., Oba, M., et al., 2014. Three-layered polyplex micelle as a multifunctional nanocarrier platform for light-induced systemic gene transfer. Nat. Commun. 5.

Nunez-Lozano, R., Cano, M., Pimentel, B., de la Cueva-Mendez, G., 2015. 'Smartening' anticancer therapeutic nanosystems using biomolecules. Curr. Opin. Biotechnol. 35, 135–140.
O'brien, M., Wigler, N., Inbar, M., Rosso, R., Grischke, E., Santoro, A., et al., 2004. Reduced cardiotoxicity and comparable efficacy in a phase III trial of pegylated liposomal doxorubicin HCl (CAELYX™/Doxil®) versus conventional doxorubicin for first-line treatment of metastatic breast cancer. Ann. Oncol. 15, 440–449.
Obata, Y., Tajima, S., Takeoka, S., 2010. Evaluation of pH-responsive liposomes containing amino acid-based zwitterionic lipids for improving intracellular drug delivery in vitro and in vivo. J. Controlled Release 142, 267–276.
Oerlemans, C., Bult, W., Bos, M., Storm, G., Nijsen, J.F.W., Hennink, W.E., 2010. Polymeric micelles in anticancer therapy: targeting, imaging and triggered release. Pharm. Res. 27, 2569–2589.
Oishi, M., Nagasaki, Y., 2010. Stimuli-responsive smart nanogels for cancer diagnostics and therapy. Nanomedicine 5, 451–468.
Ojha, T., Rizzo, L., Storm, G., Kiessling, F., Lammers, T., 2015. Image-guided drug delivery: preclinical applications and clinical translation. Expert Opin. Drug Deliv. 12, 1203–1207.
Ojugo, A.S., McSheehy, P.M., McIntyre, D.J., McCoy, C., Stubbs, M., Leach, M.O., et al., 1999. Measurement of the extracellular pH of solid tumours in mice by magnetic resonance spectroscopy: a comparison of exogenous 19F and 31P probes. NMR Biomed. 12, 495–504.
Oliver Jonas, H.M.L., Jason Fuller, E., John Santini Jr., T., Jose Baselga, Robert Tepper, I., Michael, J., Cima, Robert Langer, 2015. An implantable microdevice to perform high-throughput in vivo drug sensitivity testing in tumors. Sci. Transl. Med. 7, 1–11.
Ong, W., Yang, Y.M., Cruciano, A.C., McCarley, R.L., 2008. Redox-Triggered contents release from liposomes. J. Am. Chem. Soc. 130, 14739–14744.
Pérez-Herrero, E., Fernández-Medarde, A., 2015. Advanced targeted therapies in cancer: drug nanocarriers, the future of chemotherapy. Eur. J. Pharm. Biopharm. 93, 52–79.
Palumbo, G., 2007. Photodynamic therapy and cancer a brief sightseeing tour. Expert Opin. Drug Deliv. 4, 131–148.
Park, C., Kim, H., Kim, S., Kim, C., 2009a. Enzyme responsive nanocontainers with cyclodextrin gatekeepers and synergistic effects in release of guests. J. Am. Chem. Soc. 131, 16614.
Park, C., Lee, K., Kim, C., 2009b. Photoresponsive cyclodextrin-covered nanocontainers and their sol-gel transition induced by molecular recognition. Angew. Chem. Int. Ed. 48, 1275–1278.
Park, Y.I., Kim, H.M., Kim, J.H., Moon, K.C., Yoo, B., Lee, K.T., et al., 2012. Theranostic probe based on Lanthanide-doped nanoparticles for simultaneous In vivo Dual-Modal imaging and photodynamic therapy. Adv. Mater. 24, 5755–5761.
Park, S.M., Kim, M.S., Park, S.-J., Park, E.S., Choi, K.-S., Kim, Y.-s., et al., 2013. Novel temperature-triggered liposome with high stability: formulation, in vitro evaluation, and in vivo study combined with high-intensity focused ultrasound (HIFU). J. Controlled Release 170, 373–379.
Park, J.-H., von Maltzahn, G., Xu, M.J., Fogal, V., Kotamraju, V.R., Ruoslahti, E., et al., 2016. Cooperative nanomaterial system to sensitize, target, and treat tumors. Proc. Natl. Acad. Sci. U. S. A. 107, 981–986.
Park, K., 2010. To PEGylate or not to PEGylate, that is not the question. J. Controlled Release 142, 147–148.
Pashkovskaya, A., Kotova, E., Zorlu, Y., Dumoulin, F., Ahsen, V., Agapov, I., et al., 2010. Light-Triggered liposomal release: membrane permeabilization by photodynamic action. Langmuir 26, 5726–5733.
Pelicano, H., Carney, D., Huang, P., 2004. ROS stress in cancer cells and therapeutic implications. Drug Resist. Updat. 7, 97–110.
Peng, J., Qi, T., Liao, J., Chu, B., Yang, Q., Li, W., et al., 2013. Controlled release of cisplatin from pH-thermal dual responsive nanogels. Biomaterials 34, 8726–8740.
Phillips, E., Penate-Medina, O., Zanzonico, P.B., Carvajal, R.D., Mohan, P., Ye, Y.P., et al., 2014. Clinical translation of an ultrasmall inorganic optical-PET imaging nanoparticle probe. Sci. Transl. Med. 6, 9.
Plummer, R., Wilson, R., Calvert, H., Boddy, A., Griffin, M., Sludden, J., et al., 2011. A Phase I. Clinical study of cisplatin-incorporated polymeric micelles (NC-6004) in patients with solid tumours. Br. J. Cancer 104, 593–598.
Popovic, Z., Liu, W., Chauhan, V.P., Lee, J., Wong, C., Greytak, A.B., et al., 2016. A nanoparticle size series for In vivo fluorescence imaging. Angew. Chem. Int. Ed. 49, 8649–8652.
Provenzano, P.P., Cuevas, C., Chang, A.E., Goel, V.K., Von Hoff, D.D., Hingorani, S.R., 2012. Enzymatic targeting of the stroma ablates physical barriers to treatment of pancreatic ductal adenocarcinoma. Cancer Cell 21, 418–429.
Qian, X., Wang, W., Kong, W., Chen, Y., 2014. Hollow periodic mesoporous organosilicas for highly efficient HIFU-based synergistic therapy. RSC Adv. 4, 17950–17958.
Raemdonck, K., Demeester, J., De Smedt, S., 2009a. Advanced nanogel engineering for drug delivery. Soft Matter 5, 707–715.
Raemdonck, K., Naeye, B., Buyens, K., Vandenbroucke, R.E., Høgset, A., Demeester, J., et al., 2009b. Biodegradable dextran nanogels for RNA interference: focusing on endosomal escape and intracellular siRNA delivery. Adv. Funct. Mater. 19, 1406–1415.
Ranson, M.R., Carmichael, J., O'Byrne, K., Stewart, S., Smith, D., Howell, A., 1997. Treatment of advanced breast cancer with sterically stabilized liposomal doxorubicin: results of a multicenter phase II trial. J. Clin. Oncol. 15, 3185–3191.
Rapoport, N., Nam, K.-H., Gupta, R., Gao, Z., Mohan, P., Payne, A., et al., 2011. Ultrasound-mediated tumor imaging and nanotherapy using drug loaded, block copolymer stabilized perfluorocarbon nanoemulsions. J. Controlled Release 153, 4–15.
Rapoport, N., 2012. Phase-shift, stimuli-responsive perfluorocarbon nanodroplets for drug delivery to cancer. Wiley Interdiscip. Rev. Nanomed. Nanobiotechnol. 4, 492–510.
Rigaux, G., Roullin, V., Cadiou, C., Portefaix, C., Van Gulick, L., Bœuf, G., et al., 2014. A new magnetic resonance imaging contrast agent loaded into poly (lacide-co-glycolide) nanoparticles for long-term detection of tumors. Nanotechnology 25, 445103.
Rijcken, C.J., Snel, C.J., Schiffelers, R.M., van Nostrum, C.F., Hennink, W.E., 2007. Hydrolysable core-crosslinked thermosensitive polymeric micelles: synthesis, characterisation and in vivo studies. Biomaterials 28, 5581–5593.
Rijcken, C., 2007. Tuneable & degradable polymeric micelles for drug delivery: from synthesis to feasibility in vivo. Doctoral Dissertation. Utrecht University, Utrecht.
Robert, N., Leyland-Jones, B., Asmar, L., Belt, R., Ilegbodu, D., Loesch, D., et al., 2006. Randomized phase III study of trastuzumab, paclitaxel, and carboplatin compared with trastuzumab and paclitaxel in women with HER-2-overexpressing metastatic breast cancer. J. Clin. Oncol. 24, 2786–2792.
Roti Roti, J.L., 2008. Cellular responses to hyperthermia (40–46 degrees C): cell killing and molecular events. Int. J. Hyperthermia 24, 3–15.
Ruel-Gariepy, E., Chenite, A., Chaput, C., Guirguis, S., Leroux, J.-C., 2000. Characterization of thermosensitive chitosan gels for the sustained delivery of drugs. Int. J. Pharm. 203, 89–98.
Ruiz-Hernández, E., López-Noriega, A., Arcos, D., Vallet-Regí, M., 2010. Multifunctional nano and microparticles for drug delivery systems. Key Eng. Mater. Trans. Tech. Publ. 333–355.
Ruiz-Hernandez, E., Lopez-Noriega, A., Arcos, D., Izquierdo-Barba, I., Terasaki, O., Vallet-Regi, M., 2007. Aerosol-assisted synthesis of magnetic mesoporous silica spheres for drug targeting. Chem. Mater. 19, 3455–3463.
Ruiz-Hernandez, E., Lopez-Noriega, A., Arcos, D., Vallet-Regi, M., 2008. Mesoporous magnetic microspheres for drug targeting. Solid State Sci. 10, 421–426.
Ruiz-Hernandez, E., Baeza, A., Vallet-Regi, M., 2011. Smart drug delivery through DNA/Magnetic nanoparticle gates. ACS Nano 5, 1259–1266.
Ruiz-Hernandez, E., Hess, M., Melen, G.J., Theek, B., Talelli, M., Shi, Y., et al., 2014. PEG-pHPMAm-based polymeric micelles loaded with doxorubicin-prodrugs in combination antitumor therapy with oncolytic vaccinia viruses. Polym. Chem. 5, 1674–1681.
Ruoslahti, E., Bhatia, S.N., Sailor, M.J., 2010. Targeting of drugs and nanoparticles to tumors. J. Cell Biol. 188, 759–768.
Saleem, Q., Zhang, Z., Gradinaru, C.C., Macdonald, P.M., 2013. Liposome-coated hydrogel spheres: delivery vehicles with tandem release from distinct compartments. Langmuir 29, 14603–14612.
Sandstrom, M.C., Ickenstein, L.M., Mayer, L.D., Edwards, K., 2005. Effects of lipid segregation and lysolipid dissociation on drug release from thermosensitive liposomes. J. Controlled Release 107, 131–142.
Savic, R., Azzam, T., Eisenberg, A., Maysinger, D., 2006. Assessment of the integrity of poly(caprolactone)-b-poly(ethylene oxide) micelles under biological conditions: a fluorogenic-based approach. Langmuir 22, 3570–3578.
Schwendener, A.R., 2014. Liposomes as vaccine delivery systems: a review of recent advances. Ther. Adv. Vaccines 2, 159–182.
Serrano, M.C., Portoles, M.T., Pagani, R., De Guinoa, J.S., Ruiz-Hernandez, E., Arcos, D., et al., 2008. In vitro positive biocompatibility evaluation of glass–glass ceramic thermoseeds for hyperthermic treatment of bone tumors. Tissue Eng. Part A 14, 617–627.
Seymour, L.W., 1992. Passive tumor targeting of soluble macromolecules and drug conjugates. Crit. Rev. Ther. Drug Carrier Syst. 9, 135–187.
Sheeran, P.S., Rojas, J.D., Puett, C., Hjelmquist, J., Arena, C.B., Dayton, P.A., 2015. Contrast-enhanced ultrasound imaging and in vivo circulatory kinetics with low-boiling-point nanoscale phase-change perfluorocarbon agents. Ultrasound Med. Biology 41, 814–831.
Shi, Y., van Steenbergen, M.J., Teunissen, E.A., Novo, L.S., Gradmann, S., Baldus, M., et al., 2013. Π–Π stacking increases the stability and loading capacity of thermosensitive polymeric micelles for chemotherapeutic drugs. Biomacromolecules 14, 1826–1837.
Shi, Y., van der Meel, R., Theek, B., Oude Blenke, E., Pieters, E.H., Fens, M.H., et al., 2015. Complete regression of xenograft tumors upon targeted delivery of paclitaxel via Π–Π stacking stabilized polymeric micelles. ACS Nano 9, 3740–3752.
Shirakura, T., Kelson, T.J., Ray, A., Malyarenko, A.E., Kopelman, R., 2014. Hydrogel nanoparticles with thermally controlled drug release. ACS Macro Lett. 3, 602–606.
Siddash, D., Patil, D.G.R., Burgess, Diane J., 2005. DNA based therapeutics and DNA delivery systems: a comprehensive review. AAPS J. 1, E61–E77.
Sigward, E., Corvis, Y., Doan, B.-T., Kindsiko, K., Seguin, J., Scherman, D., et al., 2015. Preparation and evaluation of multiple nanoemulsions containing gadolinium (III) chelate as a potential magnetic resonance imaging (MRI) contrast agent. Pharm. Res. 1–12.
Singla, A.K., Garg, A., Aggarwal, D., 2002. Paclitaxel and its formulations. Int. J. Pharm. 235, 179–192.
Sirivisoot, S., Harrison, B.S., 2015. Magnetically stimulated ciprofloxacin release from polymeric microspheres entrapping iron oxide nanoparticles. Int. J. Nanomed. 10, 4447.
Slowing, I., Trewyn, B.G., Lin, V.S.Y., 2006. Effect of surface functionalization of MCM-41-type mesoporous silica nanoparticleson the endocytosis by human cancer cells. J. Am. Chem. Soc. 128, 14792–14793.

Slowing, I.I., Wu, C.-W., Vivero-Escoto, J.L., Lin, V.S.Y., 2009. Mesoporous silica nanoparticles for reducing hemolytic activity towards mammalian red blood cells. Small 5, 57–62.
Smith, C.A., de la Fuente, J., Pelaz, B., Furlani, E.P., Mullin, M., Berry, C.C., 2010. The effect of static magnetic fields and tat peptides on cellular and nuclear uptake of magnetic nanoparticles. Biomaterials 31, 4392–4400.
Staruch, R.M., Ganguly, M., Tannock, I.F., Hynynen, K., Chopra, R., 2012. Enhanced drug delivery in rabbit VX2 tumours using thermosensitive liposomes and MRI-controlled focused ultrasound hyperthermia. Int. J. Hyperthermia 28, 776–787.
Staruch, R.M., Hynynen, K., Chopra, R., 2015. Hyperthermia-mediated doxorubicin release from thermosensitive liposomes using MR-HIFU: therapeutic effect in rabbit Vx2 tumours. Int. J. Hyperthermia 31, 118–133.
Stolzoff, M., Ekladious, I., Colby, A.H., Colson, Y.L., Porter, T.M., Grinstaff, M.W., 2015. Synthesis and characterization of hybrid polymer/lipid expansile nanoparticles: imparting surface functionality for targeting and stability. Biomacromolecules 16, 1958–1966.
Stubbs, M., McSheehy, P.M., Griffiths, J.R., Bashford, C.L., 2000. Causes and consequences of tumour acidity and implications for treatment. Mol. Med. Today 6, 15–19.
Sudimack, J., Lee, R.J., 2000. Targeted drug delivery via the folate receptor. Adv. Drug Deliv. Rev. 41, 147–162.
Szakács, G., Paterson, J.K., Ludwig, J.A., Booth-Genthe, C., Gottesman, M.M., 2006. Targeting multidrug resistance in cancer. Nat. Rev. Drug Discov. 5, 219–234.
Ta, T., Convertine, A.J., Reyes, C.R., Stayton, P.S., Porter, T.M., 2010. Thermosensitive liposomes modified with poly (N-isopropylacrylamide-co-propylacrylic acid) copolymers for triggered release of doxorubicin. Biomacromolecules 11, 1915–1920.
Tagami, T., Ernsting, M.J., Li, S.D., 2011a. Efficient tumor regression by a single and low dose treatment with a novel and enhanced formulation of thermosensitive liposomal doxorubicin. J. Controlled Release 152, 303–309.
Tagami, T., Ernsting, M.J., Li, S.D., 2011b. Optimization of a novel and improved thermosensitive liposome formulated with DPPC and a Brij surfactant using a robust in vitro system. J. Controlled Release 154, 290–297.
Tagami, T., Foltz, W.D., Ernsting, M.J., Lee, C.M., Tannock, I.F., May, J.P., et al., 2011c. MRI monitoring of intratumoral drug delivery and prediction of the therapeutic effect with a multifunctional thermosensitive liposome. Biomaterials 32, 6570–6578.
Tagami, T., May, J.P., Ernsting, M.J., Li, S.-D., 2012. A thermosensitive liposome prepared with a Cu2+ gradient demonstrates improved pharmacokinetics, drug delivery and antitumor efficacy. J. Controlled Release 161, 142–149.
Tailor, T.D., Hanna, G., Yarmolenko, P.S., Dreher, M.R., Betof, A.S., Nixon, A.B., et al., 2010. Effect of pazopanib on tumor microenvironment and liposome delivery. Mol. Cancer Ther. 9, 1798–1808.
Talelli, M., Iman, M., Varkouhi, A.K., Rijcken, C.J.F., Schiffelers, R.M., Etrych, T., et al., 2010a. Core-crosslinked polymeric micelles with controlled release of covalently entrapped doxorubicin. Biomaterials 31, 7797–7804.
Talelli, M., Iman, M., Varkouhi, A.K., Rijcken, C.J., Schiffelers, R.M., Etrych, T., et al., 2010b. Core-crosslinked polymeric micelles with controlled release of covalently entrapped doxorubicin. Biomaterials 31, 7797–7804.
Talelli, M., Rijcken, C.J.F., Oliveira, S., van der Meel, R., Henegouwen, P.M.P.v.B.E., Lammers, T., et al., 2011. Nanobody – shell functionalized thermosensitive core-crosslinked polymeric micelles for active drug targeting. J. Controlled Release 151, 183–192.
Talelli, M., Oliveira, S., Rijcken, C.J.F., Pieters, E.H.E., Etrych, T., Ulbrich, K., et al., 2013. Intrinsically active nanobody-modified polymeric micelles for tumor-targeted combination therapy. Biomaterials 34, 1255–1260.
Talelli, M., Barz, M., Rijcken, C.J., Kiessling, F., Hennink, W.E., Lammers, T., 2015. Core-crosslinked polymeric micelles: principles, preparation, biomedical applications and clinical translation. Nano Today 10, 93–117.
Tamura, A., Oishi, M., Nagasaki, Y., 2009. Enhanced cytoplasmic delivery of siRNA using a stabilized polyion complex based on PEGylated nanogels with a cross-linked polyamine structure. Biomacromolecules 10, 1818–1827.
Tannock, I.F., Rotin, D., 1989. Acid pH in tumors and its potential for therapeutic exploitation. Cancer Res. 49, 4373–4384.
Theek, B., Gremse, F., Kunjachan, S., Fokong, S., Pola, R., Pechar, M., et al., 2014. Characterizing EPR-mediated passive drug targeting using contrast-enhanced functional ultrasound imaging. J. Controlled Release 182, 83–89.
Thrall, D.E., Prescott, D.M., Samulski, T.V., Dewhirst, M.W., Cline, J.M., Lee, J., et al., 1992. Serious toxicity associated with annular microwave array induction of whole-body hyperthermia in normal dogs. Int. J. Hyperthermia 8, 23–32.
Topete, A., Alatorre-Meda, M., Iglesias, P., Villar-Alvarez, E.M., Barbosa, S., Costoya, J. A., et al., 2014. Fluorescent drug-loaded, polymeric-based, branched gold nanoshells for localized multimodal therapy and imaging of tumoral cells. ACS Nano 8, 2725–2738.
Topp, M.D.C., Dijkstra, P.J., Talsma, H., Feijen, J., 1997. Thermosensitive micelle-forming block copolymers of poly(ethylene glycol) and poly(N-isopropylacrylamide). Macromolecules 30, 8518–8520.
Torchilin, V.P., Omelyanenko, V.G., Papisov, M.I., Bogdanov, A.A., Trubetskoy, V.S., Herron, J.N., et al., 1994. Poly (ethylene glycol) on the liposome surface: on the mechanism of polymer-coated liposome longevity. Biochim. Biophys. Acta (BBA)-Biomembr. 1195, 11–20.
Turley, R.S., Fontanella, A.N., Padussis, J.C., Toshimitsu, H., Tokuhisa, Y., Cho, E.H., et al., 2012. Bevacizumab-induced alterations in vascular permeability and drug delivery: a novel approach to augment regional chemotherapy for in-transit melanoma. Clin. Cancer Res. 18, 3328–3339.
Vallet-Regi, M., Ruiz-Hernandez, E., 2011. Bioceramics from bone regeneration to cancer nanomedicine. Adv. Mater. 23, 5177–5218.
Vallet-Regi, M., Ramila, A., del Real, R.P., Perez-Pariente, J., 2001. A new property of MCM-41: drug delivery system. Chem. Mater. 13, 308–311.
Vallet-Regi, M., Ruiz-Hernandez, E., Gonzalez, B., Baeza, A., 2011. Design of smart nanomaterials for drug and gene delivery. J. Biomater. Tissue Eng. 1, 6–29.
Van der Veldt, A.A., Lubberink, M., Bahce, I., Walraven, M., de Boer, M.P., Greuter, H. N., et al., 2012. Rapid decrease in delivery of chemotherapy to tumors after anti-VEGF therapy: implications for scheduling of anti-angiogenic drugs. Cancer Cell 21, 82–91.
van Elk, M., Deckers, R., Oerlemans, C., Shi, Y., Storm, G., Vermonden, T., et al., 2014. Triggered release of doxorubicin from temperature-sensitive poly(N-(2-hydroxypropyl)-methacrylamide mono/dilactate) grafted liposomes. Biomacromolecules 15, 1002–1009.
van Elk, M., Lorenzato, C., Ozbakir, B., Oerlemans, C., Storm, G., Nijsen, F., et al., 2015. Alginate microgels loaded with temperature sensitive liposomes for magnetic resonance imageable drug release and microgel visualization. Eur. Polym. J..
van der Meel, R., Vehmeijer, L.J., Kok, R.J., Storm, G., van Gaal, E.V., 2013. Ligand-targeted particulate nanomedicines undergoing clinical evaluation: current status. Adv. Drug Deliv. Rev. 65, 1284–1298.
von Maltzahn, G., Park, J.-H., Lin, K.Y., Singh, N., Schwoeppe, C., Mesters, R., et al., 2016. Nanoparticles that communicate in vivo to amplify tumour targeting. Nat. Mater. 10, 545–552.
Venditto, V.J., Szoka Jr., F.C., 2016. Cancer nanomedicines: so many papers and so few drugs!. Adv. Drug Deliv. Rev. 65, 80–88.
Vermonden, T., Censi, R., Hennink, W.E., 2012. Hydrogels for protein delivery. Chem. Rev. 112, 2853–2888.
Wang, C.H., Hsiue, G.H., 2003. New Amphiphilic poly(2-ethyl-2-oxazoline)/poly(L-lactide) triblock copolymers. Biomacromolecules 4, 1487–1490.
Wang, T., Hossann, M., Reinl, H.M., Peller, M., Eibl, H., Reiser, M., et al., 2008. In vitro characterization of phosphatidylglyceroglycerol-based thermosensitive liposomes with encapsulated 1H MR T1-shortening gadodiamide. Contrast Media Mol. Imaging 3, 19–26.
Wang, C., Henkes, L.M., Doughty, L.B., He, M., Wang, D., Meyer-Almes, F.-J., et al., 2011. Thailandepsins: bacterial products with potent histone deacetylase inhibitory activities and broad-spectrum antiproliferative activities. J. Nat. Prod. 74, 2031–2038.
Wang, A.Z., Langer, R., Farokhzad, O.C., 2012. Nanoparticle delivery of cancer drugs. Annu. Rev. Med. 63, 185–198.
Wang, H., Yi, J., Mukherjee, S., Banerjee, P., Zhou, S., 2014. Magnetic/NIR-thermally responsive hybrid nanogels for optical temperature sensing, tumor cell imaging and triggered drug release. Nanoscale 6, 13001–13011.
Wang, Z., Sun, J., Qiu, Y., Li, W., Guo, X., Li, Q., et al., 2015. Specific photothermal therapy to the tumors with high EphB4 receptor expression. Biomaterials 68, 32–41.
Wani, T.U., Rashid, M., Kumar, M., Chaudhary, S., Kumar, P., Mishra, N., 2014. Targeting aspects of nanogels: an overview. Int. J. Pharm. Sci. Nanotechnol. 7, 2612–2630.
Weiss, V., Argyo, C., Torrano, A.A., Strobel, C., Mackowiak, S.A., Schmidt, A., et al., 2016. Dendronized mesoporous silica nanoparticles provide an internal endosomal escape mechanism for successful cytosolic drug release. Microporous Mesoporous Mater. 227, 242–251.
Wicki, A., Witzigmann, D., Balasubramanian, V., Huwyler, J., 2015a. Nanomedicine in cancer therapy: challenges, opportunities, and clinical applications. J. Controlled Release 200, 138–157.
Wicki, A., Witzigmann, D., Balasubramanian, V., Huwyler, J., 2015b. Nanomedicine in cancer therapy: challenges, opportunities, and clinical applications. J. Control. Release 200, 138–157.
Winter, N.D., Murphy, R.K.J., O'Halloran, T.V., Schatz, G.C., 2011. Development and modeling of arsenic-trioxide-loaded thermosensitive liposomes for anticancer drug delivery. J. Liposome Res. 21, 106–115.
Wu, G., Fang, Y.-Z., Yang, S., Lupton, J.R., Turner, N.D., 2004. Glutathione metabolism and its implications for health. J. Nutr. 134, 489–492.
Wu, Y., Chen, W., Meng, F., Wang, Z., Cheng, R., Deng, C., et al., 2012. Core-crosslinked pH-sensitive degradable micelles: a promising approach to resolve the extracellular stability versus intracellular drug release dilemma. J. Controlled Release 164, 338–345.
Wu, L., Zou, Y., Deng, C., Cheng, R., Meng, F., Zhong, Z., 2013. Intracellular release of doxorubicin from core-crosslinked polypeptide micelles triggered by both pH and reduction conditions. Biomaterials 34, 5262–5272.
Wu, S.-Y., Chen, C.C., Tung, Y.-S., Olumolade, O.O., Konofagou, E.E., 2015. Effects of the microbubble shell physicochemical properties on ultrasound-mediated drug delivery to the brain. J. Controlled Release 212, 30–40.
Wu, M., Meng, Q., Chen, Y., Zhang, L., Li, M., Cai, X., et al., 2016. Large pore-sized hollow mesoporous organosilica for redox-responsive gene delivery and synergistic cancer chemotherapy. Adv. Mater. 28, 1963-.
Xiao, K., Li, Y.-P., Wang, C., Ahmad, S., Vu, M., Kuma, K., et al., 2015. Disulfide cross-linked micelles of novel HDAC inhibitor thailandepsin A for the treatment of breast cancer. Biomaterials 67, 183–193.
Xu, J., Zeng, F., Wu, H., Hu, C., Wu, S., 2014. Enhanced photodynamic efficiency achieved via a dual-targeted strategy based on photosensitizer/micelle structure. Biomacromolecules 15, 4249–4259.
Xu, J., Zeng, F., Wu, H., Yu, C., Wu, S., 2015. Dual-targeting nanosystem for enhancing photodynamic therapy efficiency. ACS Appl. Mater. Interfaces 7, 9287–9296.
Yamada, H., Urata, C., Ujiie, H., Yamauchi, Y., Kuroda, K., 2016. Preparation of aqueous colloidal mesostructured and mesoporous silica nanoparticles with controlled particle size in a very wide range from 20 nm to 700 nm. Nanoscale 5, 6145–6153.

Yanes, R.E., Tarn, D., Hwang, A.A., Ferris, D.P., Sherman, S.P., Thomas, C.R., et al., 2016. Involvement of lysosomal exocytosis in the excretion of mesoporous silica nanoparticles and enhancement of the drug delivery effect by exocytosis inhibition. Small 9, 697–704.
Yang, H., Wang, Q., Chen, W., Zhao, Y., Yong, T., Gan, L., et al., 2015a. Hydrophilicity/Hydrophobicity reversable and redox-sensitive nanogels for anticancer drug delivery. Mol. Pharm. 12, 1636–1647.
Yang, K., Luo, H., Zeng, M., Jiang, Y., Li, J., Fu, X., 2015b. Intracellular pH-triggered, targeted drug delivery to cancer cells by multifunctional envelope-type mesoporous silica nanocontainers. ACS Appl. Mater. Interfaces .
Yang, W., Zou, Y., Meng, F., Zhang, J., Cheng, R., Deng, C., et al., 2016. Efficient and targeted suppression of human lung tumor xenografts in mice with methotrexate sodium encapsulated in all-Function-in-One chimeric polymersomes. Adv. Mater. (Deerfield Beach, Fla) .
Yao, H., Wang, K., Wang, Y., Wang, S., Li, J., Lou, J., et al., 2015. Enhanced blood–brain barrier penetration and glioma therapy mediated by a new peptide modified gene delivery system. Biomaterials 37, 345–352.
Yarmolenko, P.S., Zhao, Y., Landon, C., Spasojevic, I., Yuan, F., Needham, D., et al., 2010. Comparative effects of thermosensitive doxorubicin-containing liposomes and hyperthermia in human and murine tumours. Int. J. Hyperthermia 26, 485–498.
Yatvin, M.B., Weinstein, J.N., Dennis, W.H., Blumenthal, R., 1978. Design of liposomes for enhanced local release of drugs by hyperthermia. Science 202, 1290–1293.
Yatvin, M.B., Muhlensiepen, H., Porschen, W., Weinstein, J.N., Feinendegen, L.E., 1981. Selective delivery of liposome-associated cis-dichlorodiammineplatinum (II) by heat and its influence on tumor drug uptake and growth. Cancer Res. 41, 1602–1607.
Yu, P., Yu, H., Guo, C., Cui, Z., Chen, X., Yin, Q., et al., 2015. Reversal of doxorubicin resistance in breast cancer by mitochondria-targeted pH-responsive micelles. Acta Biomater. 14, 115–124.
Yuan, F., Quan, L.-d., Cui, L., Goldring, S.R., Wang, D., 2012. Development of macromolecular prodrug for rheumatoid arthritis. Adv. Drug Deliv. Rev. 64, 1205–1219.
Yuan, Y., Zhang, C.J., Liu, B., 2015. A photoactivatable AIE polymer for light-controlled gene delivery: concurrent endo/lysosomal escape and DNA unpacking. Angew. Chem. Int. Ed..
Zellmer, V.R., Zhang, S., 2014. Evolving concepts of tumor heterogeneity. Cell Biosci. 4, 69.
Zeng, Y., Pitt, W.G., 2005. Poly (ethylene oxide)-b-poly (N-isopropylacrylamide) nanoparticles with cross-linked cores as drug carriers Journal of Biomaterials Science. Polym. Ed. 16, 371–380.
Zhang, W., Shi, L., Wu, K., An, Y., 2005. Thermoresponsive micellization of poly (ethylene glycol)-b-poly (N-isopropylacrylamide) in water. Macromolecules 38, 5743–5747.
Zhang, X., Zeng, X., Liang, X., Yang, Y., Li, X., Chen, H., et al., 2014. The chemotherapeutic potential of PEG-b-PLGA copolymer micelles that combine chloroquine as autophagy inhibitor and docetaxel as an anti-cancer drug. Biomaterials 35, 9144–9154.
Zhang, J., Zhang, M., Ji, J., Fang, X., Pan, X., Wang, Y., et al., 2015a. Glycyrrhetinic acid-mediated polymeric drug delivery targeting the acidic microenvironment of hepatocellular carcinoma. Pharm. Res. 1–15.
Zhang, X., Malhotra, S., Molina, M., Haag, R., 2015b. Micro- and nanogels with labile crosslinks – from synthesis to biomedical applications. Chem. Soc. Rev. 44, 1948–1973.
Zhao, Y., Vivero-Escoto, J.L., Slowing, I.I., Trewyn, B.C., Lin, V.S.Y., 2010. Capped mesoporous silica nanoparticles as stimuli-responsive controlled release systems for intracellular drug/gene delivery. Expert Opin. Drug Deliv. 7, 1013–1029.
Zhong, Y., Zhang, J., Cheng, R., Deng, C., Meng, F., Xie, F., et al., 2015. Reversibly crosslinked hyaluronic acid nanoparticles for active targeting and intelligent delivery of doxorubicin to drug resistant CD44+ human breast tumor xenografts. J. Controlled Release 205, 144–154.
Zhong, Y.N., Goltsche, K., Cheng, L., Xie, F., Meng, F.H., Deng, C., et al., 2016. Hyaluronic acid-shelled acid-activatable paclitaxel prodrug micelles effectively target and treat CD44-overexpressing human breast tumor xenografts in vivo. Biomaterials 84, 250–261.
Zhou, H.Y., Chen, X.G., Kong, M., Liu, C.S., 2009. Preparation of chitosan-based thermosensitive hydrogels for drug delivery. J. Appl. Polym. Sci. 112, 1509–1515.
Zhou, M., Li, J., Liang, S., Sood, A.K., Liang, D., Li, C., 2015a. CuS nanodots with ultrahigh efficient renal clearance for positron emission tomography imaging and image-guided photothermal therapy. ACS Nano 9, 7085–7096.
Zhou, B., Hui, W., Liu, R., Wang, M., Deng, H., Giglio, B., et al., 2015b. PET imaging of human glioblastoma and colorectal cancer xenografts using 64Cu-labeled Dll4 antibody. J. Nucl. Med. 56, 1142.
Zou, Y., Meng, F., Deng, C., Zhong, Z., 2016a. Robust, tumor-homing and redox-sensitive polymersomal doxorubicin: a superior alternative to Doxil and Caelyx? J. Controlled Release 239, 149–158.
Zou, Y., Fang, Y., Meng, H., Meng, F., Deng, C., Zhang, J., et al., 2016b. Self-crosslinkable and intracellularly decrosslinkable biodegradable micellar nanoparticles: a robust, simple and multifunctional nanoplatform for high-efficiency targeted cancer chemotherapyJ. Controlled Release . . Available online 28 May 2016, ISSN 0168-3659 http://dx.doi.org/10.1016/j.jconrel.2016.05.060.